SLAC–PUB–6439
February 1994
(M)

POLARIZED LEPTON–NUCLEON SCATTERING[⋆]

Emlyn Hughes
Stanford Linear Accelerator Center
Stanford University, Stanford, CA 94309

ABSTRACT

Deep inelastic polarized lepton-nucleon scattering is reviewed in three lectures. The first lecture covers the polarized deep inelastic scattering formalism and foundational theoretical work. The second lecture describes the nucleon spin structure function experiments that have been performed up through 1993. The third lecture discusses implications of the results and future experiments aimed at high-precision measurements of the nucleon spin structure functions.

Invited talk presented at the 21st Annual SLAC Summer Institute on Particle Physics: Spin Structure in High-Energy Processes, Stanford, CA, July 26–August 6, 1993

[⋆] Work supported by Department of Energy contract DE–AC03–76SF00515 (SLAC).

Dedication

These lectures are dedicated to the memory of William W. Ash, who built the polarized target for the first polarized electron-nucleon deep inelastic scattering experiment, SLAC E–80.

TABLE OF CONTENTS

Lecture I: Introduction and Formalism

Lecture II: The Experiments

(Continued)

Lecture III: Implications and Future Programs

Lecture I: Introduction and Formalism

1 Introduction

Polarized lepton-nucleon scattering provides information on the spin structure of the proton and neutron. The experimental breakthrough in the field came in 1972, when a group from Yale University pioneered the production of polarized electron beams using the principle of photoionization of electrons from polarized alkali atoms.[1] The difficulty of producing a polarized electron beam prior to this fairly late development was driven by the inability to polarize electrons through Stern-Gerlach techniques due to the Heisenberg uncertainty principle.[2] Polarized atomic beams from the Stern–Gerlach discovery had long been developed.

The first experiment[3] to scatter elastically polarized electrons at low energies off polarized hydrogen is an instructive example of polarized lepton-nucleon scattering. In this experiment, a polarized beam of Cesium atoms is stripped of its electrons and accelerated into the beam transport line (see Fig. 1). The electron beam is directed into a polarized hydrogen beam injected into an interaction

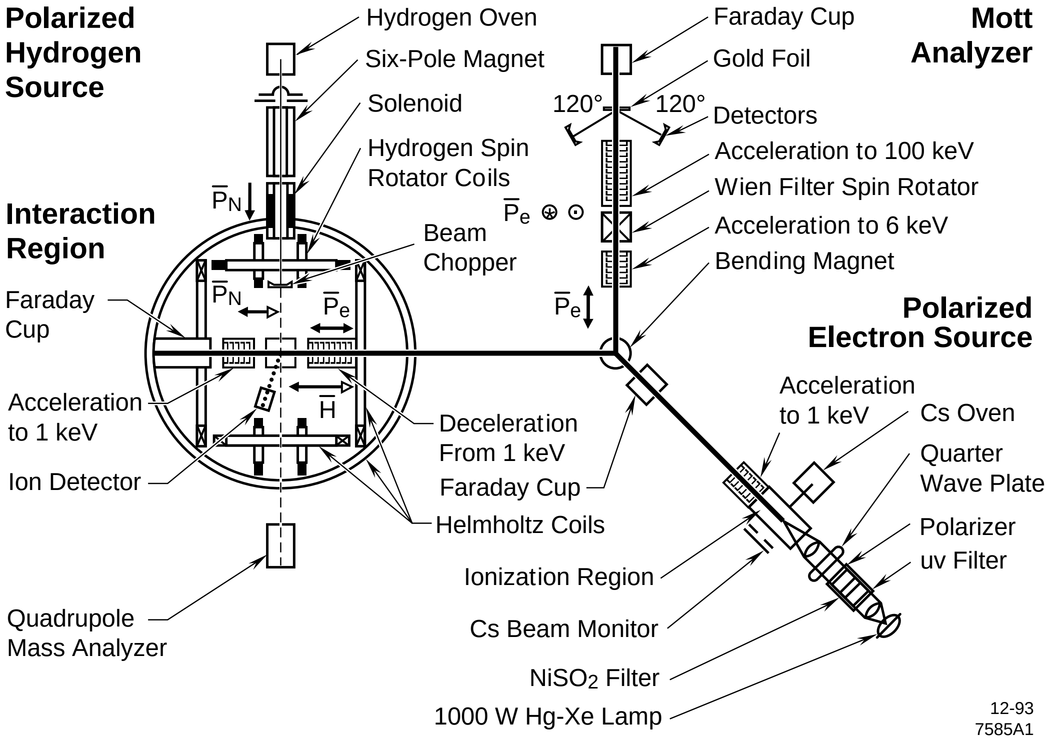

Fig. 1. Experimental setup for polarized electron polarized hydrogen elastic scattering experiment.

region, where the scattered hydrogen ions are detected. The motivation for the experiment was to study in a simple process spin-dependent scattering and spin-dependent interactions. "Theoretically, electron-hydrogen elastic scattering is the simplest and most fundamental of all electron-atom collision problems. Nonetheless, it cannot be solved in closed form." The results are presented in Fig. 2. Large asymmetries in the scattering are observed and compared to theoretical predictions. The theoretical models vary enormously in their predictions and the experimental results disagree with all models, which is typical in the field of spin-dependent scattering.

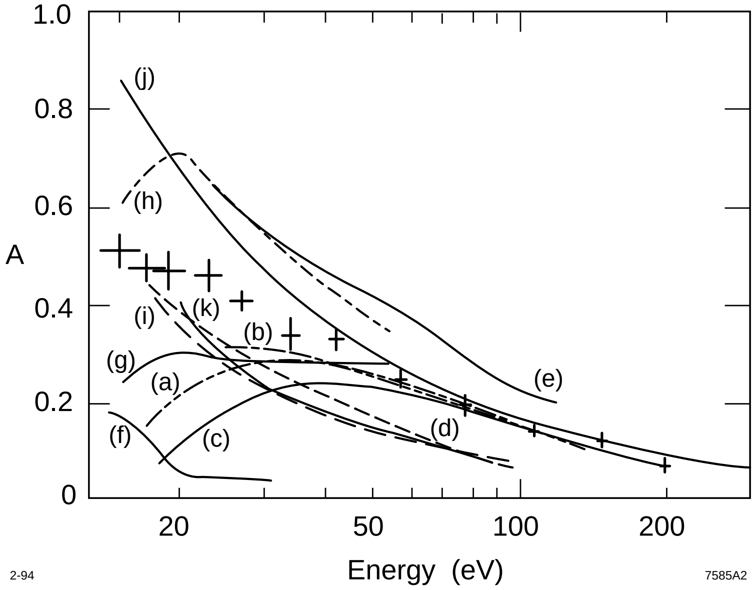

Fig. 2. Results on asymmetry versus energy for elastic scattering experiment. For references to theoretical models, see Ref. 3.

Energies for scattering polarized leptons off polarized nucleons extend from the 1 eV level, as just discussed, to the 200 GeV level from polarized muon scattering at CERN. These lectures will concentrate on polarized electron nucleon scattering at high energies, greater than 10 GeV. Low-energy polarization experiments are discussed here only to the extent that they aid in understanding the high-energy results. These lectures will concentrate on physics provided by scattering polarized leptons off polarized targets. Experiments with neutrino beams (which are naturally polarized) and experiments with polarized electrons scattering off unpolarized targets (which are used in the study of electroweak parity violation) are not discussed.

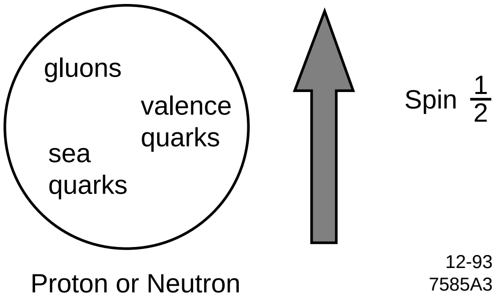

Fig. 3. Pictorial of Quark Parton Model constituents in the nucleon.

The primary goal of high-energy deep inelastic scattering of polarized leptons by polarized nucleons is to study the internal spin structure of the proton and neutron. It has long been known that the nucleon has substructure (see Fig. 3). The questions being asked here include:

- ◇ Do quarks carry the spin of the nucleon?
- ◇ What is the distribution of the nucleon spin between the different quark flavors?
- ◇ What is the role of the orbital angular momentum of the constituents in the nucleon?
- ◇ What role do the gluons play?
- ◇ Does QCD adequately account for the behavior of the nucleon spin?

The answers to these questions require input ranging from nuclear physics to the current algebra of quarks, from the atomic and solid-state physics of polarized targets and polarized beams to high-energy particle physics detectors. This lecture series is divided into three parts. The first lecture reviews the formalism of deep inelastic scattering and how it is applied to polarized lepton-nucleon scattering. It discusses some of the foundational theoretical work which motivated the field and identified the language for interpreting the experimental results. While the formalism of polarized deep inelastic scattering has been reviewed previously by Fred Gilman,[4] the language is somewhat outdated. The second lecture focuses on experimental techniques and presents results on experiments which have been performed up to the end of 1993. Crucial to the experimental developments have been the large role played by solid state and atomic physics. The third lecture addresses the theoretical implications of the results and the difficulties faced in interpreting the results. The goal of this lecture series is both to educate the nonexpert and to review the status of the field.

2 Unpolarized Deep Inelastic Scattering

Deep inelastic fixed target experiments scatter high-energy (E) lepton beams of electron, muons, and neutrinos off targets, detect the scattered lepton, and measure its angle of deflection (θ) and its outgoing energy (E') (see Fig. 4). From the three measured quantities E, E', and θ, one can extract three independent scaling variables Q^2, x, and y where the scaling variables are given by

$$\begin{aligned} Q^2 &= 4EE' \ \sin^2[\theta/2] \ , \\ x &= Q^2/2M(E-E') \ , \\ y &= [E-E']/E \ . \end{aligned}$$

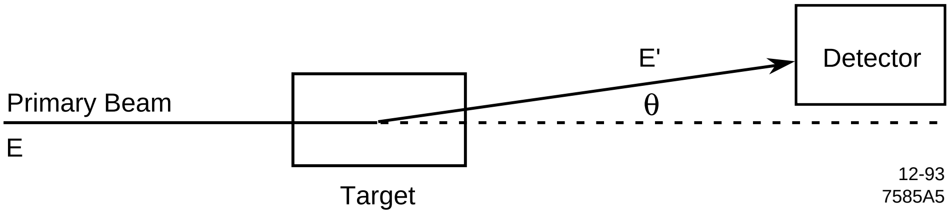

Fig. 4. The variables E, E', and θ as defined in fixed target deep inelastic scattering experiments.

Here, M is the nucleon mass. In the Quark Parton Model (see Fig. 5), these three variables have a simple meaning. In the view that deep inelastic scattering is a process describing the scattering of a lepton off a quark in the nucleon via the exchange of a virtual photon, Q^2 is the four-momentum of the virtual photon, x is the fraction of the total nucleon momentum carried by the struck quark, and y is the fraction of incoming energy carried by the virtual photon.

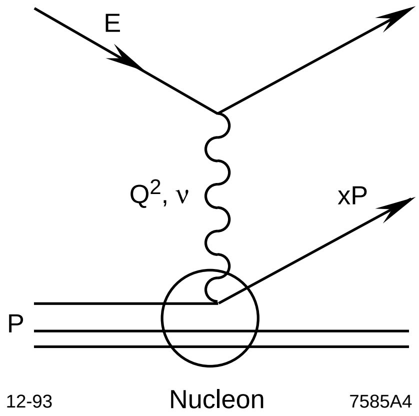

Fig. 5. Scaling variables in lepton-nucleon scattering.

The cross section for unpolarized deep inelastic scattering can be described by two "structure functions" (W_1 and W_2) that are functions of only x and Q^2:

$$\frac{d^2\sigma}{d\Omega\, dE'} = \frac{\alpha^2}{4E^2} \cdot \frac{\cos^2(\theta/2)}{\sin^4(\theta/2)} \left[W_2 + 2W_1 \ \tan^2(\theta/2)\right] . \tag{1}$$

Here α is the fine structure constant and Ω is the solid angle available for the scattered leptons.

Knowledge of the structure functions W_1 and W_2 is sufficient to calculate scattering rates for any deep inelastic experiment with proton and neutron targets. Experiments using polarized beams and targets require only small modifications to these rates, since the effects of polarized scattering is relatively small compared to the unpolarized case. For calculating electron scattering rates in order to estimate factors such as spectrometer performance, knowledge of the unpolarized scattering cross sections is sufficient.

The language and conventions that describe unpolarized structure functions have evolved with time. Historically, W_1 and W_2 were denoted as the unpolarized structure functions. Bjorken[5] postulated that these structure functions taken at high momentum transfer Q^2 and high virtual photon energy transfer $\nu = E - E'$ become functions (F_1 and F_2) of only x,

$$\begin{aligned} MW_1(\nu, Q^2) &\rightarrow F_1(x) , \\ \nu W_2(\nu, Q^2) &\rightarrow F_2(x) . \end{aligned}$$

A simple relation developed by Callan and Gross[6] between F_1 and F_2 emerges in the naive Quark Parton Model,

$$F_2(x) = 2xF_1(x) \tag{2}$$

In today's language, results are usually presented as a mixture of the old convention. The two structure functions now quoted in most papers or review articles are given as $F_2(x, Q^2)$ and $R(x, Q^2)$, where R measures the deviation of F_1 and F_2 at finite Q^2 from the Callan-Gross relation,

$$R(x, Q^2) \ = \ \frac{F_2(x, Q^2)}{2xF_1(x, Q^2)} \left[1 + \frac{Q^2}{\nu^2}\right] - 1 , \tag{3}$$

and

$$F_2(x, Q^2) \ = \ \nu W_2(x, Q^2) . \tag{4}$$

From F_2 and R, one can extract W_1 and W_2 and calculate scattering cross sections. Modern results on F_2 for the deuteron from CERN[7] and R from SLAC[8] are presented in Figs. 6 and 7, respectively. The ratio R is difficult to measure with precision, since it represents the small difference between two structure functions, F_2 and $2xF_1$.

From the scattering cross section, it is straightforward to calculate the number of scattered electrons per energy E'. The total number of scattered electrons at a particular energy is

$$N = I_b \, \rho \, L N_A \, \Omega \, d^2\sigma \ . \tag{5}$$

Here I_b is the number of incident electrons, ρ is the target density, L is the target length, N_A is Avogadro number, Ω is the spectrometer solid angle, and $d^2\sigma$ is the double differential scattering cross section with energy and solid angle. A useful mnemonic for calculating the density of target nucleons is

$$\text{Number of target nucleons / cc} \ = \ \rho N_A \ ,$$

with ρ in units of gm/cc.

Consider the following example: If one scatters a 50 GeV electron beam with a current of 1 μA off a 1-cm-long hydrogen (Z = 1) target with a density of 1 gm/cc and detects the scattered electrons in a 1 msr spectrometer set up at 7°,

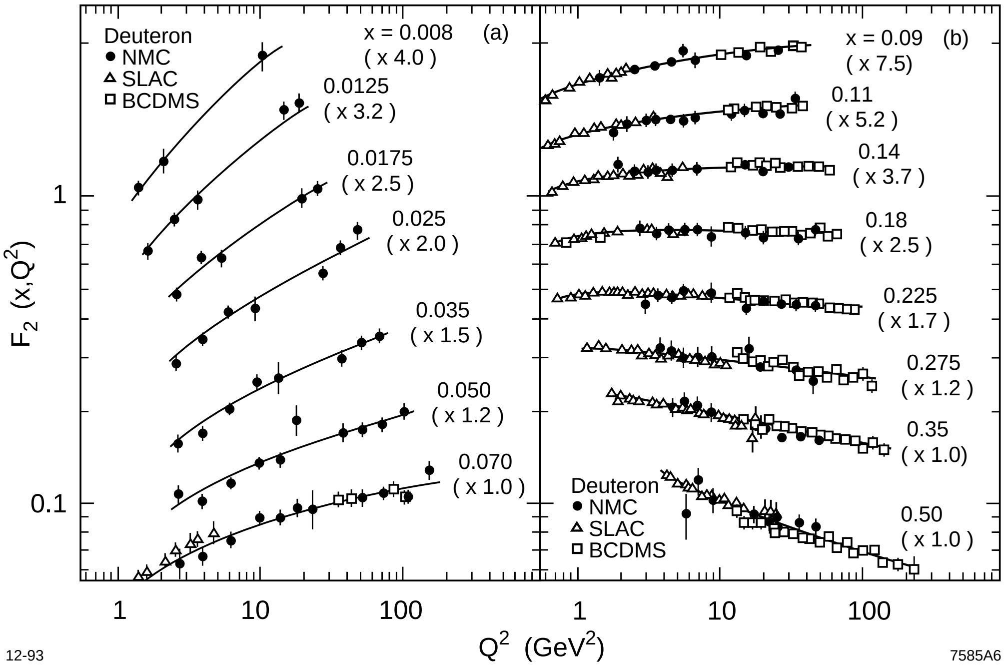

Fig. 6. Structure function F_2 of the deuteron versus Q^2 for different values of x.

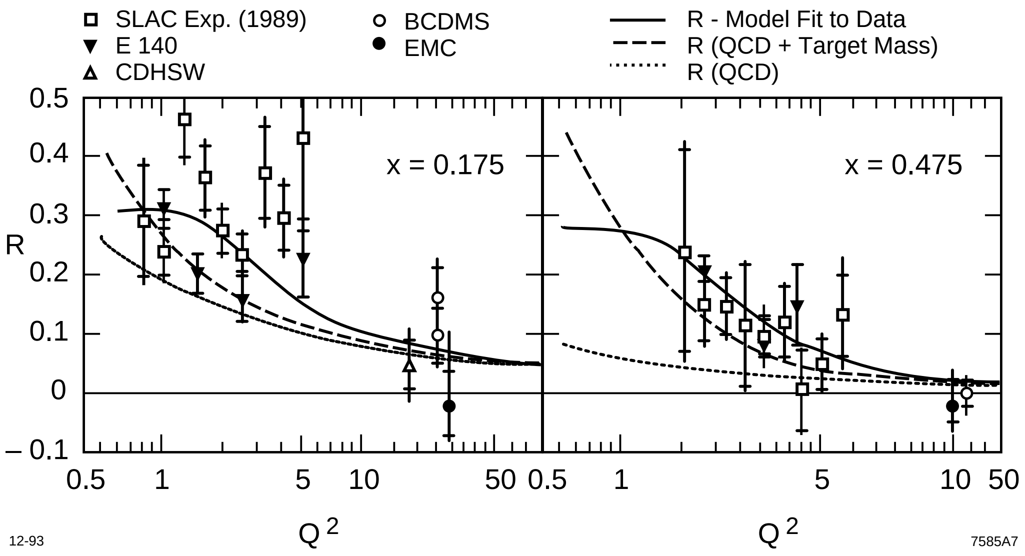

Fig. 7. The longitudinal-to-transverse structure function ratio R as a function of Q^2 for two values of x.

how many scattered electrons per second are observed with energies between 10 and 11 GeV?

The kinematics are well defined, and give the values of W_1 and W_2. For the above conditions,

$$Q^2 \;=\; 4 \cdot 50 \text{ GeV} \cdot 10.5 \text{ GeV} \cdot \sin^2(7^\circ/2) = 7.8 \text{ GeV}^2 \;,$$

$$x \;=\; \frac{Q^2}{2M\nu} \;=\; \frac{7.8 \text{ GeV}^2}{2(0.938 \text{ GeV})\ (50 \text{ GeV} - 10.5 \text{ GeV})} \;=\; 0.11 \;.$$

From Figs. 6 and 7, one can read off the values of $F_2(x, Q^2)$ and $R(x, Q^2)$ at these values of x and Q^2,

$$F_2(0.11, 7.8) \;\approx\; 0.35 \;, \qquad\qquad R(0.11, 7.8) \;\approx\; 0.1 \;,$$

and extract W_1 and W_2,

$$W_1 \;=\; \frac{F_1}{M} \;\approx\; 1.5 \;, \qquad W_2 \;=\; \frac{F_2}{\nu} \;\approx\; 0.009 \;,$$

applying $F_1 \approx F_2/2x(1+R)$.

The scattering cross section [Eq. (1)], is

$$d^2\sigma \approx \frac{(1/137)^2}{4 \cdot (50 \text{ GeV})^2} \cdot \frac{\cos^2(7/2)}{\sin^4(7/2)} \cdot [0.009 + 2(1.5)\ \tan^2(7/2)] \;.$$

Numerically, this gives

$$d^2\sigma \;\approx\; 7.7 \times 10^{-6}\ \mathrm{GeV}^{-2}\ \mathrm{sr}^{-1} \;=\; 3 \times 10^{-33}\ \mathrm{cm}^2/\mathrm{sr}\ ,$$

using the conversion factor that 1 $\mathrm{GeV}^{-2} = 3.89 \times 10^{-28}$ cm^2. The number of scattered electrons [Eq. (5)] per second with energies between 10 and 11 GeV detected by the spectrometer is

$$N_e \;\approx\; \frac{10^{-6}\,\mathrm{A}}{1.6{\times}10^{-19}\,\mathrm{A/e^-}} \cdot 1\,\mathrm{gm/cc} \cdot 1\,\mathrm{cm} \cdot 6{\times}10^{23} \cdot 10^{-3}\,\mathrm{sr} \cdot 3{\times}10^{-33}\,\mathrm{cm}^2/\mathrm{sr}\ .$$

The result becomes

$$N_e \;\approx\; 11\ \mathrm{electrons/second}$$

This example is typical of the zeroth-order calculations done in deep inelastic scattering. It should be emphasized that this is an over-simplified case. In reality, issues such as radiative corrections (Sec. 3.1) must be taken into account, which complicates the situation significantly.

3 Polarized Deep Inelastic Scattering

Deep inelastic scattering experiments using polarized lepton beams off polarized targets provide information on the spin structure function of the nucleon.[9] These experiments typically measure differences between the scattering cross sections for the case where the beam and target spins are in various orientations (see Fig. 8). The relationship between the spin-dependent scattering cross sections and the nucleon spin-dependent structure functions has a parallel formalism to the unpolarized case. Once again, there are two primary spin structure functions $G_1(x,Q^2)$ and $G_2(x,Q^2)$ (analogous to W_1 and W_2) and the scattering cross sections and the spin structure functions are related by,[10−12]

$$\frac{d^2\sigma^{\uparrow\downarrow}}{dQ^2d\nu} - \frac{d^2\sigma^{\uparrow\uparrow}}{dQ^2d\nu} \;=\; \frac{4\pi\alpha^2}{Q^2E^2}\left[M(E+E'\cos\theta)\,G_1(Q^2,\nu) - Q^2\,G_2(Q^2,\nu)\right]\ , \quad (6)$$

and

$$\frac{d^2\sigma^{\uparrow\rightarrow}}{dQ^2d\nu} - \frac{d^2\sigma^{\downarrow\rightarrow}}{dQ^2d\nu} \;=\; \frac{4\pi\alpha^2E'}{Q^2E^2}\ \sin\theta\left[M\,G_1(Q^2,\nu) + 2E\,G_2(Q^2,\nu)\right]\ . \quad (7)$$

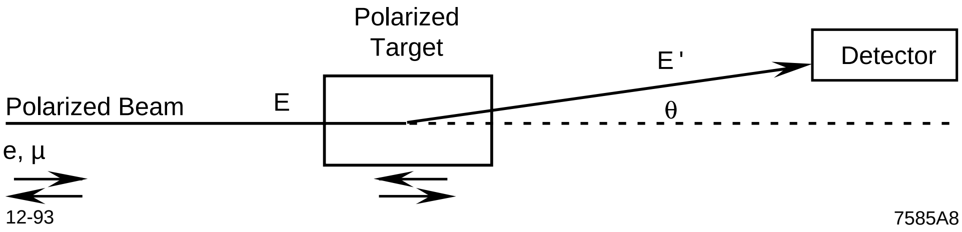

Fig. 8. Spin orientations of beam and targets in polarized lepton polarized nucleon scattering.

Here $\sigma^{\uparrow\uparrow}$, $\sigma^{\uparrow\downarrow}$, and $\sigma^{\uparrow\rightarrow}$ correspond to the scattering cross sections with beam and target spins parallel, antiparallel, or at 90° to one another. Like W_1 and W_2, these structure functions scale at high Q^2. As $Q^2 \rightarrow \infty$,

$$M^2\nu\, G_1(\nu, Q^2) \rightarrow g_1(x)\ , \qquad \text{and} \qquad M\nu^2\, G_2(\nu, Q^2) \rightarrow g_2(x)\ . \tag{8}$$

Modern convention presents results in terms of structure functions $g_1(x, Q^2)$ and $g_2(x, Q^2)$, which are dimensionally the same as the g_1 and g_2 defined above.

Since the difference between the various spin-dependent cross sections are usually quite small, the formalism of spin-dependent deep inelastic scattering experiments has developed around the use of asymmetries or the difference over the sum of the scattering cross sections. The next section describes the various types of spin-dependent asymmetries which appear in the literature.

3.1 Asymmetries in Spin-Dependent Deep Inelastic Scattering

The goal of most deep inelastic spin-dependent scattering experiments today is to extract the virtual photon nucleon asymmetries $A_1(x, Q^2)$ and $A_2(x, Q^2)$, where A_1 refers to the difference in scattering cross sections for the case where the virtual photon and nucleon spins are parallel versus antiparallel,

$$A_1 = \frac{d^2\sigma^{\uparrow\downarrow} - d^2\sigma^{\uparrow\uparrow}}{d^2\sigma^{\uparrow\downarrow} + d^2\sigma^{\uparrow\uparrow}}\ . \tag{9}$$

Similarly, the transverse asymmetry A_2 represents the comparison in which the nucleon target spin is transverse to the photon spin,

$$A_2 = \frac{d^2\sigma^{\uparrow\rightarrow} - d^2\sigma^{\downarrow\rightarrow}}{d^2\sigma^{\uparrow\rightarrow} + d^2\sigma^{\downarrow\rightarrow}}\ . \tag{10}$$

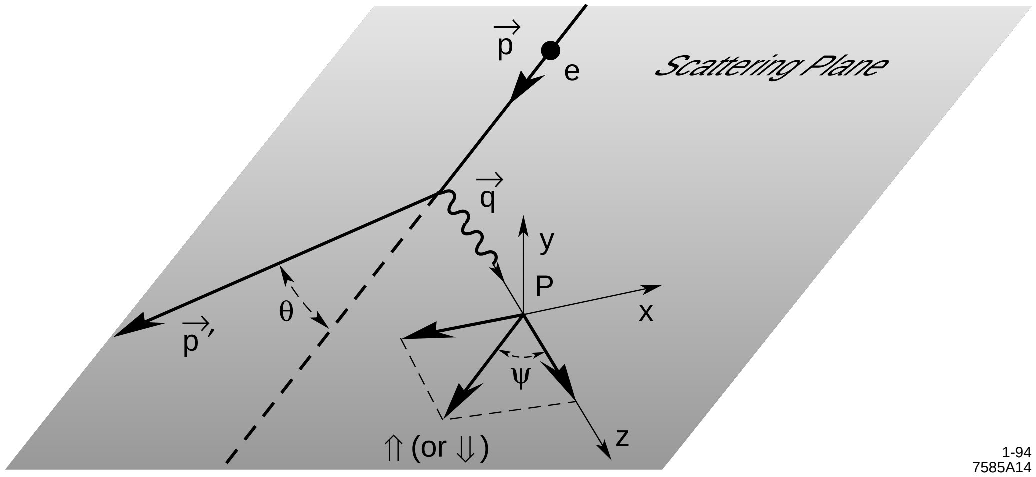

Fig. 9. Coordinate system for polarized lepton-nucleon scattering.

In practice, the virtual photon does not have 100% polarization (even if the lepton does!), nor does it scatter head-on. Even if the lepton scatters head-on, the virtual photon will scatter at some angle ψ that depends on the electron energy before and after the scatter (see Fig. 9). If $A^{\|}$ and $A^{\perp}$ represent the cross section asymmetries for scattering a 100% longitudinally polarized lepton off a polarized nucleon, then the relationship between $A^{\|}$ and $A^{\perp}$ and A_1 and A_2 is given by kinematics,

$$A^{\|} \;=\; D \cdot (A_1 + \eta A_2) \; , \tag{11}$$

$$A^{\perp} \;=\; d \cdot (A_2 + \zeta A_1) \; . \tag{12}$$

The factors η and ζ are typically small, providing a strong correlation between the asymmetries $A^{\|}$ and A_1, and between the asymmetries $A^{\perp}$ and A_2. Here the two depolarization factors are given by kinematics,

$$D \;=\; \frac{E - E'\epsilon}{E(1 + \epsilon R)} \; , \tag{13}$$

and

$$d \;=\; D \sqrt{\frac{2\epsilon}{1+\epsilon}} \; , \tag{14}$$

and the factors η and ζ are found via,

$$\eta \;=\; \frac{\epsilon \sqrt{Q^2}}{E - E'\epsilon} \; , \tag{15}$$

$$\zeta \;=\; \eta \left(\frac{1+\epsilon}{2\epsilon} \right) \;, \tag{16}$$

where ϵ characterizes the virtual photon polarization,

$$\epsilon \;=\; \frac{1}{1+2\left(1+\frac{\nu^2}{Q^2}\right)\,\tan^2\left(\frac{\theta}{2}\right)} \;. \tag{17}$$

The depolarization factor D is a pure QED factor and has a simple interpretation. It can be divided into two multiplicative terms, the first representing the angle ψ between the virtual photon and the struck nucleon, and the second representing the polarization P^γ of the virtual photon in the interaction. The scattering angle ψ and polarization P^γ can be extracted from kinematics,

$$\cos\psi \;=\; \frac{E-E'\epsilon}{E\,\sqrt{1-\epsilon^2}} \;, \qquad \text{and} \qquad P^\gamma \;=\; \frac{\sqrt{1-\epsilon^2}}{1+\epsilon R} \;, \tag{18}$$

where R is once again the ratio of longitudinal-to-transverse structure functions defined earlier. The entire depolarization factor is simply

$$D = P^\gamma \cdot \cos\psi \;, \tag{19}$$

which reduces to Eq. (13).

With a 100% polarized lepton beam scattering from a 100% polarized nucleon, A_1 and A_2 can be extracted by measuring $A^{\|}$ and $A^{\perp}$ and knowing the event kinematics, in order to determine the constants D, d, η, and ζ. In reality, however, the target has a polarization P_t, only a fraction f of the nucleons are polarized, and the beam polarization is less than 100%. As a result, the measured raw event asymmetry A^{meas} is smaller than $A^{\perp}$ or $A^{\|}$. In fact, to extract $A^{\|}$,

$$A^{\text{meas}} = A^{\|} \cdot P_t \cdot P_b \cdot f \;. \tag{20}$$

Figure 10 presents a schematic of how the various dilutions appear in the interaction, compared to the 'pure' case in which a fully polarized virtual photon collides head-on with a fully polarized nucleon. The smaller asymmetry A^{meas} represents a technical challenge to the experiments.

To extract A_1 from the experiment, it is necessary to unravel the impact of radiative corrections on the deep inelastic scattering measurements.[13] Theoretical models of A_1 and sum rules assume that the scattering corresponds to the single photon exchange Born approximation. Therefore, to compare to theory, it is necessary to calculate the radiative correction diagrams (see Fig. 11) and then to

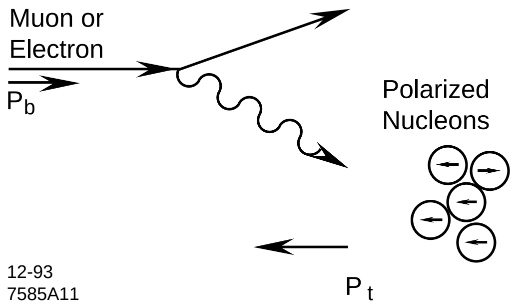

Fig. 10. Experimental dilutions in polarized lepton-nucleon scattering.

apply these corrections to the measured A_1 asymmetries in order to find A_1 values corresponding to the Born approximation. This process is laborious and requires an interative approach, since the size of the corrections is strongly correlated to values of A_1. Figure 11 presents the primary diagrams needed to extract A_1 from the measured asymmetry. A few of the important properties of the radiative corrections and their effect on the data are:

- ◇ The difference between the radiative corrections to the scattering cross sections $\sigma^{\uparrow\uparrow}$ and $\sigma^{\uparrow\downarrow}$ is small.
- ◇ The dominant corrections are pure QED diagrams, and the largest effect comes from the bremsstrahlung diagrams.
- ◇ Radiative corrections move events from high E' bins to lower E' bins (which is easy to understand in terms of bremmstrahlung).
- ◇ To the extent that the asymmetries are flat as a function of x, there is little change in the central value of the asymmetries due to radiative corrections. This is a direct consequence of the first point. However, even without an x-dependence in the asymmetry, the statistical error bars on the asymmetry at low x will increase after radiative corrections due to the subtraction of events from the high E' bins, which have contaminated the low E' bins.
- ◇ Solid targets have typically larger radiative corrections compared to gas targets due to 'external' radiative corrections.[14] These corrections scale with the thickness of the targets (in radiation lengths) and can be comparable in magnitude to the internal radiative corrections.

An example of radiative corrections to the proton target used in the EMC proton experiment[15] is given in Fig. 12. The increase in the size of the correction for low x is evident, and is a result of the contamination of events at low x.

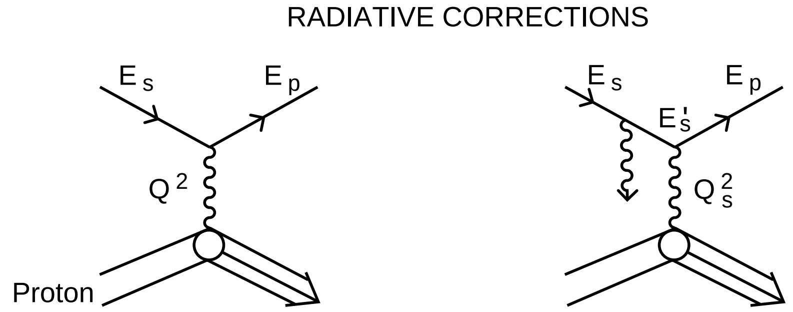

(a) Lowest Order Graph

(b) Internal Bremsstrahlung (s-peak)

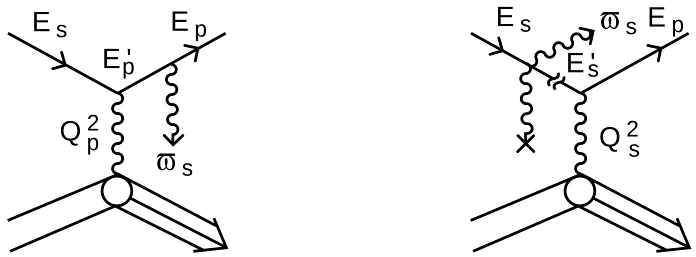

(c) Internal Bremsstrahlung (p-peak)

(d) External Bremsstrahlung (s-peak)

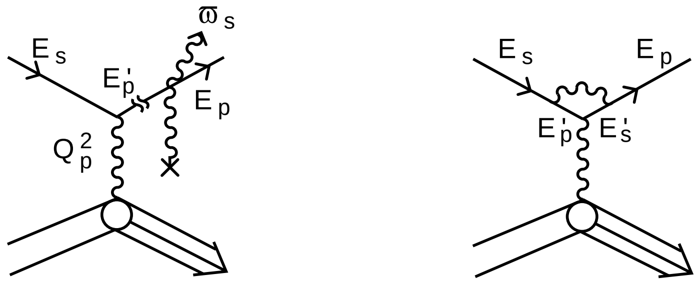

(e) External Bremsstrahlung (p-peak)

(f) Vertex Correction

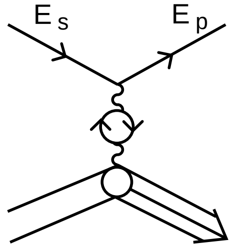

(g) Vacuum Polarization

Fig. 11. Primary radiative correction diagrams in deep inelastic scattering.

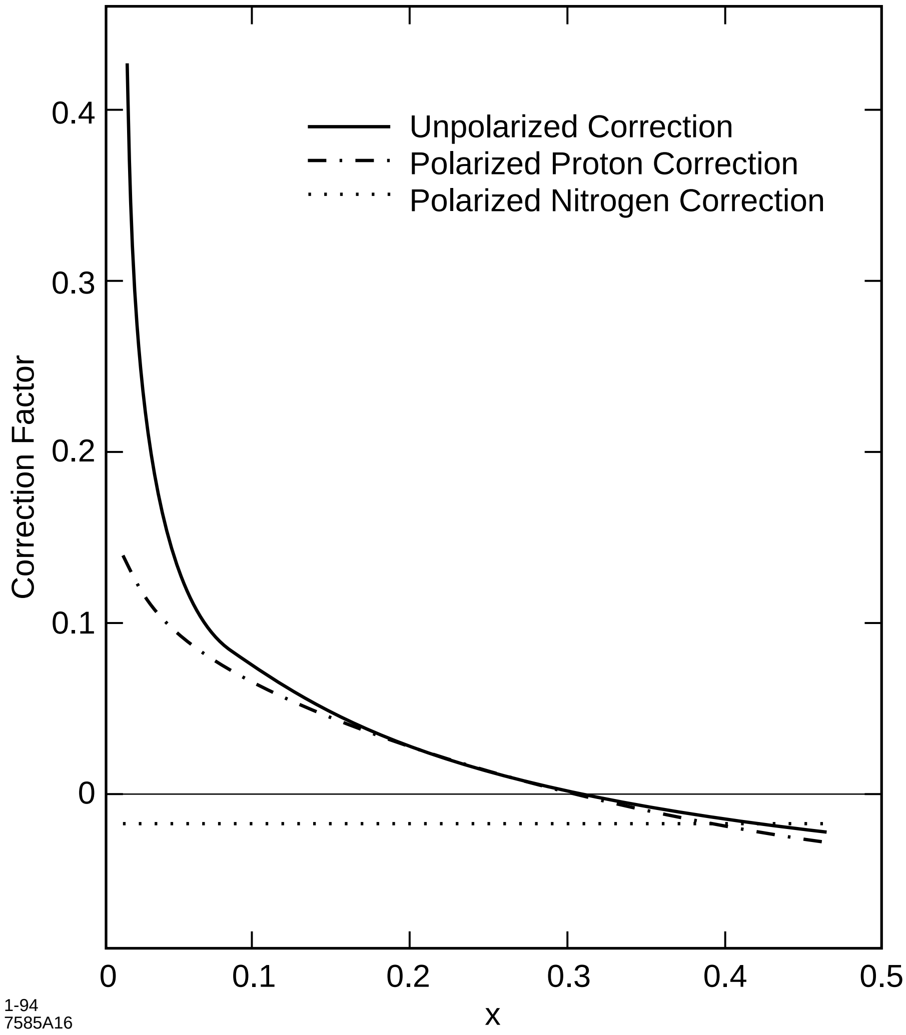

Fig. 12. Radiative corrections as a function of x for the EMC proton experiment.

The transverse spin asymmetry A_2 has a different behavior. For this asymmetry, the nucleon spin must lie in the scattering plane defined by the incoming and outgoing scattered electron. Transverse spin-dependent scattering in which the target nucleon spin is outside the scattering plane will result in no asymmetry due to CP conservation. A_2 has a number of interesting properties:

◇ Its value is bounded by the value of the unpolarized longitudinal structure function, namely $|A_2(x, Q^2)| < \ \overline{R}$. This behavior results from positivity bounds.[16] Initial experiments which extracted A_1 used this bound on A_2 and Eq. (11). However, future precision experiments on A_1 will require direct measurements of $A^{\perp}$.

- In the Quark Parton Model (QPM) the value of A_2 is believed to be small, since it is proportional to the quark masses. In the QPM, the helicity flip probability varies as m_q/E, and vanishes to the extent that quarks are massless.
- The transverse spin structure function g_2 extracted from A_2 obeys a sum rule (Burkhardt-Cottingham)[17] which implies an overall small contribution,

$$\int_0^1 g_2(x)dx \;=\; 0 \;. \tag{21}$$

The next section discusses the old QPM predictions of the values of A_1 and its behavior as a function of x and Q^2.

4 The Virtual Photon Asymmetry $\mathbf{A_1}$

Historically, the asymmetry A_1 and its dependence on x, in particular, was the primary variable which theoretical models of nucleon spin structure tried to predict. The following sections discuss some of the simplest early theories on A_1 and how it behaves.

4.1 The SU(6) Model

The simplest QPM prediction of the quark distribution in the nucleon[18] is SU(6). This model presents a static picture of the nucleon in which the proton (neutron) consists of purely valence quarks with two up (down) quarks and one down (up) quark. The wavefunction for the proton and neutron is found by counting all the possible antisymmetric combinations of three quark states, with one quark spin antiparallel to the other two quark spins. From the nucleon wavefunction, it is straightforward to extract the probability of finding an up or down quark with its spin parallel $\uparrow$ or antiparallel $\downarrow$ to the nucleon spin.

$$u^{\uparrow} = 5/9 \;, \qquad\qquad u^{\downarrow} = 1/9 \;,$$

$$d^{\uparrow} = 1/9 \;, \qquad\qquad d^{\downarrow} = 2/9 \;.$$

The value of A_1 for the proton is given by the charge squared of the quarks times the quark spin probability given above,

$$A_1^p = \frac{4/9(u^{\uparrow} - u^{\downarrow}) + 1/9(d^{\uparrow} - d^{\downarrow})}{4/9(u^{\uparrow} + u^{\downarrow}) + 1/9(d^{\uparrow} + d^{\downarrow})} \quad . \tag{22}$$

The proton asymmetry yields 5/9, and the neutron asymmetry is 0.

Although SU(6) is known to breakdown due to the existence of sea quarks and gluons, the SU(6) predictions appear to work at x near 0.3. For example, the measured values of A_1 for the proton and neutron appear to be in fine agreement with SU(6) at $x = 0.3$.

4.2 Regge Theory and Small x

The small x behavior of A_1 and A_2 is a topic of great interest in terms of understanding the "sum rules" discussed at the end of this lecture. Small x measurements correspond in QPM to scattering in which the struck quarks are carrying a small fraction of the nucleon momentum. The loss of information from the initial static state can be understood in terms of the emission of gluons, "taking spin away" from the struck quark. As a result, the asymmetries tend to zero as x approaches zero. The convergence of the asymmetries to zero is described by the data over the measured range, and this tendency to coverge is apparent in all existing data samples.

For understanding the data below the x range of the measurements, a Regge parameterization is taken. A long, complicated history of Regge theory[19,20] has evolved and is used to describe the low-x behavior of structure functions, in general. The results of the Regge theory prediction for the convergence of the asymmetries to zero has some particular properties,[21]

- ◇ As x approaches zero, the structure functions and asymmetries become independent of Q^2.
- ◇ The value of the cross sections needed for the structure functions and asymmetries is given by the optical theorem,

  $$\mathrm{Im}\, A \;=\; s \cdot \sigma^{\mathrm{tot}} \;,$$

  where A is the scattering amplitude, s is the center-of-mass energy, and σ^{tot} is the total scattering cross section.
- ◇ Regge theory predicts how the amplitude varies as x approaches zero,

  $$A(s,0) \;=\; s^{\alpha(0)} \;,$$

  where $\alpha(0)$ is a Regge intercept given by $a_1(1270)$ and $f_1(1285)$ evaluated from pion-proton scattering.[22]

At low x, the value of x can be related to the center-of-mass energy via

$$x \approx Q^2/s \approx 1/s .$$

Therefore, when s is large and x is small,

$$F_2 \approx \sigma^{\rm tot} \approx x^{1-\alpha_1(0)} \qquad \Rightarrow \qquad F_1 \approx x^{-\alpha_1(0)} ,$$

and similarly

$$g_1 \approx x^{-\alpha_2(0)} .$$

Since $A_1 \approx g_1/F_1$,

$$A_1 \approx x^{\alpha_1(0)-\alpha_2(0)} .$$

The same behavior of x evaluated to a power[23] is invoked to extract the low-x behavior of the spin structure function g_1 described later in Sec. 5.1.

4.3 The Quark Parton Model and High x

The large x behavior of the structure functions is also predicted by the Quark Parton Model (QPM). Figure 13 presents the Feynman diagram for scattering off a quark that carries all of the nucleon momentum (i.e., x approaches 1). For this case, the measured asymmetry for the proton (or neutron) will come from the scattering off a single quark,

$$A_1(x \to 1) = \frac{q^\uparrow - q^\downarrow}{q^\uparrow + q^\downarrow} .$$

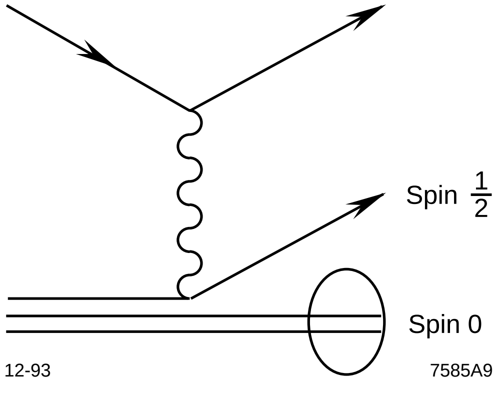

Fig. 13. Diquark production in scattering at high x.

For the case of massless quarks at high x, the probability of spin-flip varies as $\sigma_{1/2} \approx z_i^2$ ($q^{\uparrow}$ finite) and $\sigma_{3/2} \approx 0$ ($q^{\downarrow}$ zero). The formula above implies that the asymmetry A_1 will approach one as x approaches one.[24]

This behavior appears reasonable, since the struck quark carries the nucleon spin, and the two remaining quarks pair off with a net zero spin. If the struck quark is decoupled from the other two quarks or from polarized gluons at high x, then the single-struck quark aligned with the nucleon spin (with no mechanism to undergo spin-flip), is the only scattering channel.

This model of the nucleon at high x also predicts[25] that the ratio of the neutron-to-proton cross sections in deep inelastic scattering should tend to 1/4 as x approaches 1. The experimental data appears to support this conclusion.[26]

4.4 The Carlitz-Kaur Model

In 1977, Carlitz and Kaur developed a model[27] that supports the low-, middle-, and high-x predictions discussed in the last three sections. The results for the asymmetry predictions as a function of x from the Carlitz-Kaur model is given in Fig. 14. This model also obeys a sum rule developed by Ellis and Jaffe discussed at the end of this lecture. This model has become a standard to which experimental data can typically be compared.

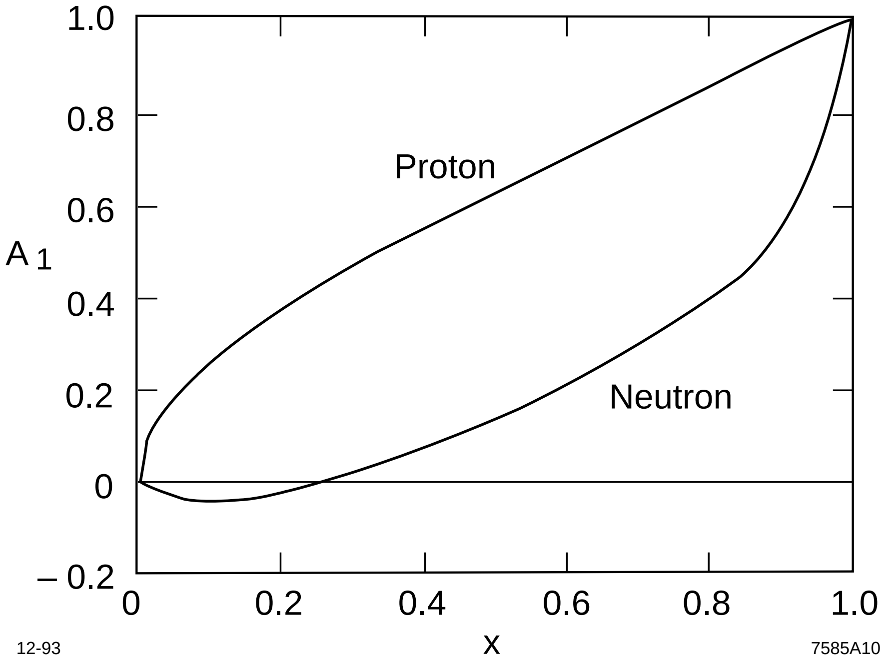

Fig. 14. Carlitz-Kaur model of A_1 versus x for the proton and neutron.

5 The Spin Structure Function g_1

Knowledge of the spin-dependent asymmetries A_1 and A_2 and the unpolarized structure functions F_2 and R completely determines the spin structure function g_1,

$$g_1(x, Q^2) = F_1(x, Q^2) \cdot [A_1(x, Q^2) + \gamma A_2(x, Q^2)] \ , \tag{23}$$

where γ is a kinematic factor given by $\gamma = \sqrt{Q^2}/\nu$. Terms proportional to γ^2 have been neglected. In the QPM, the structure function g_1 has a simple interpretation,

$$g_1(x) = \Sigma z_i^2 [q_i^{\uparrow}(x) - q_i^{\downarrow}(x)] \ , \tag{24}$$

where the sum is over the different quark flavors. This relationship is analogous to the relationship between F_2 and the quark distributions for unpolarized scattering,

$$F_1(x) = \Sigma z_i^2 [q_i^{\uparrow}(x) + q_i^{\downarrow}(x)] \ , \tag{25}$$

The asymmetry A_1 develops a simple meaning in the Quark Parton Model, since $A_1 = g_1/F_1$ (ignoring higher order corrections). The kinematic factor γ is generally small, and suppresses the A_2 contribution to the spin structure function g_1.

A number of interesting idiosynchrasies of the structure function g_1 appear:

- ◇ As x gets large, F_1 approaches zero, implying that g_1 approaches zero. Similarly, the uncertainty on g_1 becomes small, since it is bounded by $g_1 < F_1$.
- ◇ At low x, g_1 varies as A_1/x. This implies that the precision on determining g_1 quickly becomes limited due to the divergent $1/x$ behavior. As a result, the statistical error bars on g_1 from any measurement tend to increase as x gets small, even though the error bars on the asymmetry measurements may be small and independent of x.

For completeness, the transverse spin structure function g_2 is given,

$$g_2 \ = \ F_1 \cdot \left(\frac{A_2}{\gamma} + \gamma A_2 - A_1 \right) \ . \tag{26}$$

As discussed earlier the integral over g_2 is expected to vanish.[27] Interestingly, this implies that $A_2 \neq 0$!

5.1 The Spin Structure Function at Low x

An important quantity in the study of spin structure functions is the integral over the full x range of the spin structure function g_1, namely $\int_0^1 g_1(x)dx$. The integral values are useful for testing ‘sum rules’ discussed in the next section. Since the measurements are only valid over an x-range limited to typically greater than 0.005 and less than 0.7, extrapolations of the measurements must be invoked in order to extract the full integral.

For the low-x extrapolation, one uses Regge theory as described in Sec. 4.2. At low x, g_1 is expected to be independent of Q^2, and varies as

$$g_1 \;=\; \left(\frac{x}{x_0}\right)^{\alpha} ,$$

where x_0 is the lowest x value determined by the experiment. The contribution of the integral from the low-x unmeasured region then becomes

$$\epsilon \;=\; \int_0^{x_0} g_1(x)\; dx \;=\; \frac{x_0\, g_1(x_0)}{1-\alpha} .$$

The value of the integral diverges as α approaches one. Calculations[28] give a range in α for spin-dependent scattering to be $-0.5 < \alpha < 0$. With this constraint, the low-x extrapolation becomes

$$0.66\; x_0\, g_1(x_0) < \epsilon < x_0\, g_1(x_0) .$$

To maintain as small a low-x extrapolation as possible, it is important to both measure the low-x structure function $g_1(x_0)$ as accurately as possible and to make sure that x_0 is as small as possible. In general, high-energy (200 GeV) muon beams can measure the structure functions to values of x_0 less than 0.01, but with limited statistics on $g_1(x_0)$; whereas, low-energy electron beams (30 GeV) can measure the structure function only down to values of x_0 near 0.02, but with high precision on $g_1(x_0)$.

It should be stressed that without a theory for the low-x extrapolation, the value of ϵ is unbounded.

6 The Bjorken Sum Rule

In 1966, prior to the development of QCD, Bjorken^{29} discussed applications of $\mathrm{SU}(6)\times\mathrm{SU}(6)$ current algebra. Within this famous paper, he derived what at the time was an obscure relationship between spin-dependent deep inelastic scattering cross sections and the weak coupling constant found in neutron beta decay. This relationship known as the 'Bjorken Sum Rule' has become the holy grail for experiments in spin-dependent deep inelastic scattering. The sum rule is regarded as inviolable, since it depends only on current algebra assumptions and the assignment of charges to the quarks. Corrections to the sum rule for experiments which measure the spin structure functions at finite Q^2 are given by QCD, implying that a violation of the sum rule would be a direct threat to QCD. Feynman^{30} wrote that the Bjorken sum rule's "verification, or failure, would have a most decisive effect on the direction of future high-energy theoretical physics."

The sum rule without QCD corrections stands on three pillars: current algebra, quark currents, and beta decay.

The calculations to extract the current algebra part of the sum rule are laborious and not reproduced here. The result of Bjorken's calculation relates the integral over x of the spin structure function g_1 to the equal time commutator of the transverse components of the electromagnetic current densities $J_x(x,0)$ and $J_y(0)$. The derived relationship gives at infinite momentum transfer Q^2,

$$\int_0^1 g_1(x)\,dx \;=\; \frac{i}{4}\int d^3x\,\langle P\mid[J_x(x,0),J_y(0)]\mid P\rangle\ .$$

The above relationship requires no models of hadronic structure.

Previous work with electromagnetic currents^{31} had already connected the transverse components of the electromagnetic currents to the axial current of the interaction, yielding

$$[J_x(x,0),J_y(0)] \;=\; 2i\,\delta^3(x)\;J^5_\mu \;+\; \text{Schwinger terms}\ .$$

Substituting the above equation into the Bjorken relationship previously given yields trivially,

$$\int_0^1 g_1(x)\;dx \;=\; \frac{1}{2}\;\left\langle P|J^5_\mu|P\right\rangle\ . \tag{27}$$

The second step in the Bjorken sum rule derivation is the assignment of the quark currents. The vector quark current can be written in Dirac notation, in which $J_\mu = \psi\gamma_\mu \mathrm{Q}\bar{\psi}$, where ψ is the Dirac spinor for three quarks (u,d,s) and Q is the quark charge matrix with specific quark charges assigned to the up, down, and strange quarks,

$$\mathrm{Q} \;=\; \begin{pmatrix} 2/3 & 0 & 0 \\ 0 & -1/3 & 0 \\ 0 & 0 & -1/3 \end{pmatrix} \quad .$$

The axial vector quark currents of this problem are

$$J^5_\mu \;=\; \frac{1}{2}\,\psi\,\gamma_5\,\gamma_\mu\,\mathrm{Q}^2\,\bar{\psi}\ .$$

Defining the matrices for hypercharge Y and isospin I$_3$,

$$\mathrm{Y} \;=\; \begin{pmatrix} 1/3 & 0 & 0 \\ 0 & 1/3 & 0 \\ 0 & 0 & -2/3 \end{pmatrix} \quad , \qquad \mathrm{I}_3 \;=\; \begin{pmatrix} 1/2 & 0 & 0 \\ 0 & -1/2 & 0 \\ 0 & 0 & 0 \end{pmatrix} \quad .$$

By simple matrix manipulation, it can be shown that

$$\mathrm{Q}^2 \;=\; \frac{2}{9} + \frac{1}{3}\,\mathrm{Q} \;=\; \frac{2}{9} + \frac{1}{3}\,\left(\mathrm{I}_3 + \frac{1}{2}\,\mathrm{Y}\right)$$

In taking the difference between the matrix elements of the axial vector current between a proton and a neutron, only the isospin component will survive as nonzero.

$$\begin{aligned} &\left\langle \mathrm{proton}\left|J^5_\mu\right|\mathrm{proton}\right\rangle \;-\; \left\langle \mathrm{neutron}\left|J^5_\mu\right|\mathrm{neutron}\right\rangle \\ &\quad= \left\langle \mathrm{proton}\left|\frac{1}{3}\,\psi\gamma_5\gamma_\mu I_3\bar{\psi}\right|\mathrm{proton}\right\rangle - \left\langle \mathrm{neutron}\left|\frac{1}{3}\,\psi\,\gamma_5\,\gamma_\mu\,I_3\bar{\psi}\right|\mathrm{neutron}\right\rangle \\ &\quad= \frac{2}{3}\,\left\langle P\left|\psi\,\gamma_5\,\gamma_\mu\,I_3\bar{\psi}\right|P\right\rangle\ . \end{aligned}$$

The last relation arises from the fact that the proton and neutron isospin values are equal and opposite in sign.

Substitution from Eq. (27) provides for the result in terms of the proton and neutron spin structure function integrals,

$$\int_0^1 g_1^p(x)\,dx - \int_0^1 g_1^n(x)\,dx = \frac{1}{6}\,\cdot\,2\left\langle P\left|\psi\gamma_5\gamma_\mu I_3\bar{\psi}\right|P\right\rangle\ . \qquad (28)$$

The final step in the derivation of the Bjorken sum rule is the equating of the above matrix element to the matrix element that describes neutron beta decay. The weak coupling constant from beta decay g_A is related to an axial vector current between a proton and a neutron state,

$$g_A \;=\; \left\langle \text{proton} \left| \psi\, \gamma_5\, \gamma_\mu\, I^+ \bar{\psi} \right| \text{neutron} \right\rangle$$

Here g_V is set equal to one by convention, so that the expression $g_A/g_V = g_A$. By introducing the lowering operator $T^- = \int \psi \gamma_0 I^- \bar{\psi} d^3x$, the coupling constant g_A can be related to the third component of the isospin operator in the following manner,

$$\begin{aligned} g_A &= \left\langle P \left| \psi\, \gamma_5\, \gamma_\mu I^+ \bar{\psi}\, T^- \right| P \right\rangle \\ &= \left\langle P \left| \psi\, \gamma_5\, \gamma_\mu\, [I^+, I^-]\, \bar{\psi} \right| P \right\rangle \\ &= 2 \cdot \left\langle P \left| \psi\, \gamma_5\, \gamma_\mu\, I_3 \bar{\psi} \right| P \right\rangle \end{aligned}$$

Substituting the above result into Eq. (28) yields the Bjorken sum rule, which states that at infinite Q^2,

$$\int_0^1 g_1^p(x)\; dx - \int_0^1 g_1^n(x)\; dx \;=\; \frac{1}{6}\, g_A\ . \tag{29}$$

At this stage the weakest assumptions inherent in the Bjorken sum rule is probably the charge assignments to the quarks. The current algebra derivation of the Bjorken sum rule is today typically replaced by Operator Product Expansion techniques.[32]

In any case, the foundations of QCD rest upon the algebra which yields the Bjorken sum rule.

Experimentally, infinite momentum transfer in an interaction is of course unattainable. Experiments are performed at a particular Q^2 or even more realistically over a range of Q^2. In order to test the Bjorken sum rule, it is necessary to make measurements at similar Q^2 between the proton and neutron integrals and then compare the results to the Bjorken sum rule including perturbative and nonperturbative QCD corrections. Perturbative QCD corrections to the Bjorken sum have been performed up to third order in the strong coupling constant α_s (see Lecture III, Sec. 7),

$$\int_0^1 g_1^p(x)\; dx - \int_0^1 g_1^n(x)\; dx \;=\; \frac{1}{6}\,\frac{g_A}{g_V}\,\left(1 - \Delta^{QCD}\right)\ . \tag{30}$$

The theoretical prediction for Δ^{QCD} is to be compared to the pure experimental quantities in the Bjorken sum rule equation, namely

$$\Delta^{\exp} = 1 - \frac{6\int_0^1 g_1^p(x)\, dx - 6\int_0^1 g_1^n(x\,)dx}{g_A/g_V}\ .$$

Nonperturbative QCD corrections which vary typically as $1/Q^n$ also may influence Δ^{QCD}, and are discussed in some detail in Lecture III, and by Stan Brodsky.[33]

7 The Ellis-Jaffe Sum Rule

In the early days of the experiments, only polarized proton targets were available, implying that only the proton spin structure function was measurable. Since no polarized neutron targets existed, the Bjorken sum rule (which requires both the proton and neutron spin structure functions) could not be tested. It was, therefore, of great interest to have a prediction for the proton spin structure function integral by itself.

In 1974, Ellis and Jaffe[34] using SU(3) symmetry between the up, down, and strange quarks, derived a unique prediction for both the proton and neutron spin structure function integrals. The relationship became known as the Ellis-Jaffe sum rule, and its derivation is reproduced below.

As noted earlier, the spin structure functions have a simple description in the QPM. The integral over the proton spin structure function can be written in terms of a sum of integrals over the spin-dependent quark distributions, weighted by the charge square of the quark:

$$g_1^p(x)\ dx = \frac{4}{18}\Delta u + \frac{1}{18}\Delta d + \frac{1}{18}\Delta s \tag{31}$$

where $\Delta u = \int_0^1[u^{\uparrow}(x) - u^{\downarrow}(x)]$ and $u^{\uparrow}$ $(u^{\downarrow})$ corresponds to the case where the up quark is parallel (antiparallel) to the nucleon spin. The quantities Δu, Δd, and Δs can be interpreted as a measure of the polarization of the quarks in a polarized proton.

The integral over the neutron spin structure function yields the same relation except that the up and down quark distributions are interchanged by isospin symmetry,

$$g_1^n(x)\ dx\ =\ \frac{4}{18}\ \Delta d + \frac{1}{18}\ \Delta u + \frac{1}{18}\ \Delta s\ . \tag{32}$$

Substituting Eqs. (31) and (32) into the Bjorken sum rule (Eq. 29) yields,

$$\Delta u - \Delta d\ =\ \frac{g_A}{g_V}\ . \tag{33}$$

Notice that the strange sea contribution cancels out.

A relation from SU(3) symmetry is used to extract information on the individual proton and neutron integral. In SU(3), rotations are performed on the baryon octet presented in Fig. 15 to extract relations to coupling constants. For example, SU(3) symmetry postulates that the quark distribution in the proton is just a V-spin rotation of that in a cascade,

$$(uds)^{\rm proton} = (sdu)^{\rm cascade}$$

Applying a V-spin rotation one transforms Eq. (33) with the following substitution,

$$\Delta u - \Delta d \ \rightarrow \ \Delta d - \Delta s \ .$$

The matrix elements of the neutron and cascade decay are given below in terms of the symmetric and antisymmetric tensor constants F and D,

$$\left(\frac{g_A}{g_V}\right)^{\rm proton} = {\rm F} + {\rm D}\ , \qquad\qquad \left(\frac{g_A}{g_V}\right)^{\rm cascade} = {\rm F} - {\rm D}\ .$$

Applying the V-spin rotation yields the equation,

$$\Delta d - \Delta s = {\rm F} - {\rm D}\ . \tag{34}$$

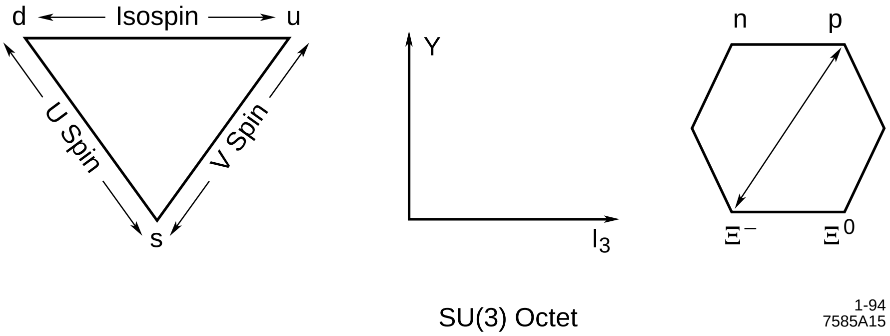

Fig. 15. Schematic of SU(3) baryon octet.

With the strange sea left unconstrained, one can use Eqs. (33) and (34) and substitute into Eqs. (31) and (32) to yield an independent relation for the proton and neutron integrals.

$$\text{Proton} \qquad \int_0^1 g_1^p(x)\,dx \;=\; \frac{1}{18}\,(9\mathrm{F}-\mathrm{D}) + \frac{1}{3}\,\Delta s \;\approx\; 0.17\;, \qquad (35)$$

$$\text{Neutron} \qquad \int_0^1 g_1^n(x)\,dx \;=\; \frac{1}{18}\,(6\mathrm{F}-4\mathrm{D}) + \frac{1}{3}\,\Delta s \;\approx\; -0.02\;. \qquad (36)$$

The numerical values for the integrals use updated values of the F and D constants,[35] F = 0.47 ± 0.04 and D = 0.81 ± 0.03, and assume that the strange sea is unpolarized ($\Delta s = 0$). That Δs should be small is regarded as reasonable, since the strange sea provides only a small fraction of the total quark contribution to the nucleon.

The first data on the neutron spin structure function has come into existence only in this past year. As a result, only the Ellis-Jaffe sum rule for the proton has played a role in evaluating results prior to 1993. Lecture II reviews experimental results up to the end of 1993, and Lecture III discusses the implications of these results and future programs that will study QCD and nucleon spin structure in more detail.

References

1. V.W. Hughes et al., Phys. Rev. **5A** (1972) 195.
2. For a complete introduction to polarized electrons and a discussion of why Stern-Gerlach techniques cannot be applied to electrons, see J. Kessler, *Polarized Electrons*, Chap. 1 (Springer-Verlag, New York, 1985).
3. M.J. Alguard, V.W. Hughes, M.S. Lubell, and P.F. Wainwright, Phys.Rev. Lett. **39** (1977) 334.
4. F. Gilman, Proc. SLAC Summer Institute on Particle Physics, Vol. 1 (Stanford Linear Accelerator Center, Stanford, 1973) p. 71.
5. J.D. Bjorken, Phys. Rev. **179** (1969) 1547.
6. C.G. Callan and D.G. Gross, Phys. Rev. Lett. **21** (1968) 311; **22** (1969) 156.
7. P. Amaudruz et al., Phys. Lett. **B295** (1992) 159.
8. S. Dasu et al., Phys. Rev. Lett. **61** (1988) 1061.
9. J. Kuti and V.W. Hughes, Ann Rev. Nucl. Part. Sci. **33** (1983) 611.

10. L.Galfi, J. Kuti, and A.Patkos, Phys. Lett. **31B** (1970) 465.

11. A.J.G. Hey and J.E. Mandula, Phys. Rev. **D5** (1972) 2610. For a review of the formalism, see R. Oppenheim, Ph.D. thesis, Yale University, 1982.

12. C.E. Carlson and W. Tung, Phys. Rev. **D5** (1972) 721.

13. T.V. Kukhto and N.M. Shumeiko, Nucl. Phys. **B219** (1983) 412.

14. L.W. Mo and Y.S. Tsai, Rev. Mod. Phys. **41** (1969) 205.

15. J. Ashman et al., Nucl. Phys. **B328** (1989) 1.

16. M.G. Doncel and E. de Rafael, Nuovo Cimento **4A** (1971) 363.

17. H. Burkhardt and W.N. Cottingham, Ann. Phys. **56** (1970) 453.

18. J.J. Kokkedee, *The Quark Model* (W.A. Benjamin, New York, 1969).

19. H.D.I. Abarbanel, M.L. Goldberger, and S.B. Treiman, Phys. Rev. Lett. **22** (1969) 500.

20. P.D.B. Collins, *An Introduction to Regge Theory and High Energy Physics,* (Cambridge University Press, 1977).

21. B. Badelek et al., Rev. Mod. Phys. **64** (1992) 927.

22. J. Ellis and M. Karliner, Phys. Lett. **B213** (1988) 73.

23. R.L. Heimann, Nucl. Phys. **B64** (1973) 429.

24. G.R. Farrar and D.R. Jackson, Phys. Rev. Lett. **35** (1975) 1416.

25. R. Carlitz, Phys. Lett. **B58** (1975) 345.

26. D. Allasia et al., Phys. Lett. **B249** (1990) 366.

27. R. Carlitz and J. Kaur, Phys. Rev. Lett. **38** (1977) 673.

28. A. Schaefer, Phys. Lett. **B208** (1988) 175.

29. J.D. Bjorken, Phys. Rev. **148** (1966) 1467; **D1** (1970) 1376.

30. R. Feynman, *Photon Hadron Interactions,* (Benjamin, Reading, Massachusets, 1972) p. 159.

31. J. Schwinger, Phys. Rev. Lett. **3** (1959) 296.

32. For a review of Operator Product Techniques applied in QCD see: A. Manohar, lectures presented at the Lake Louise Winter Institute,

UCSD/PTH 92–10 (February 1992); M.E Peskin and D.V. Schroeder, *An Introduction to Quantum Field Theory,* (Addison-Wesley, Menlo Park, 1993).

33. S. Brodsky, these proceedings.

34. J. Ellis and R. Jaffe, Phys. Rev. **D9** (1974) 1444.

35. R.L. Jaffe and A. Manohar, Nucl. Phys. **B337** (1990) 509.

Lecture II: The Experiments

Despite a twenty-five year history, only five polarized beam polarized target deep inelastic scattering experiments have been performed, three at SLAC and two at CERN. This lecture describes each of the five experiments. The impact of the results from these experiments has been large, each motivating extensive theoretical activity. This activity (discussed in Lecture III) has in turn continued to provide fuel for more experiments with higher precision at higher energies.

This lecture covers the five experiments and their results, one-by-one in chronological order. Lecture III will discuss the implications of the experimental results and future experimental programs.

1 SLAC Experiment E-80

The first experiment to scatter a polarized electron beam off a polarized target was performed at SLAC in End Station A.[1,2] Although deep inelastic scattering experiments with polarized targets had been performed previously,[3] SLAC experiment E-80 was the first to run with a polarized electron beam. The primary electron energies in the experiment ranged from 6 to 13 GeV and scattered off a polarized alcohol (butanol) target. Scattered electrons were detected using the 8 GeV spectrometer built for the full range of deep inelastic scattering experiments.[4] The outstanding features of experiment E-80 were the relatively high average beam (50%) and target (60% peak value) polarizations.

The E-80 polarized electron source relied on the photoionization of alkali atoms by a pulsed ultraviolet light source. The electrons stripped from these polarized atoms remained polarized, since the excitation takes place through an electric dipole transition. The method for polarizing electrons follows a number of technical steps (see Fig. 16):

(1) polarization of the ^{6}Li atoms via passage through a six-pole magnet,

(2) ^{6}Li ionization using a high-intensity ultraviolet lamp producing transversely polarized electrons,

(3) acceleration of the electrons in an electric field concurrent with the ionization, and

(4) rotation of the electron spin to the longitudinal direction using a polarizing coil.

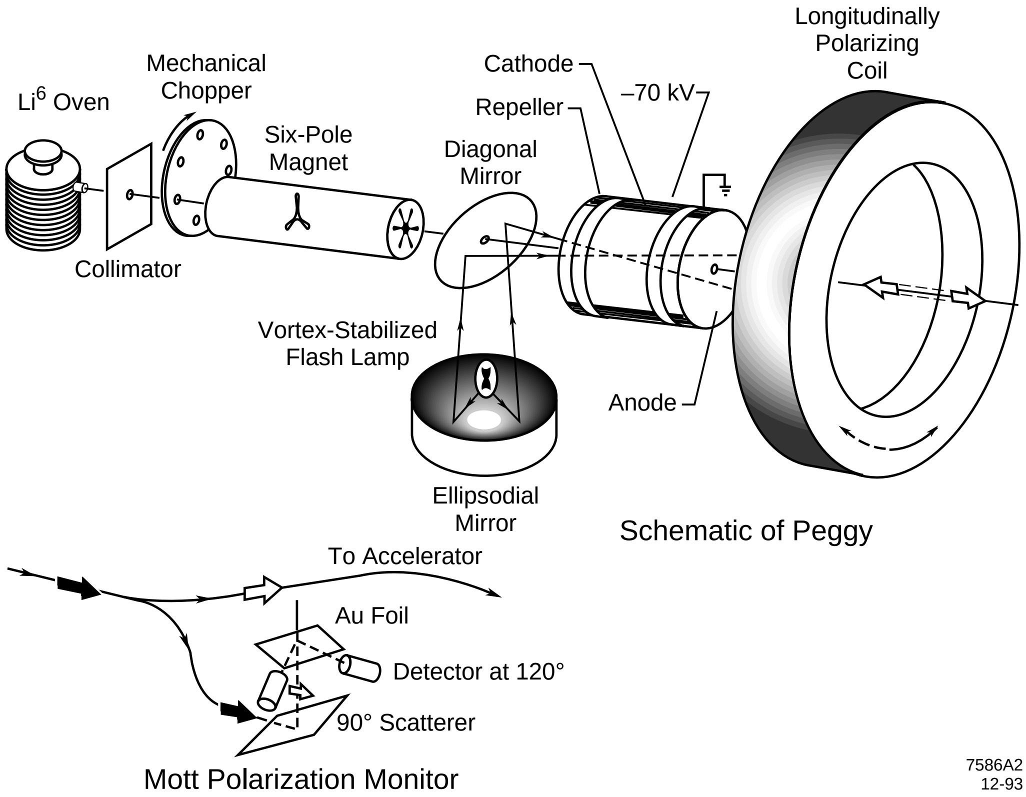

Fig. 16. Stanford Linear Accelerator Center E-80 polarized electron source and Mott polarimeter.

The development of the source was a large technical effort and a great success for the first production of a longitudinally polarized beam of electrons. The E-80 polarized source was limited in beam current, since the number of electrons depends on the number of polarized atoms ($\sim 10^8$ electrons per pulse). The low current was, however, not an issue for the experiment, since the polarized target was sensitive to radiation damage and could not handle higher currents. In fact, the beam was scanned across the target ("rastered") on a pulse-to-pulse basis so as to reduce the hot-spot radiation damage.

Determination of the electron beam polarization was an experiment in itself. Experiment E-80 used both Möller and Mott polarimetry to measure the electron beam polarization. Mott polarimetry was used to monitor the electron beam polarization at the front end of the SLAC accelerator. This type of polarimeter involved scattering transversely polarized electrons off a gold nucleus, and studying an asymmetry in the spatial distribution of the backscattered electrons.[5] This asymmetry comes about from the spin orbit interaction between the electron and the gold nucleus. The size of the asymmetry is a function of energy and scattering angle, called the Sherman function, and is known to approximately 2%. The E-80 Mott polarimeter (see Fig. 16) monitored the polarization of the electrons as they were emitted from the polarized source, but did not determine the electron polarization at high energy near the interaction in End Station A. Depolarization of the beam in the transport from the source to the polarized target was expected to be small, but was not excluded.

As a consequence, a special Möller scattering experiment was performed at the conclusion of the E-80 experiment.

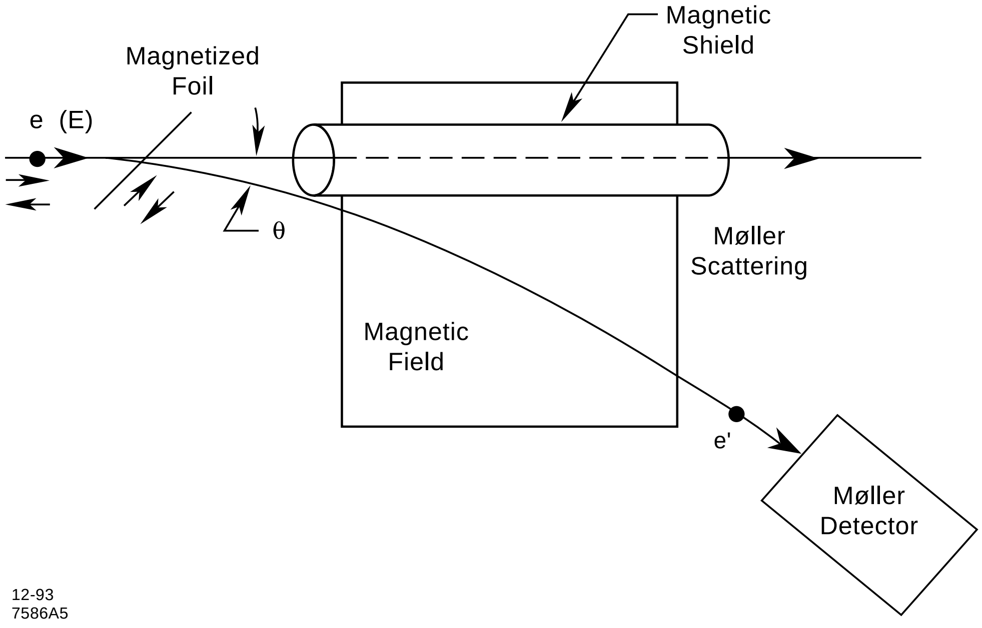

Fig. 17. Schematic of a Möller polarimeter setup.

Möller polarimetry determines the polarization of the electron beam by measuring the cross section asymmetry in the scattering of polarized electrons by polarized electrons. Polarized electrons are scattered off a polarized ferromagnetic foil, and the elastic scattered electrons are produced at a particular scattering angle that maximizes the asymmetry (90° scattering in the center-of-mass). The Möller electrons after the interaction pass through a magnetic field and are detected by a detector package. The primary unscattered electron beam is shielded from the magnetic field used for analyzing the Möller scattered electrons (see Fig. 17). A difference in cross sections for the scattering of beam electrons with spins parallel or antiparallel to the target foil electron spin results in a scattering asymmetry:

$$A = \frac{\sigma^{\uparrow\uparrow} - \sigma^{\uparrow\downarrow}}{\sigma^{\uparrow\uparrow} + \sigma^{\uparrow\downarrow}} = \frac{y(2+3y+2y^2)}{(1+y+y^2)^2} \ . \tag{1}$$

Here y varies with the center of mass scattering angle and is given in the laboratory frame by $y = E\theta^2/2M_e$. The measured raw asymmetry is related to this pure QED asymmetry A (calculated from Feynman diagrams in electron electron scattering) via

$$A^{\rm meas} \;=\; A \cdot P_{\rm beam} \cdot P_{\rm foil}\ . \tag{2}$$

Here $P_{\rm beam}$ and $P_{\rm foil}$ are the beam and target foil polarizations, respectively. Only two of the twenty-six electrons in iron are polarized, yielding a dilution of the target foil polarization $P_{\rm foil}$. The foil polarization is determined by measurements of the magnetization of the foil and its thickness.[6] From the measured asymmetry below the elastic peak (see Fig. 18), the beam polarization is determined directly. For experiment E-80, the polarized target consisted of an iron-cobalt compound called supermendur.[6] The target was set up in End Station A at the same position as the true polarized target, and the 8 GeV spectrometer (see Fig. 18) was used to detect the scattered electrons and to scan the elastic peak.

The E-80 butanol ($C_6O_4H_8$) target[7] was polarized using the principle of dynamic nuclear polarization.[8] A high magnetic field and low temperature is used to achieve high polarization and to calibrate the absolute polarization P_t of the target via $P_t = \tanh[\mu H/kT]$. Application of 140 GHz microwaves polarizes the target. A summary of the target parameters is given[2] in Table 1. A review of dynamic nuclear polarization using solid frozen targets is given by Gordon Cates.[9]

Although the target material is not pure hydrogen, only the hydrogen atoms contribute to the polarized scattering; carbon and oxygen are spin-0 nuclei. The dilution factor [used in Lecture I, Eq. (20)] is merely the number of scattered electrons originating from polarized hydrogen compared to the total number of scattered electrons coming from the entire target. For butanol, this fraction is approximately $f \approx 10/74 \approx 0.11$. Figure 19 presents a schematic view of the E-80 polarized target with the microwave guide for polarizing, cryostat for temperature

Fig. 18. The 8 GeV spectrometer and an example of a Möller elastic peak.

Table 1: E–80 Polarized Proton Target

Characteristic	Value
Magnetic Field	50 kG
Temperature	1.05° K
Target material	butanol–porphyrexide beads
Initial polarization of free protons	0.5 to 0.65
Depolarizing dose (1/e)	$\sim 3 \times 10^{14}$ e$^-$/cm^2
Polarizing time (1/e)	∼ 4 minutes
Annealing time	∼ 45 minutes

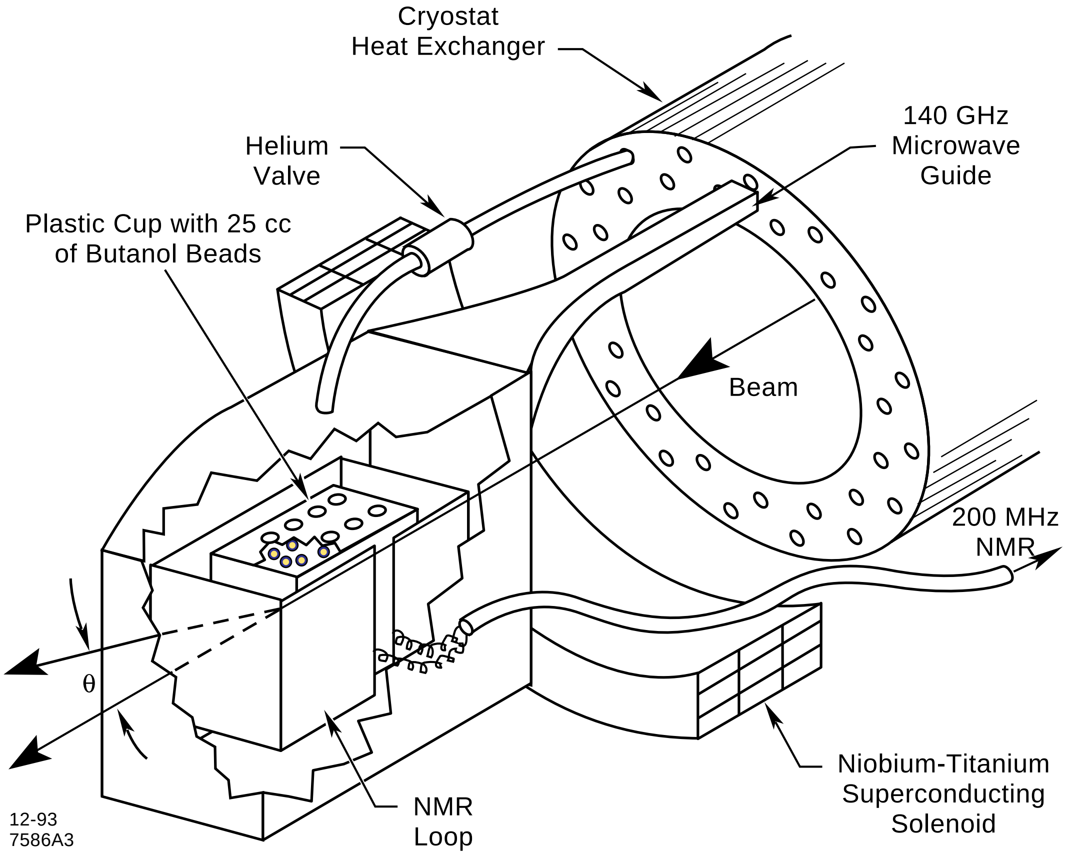

Fig. 19. Stanford Linear Accelerator Center E–80 polarized butanol target.

control and assembly container for the 25 cc of butanol target beads. Measurement of polarization was accomplished using standard NMR techniques. The dominant systematic error in the polarization measurement of the target came from the measurement of the small calibration signal from thermal polarization.

Scattered electrons from the polarized target were detected in the 8 GeV spectrometer. This spectrometer accepted electrons with energies up to 8 GeV, and was situated on rails which allowed for measurements over a range of scattering angles θ. Figure 20 presents a floor plan and side view of the spectrometer set up for experiment E-80. The spectrometer magnets were selected in an orientation that allowed for focussing of the scattered electrons in two dimension, which gave

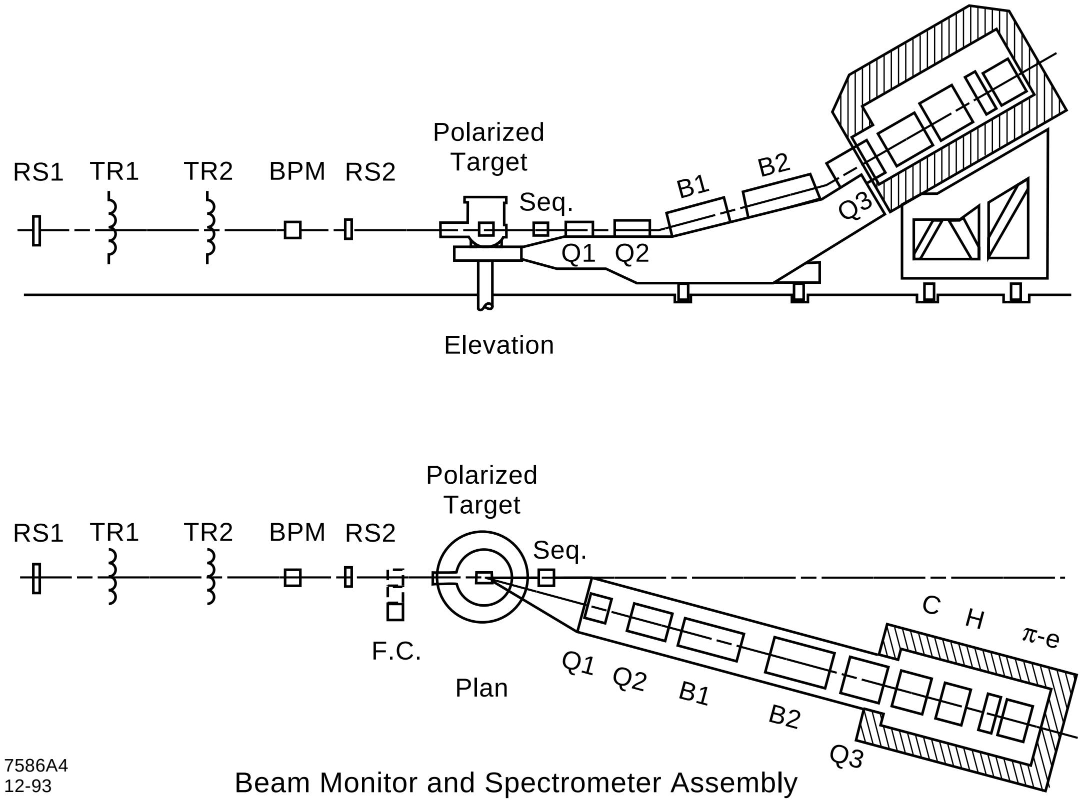

Fig. 20. Stanford Linear Accelerator Center E–80 experimental setup.

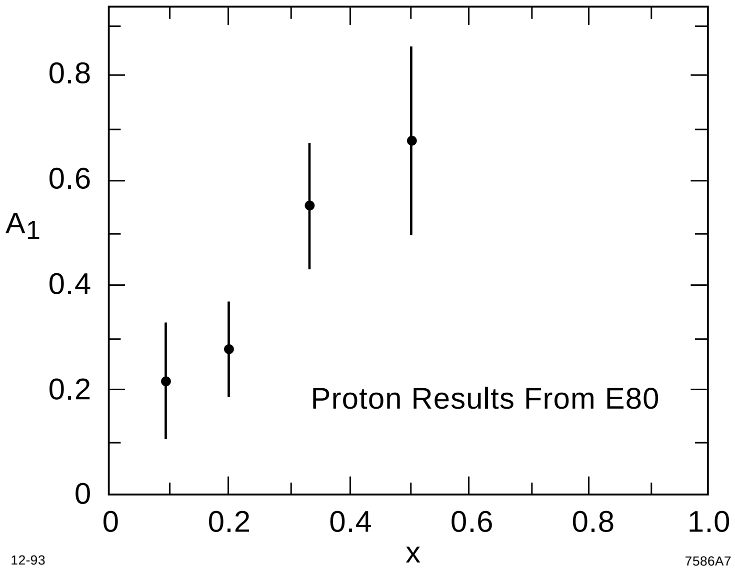

Fig. 21. Results of A_1^p versus x from experiment E–80.

a direct measurement of the electron scattering angle and momentum. The detector package used in this experiment consisted of a Čerenkov counter for electron identification, tracking hodoscopes for electron momentum measurements and a lead-glass shower counter for pion rejection. Data for experiment E-80 was collected at scattering angles ranging from 7° to 11°.

In total, the experiment collected about two million scattered electron events. As predicted by Bjorken, the experiment found large asymmetries A_1^p for the proton (see Figure 21). This result was regarded as a success for the Quark Parton Model and gave asymmetries with values close to the SU(6) prediction of 5/9 (see Lecture I, Sec. 4.1). The average Q^2 was low ($Q^2 \sim 2$ GeV^2), which helped motivate the follow up experiment to measure the proton spin structure function at higher x and higher Q^2. The desire to measure structure functions at high Q^2, closer to scaling where theoretical corrections become small, is a continuing goal in the field.

2 SLAC Experiment E-130

The desire to re-measure the proton spin structure function at higher energy to observe the Q^2 dependence of the asymmetries and to characterize their high-x behavior motivated a second SLAC experiment (E-130).[10,11] The experiment had the same basic philosophy as E-80, but with some substantial modifications. For this experiment, the beam energy was set to an energy of 22.66 GeV, while the spectrometer was set up at a fixed scattering angle of 10° and had a fifteen times larger effective acceptance. The target was improved and ran with a higher average polarization of 60%, and the beam polarization was increased to $\sim 80\%$ by focusing the ultraviolet light at the source more effectively. Finally, the experiment built a special Möller polarimeter (*in situe*) in End Station A, which allowed for beam polarization measurements to be done continuously during the experiment. Figure 22 presents a layout of the E-130 experiment in End Station A, as seen in a top view. The front half of the beam line is devoted to the Möller polarimeter. A polarized target foil was placed far upstream, followed by a strong bend magnet (18D72), and an array of proportional tube detectors. The 8 and 20 GeV spectrometers shown were not used in the experiment. Downstream of the Möller polarimeter was the polarized butanol target and the single arm E-130 spectrometer. Čerenkov and lead-glass counters were used to identify the scattered electrons and measure their energy. Wire chambers were used for tracking and pion rejection in coincidence with the lead-glass counters.

The experiment concentrated on the measurement of the proton spin structure function at high x where the scattering cross section is low. As a result, the experiment only collected about one million events. The kinematic coverage extended from $0.2 < x < 0.65$ and 2 $\mathrm{GeV}^2 < Q^2 < 6$ GeV^2. Figure 23 presents the results

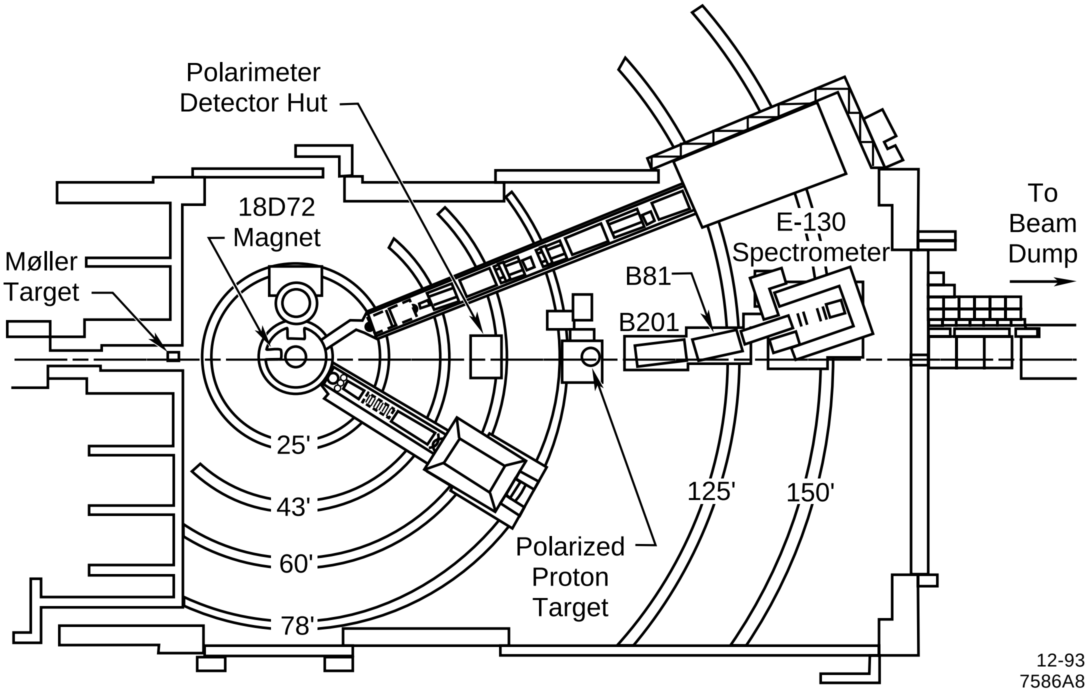

Fig. 22. The SLAC E-130 experimental setup.

for the proton asymmetry measurements A_1^p for E-130 and E-80 together. Notice that the average result is in good agreement with the SU(6) prediction of 5/9.

The E-130 results agree well with those of E-80. No discrepancies appear within error bars, despite the substantial difference in Q^2 of the two experiments The observation of a rise in the asymmetries as x gets large appears to be confirmed. As x approaches one, the prediction that A_1^p approaches one looks reasonable (as discussed in Lecture I, Sec. 4.3). Figure 24 presents a comparison of the E-80 and E-130 results to various theoretical model predictions. A discrepancy between the data and some models is evident. The Carlitz-Kaur Model (Lecture I, Sec. 4.4) gives a good fit to the experimental data.

The confirmation of large asymmetries as predicted by the Quark Parton Model (QPM) appeared to indicate that the discovery potential for new physics

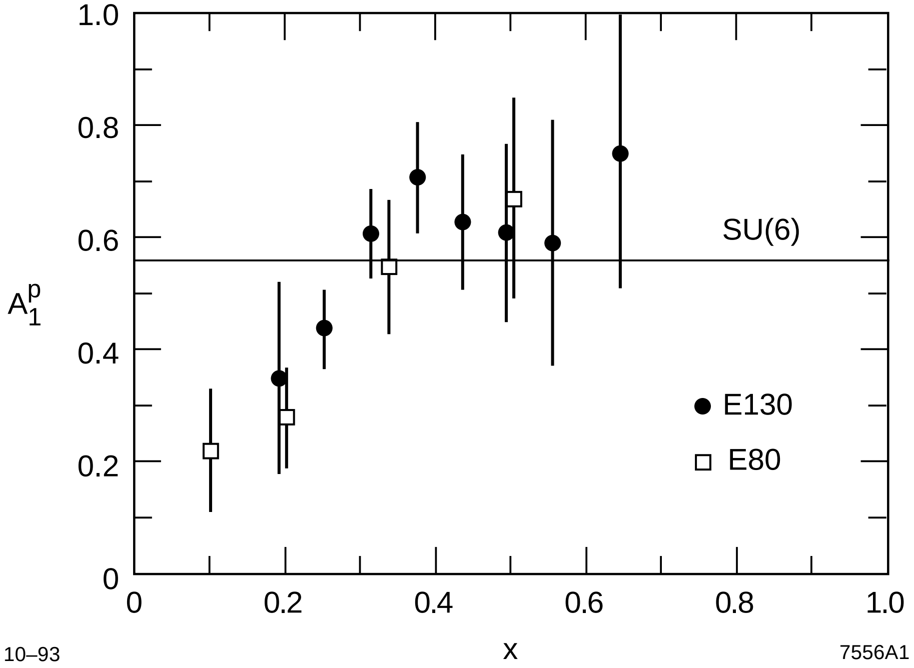

Fig. 23. Results of A_1^p versus x for experiments E–130 and E–80.

was low. The continuation of the spin structure function measurements at SLAC ended as the SLC collider project began. The field of spin structure function measurements then moved to CERN, and the surprises began.

Although not apparent from Figs. 23 and 24, the measurement of the proton asymmetries at low x (below 0.1) is very important, since the spin structure function g_1 varies as A_1/x, and its contribution to the proton integral $g_1^p(x)\,dx$ could be large. In fact, from the combined E-80 and E-130 results, a proton integral of $g_1^p(x)\,dx = 0.17 \pm 0.05$ is obtained. The result is in agreement with the Ellis-Jaffe sum rule prediction, but the large error bar is due to the extrapolation of the integral over the unmeasured x range from 0 to 0.1. A measurement of the low-x asymmetries in order to test the Ellis Jaffe sum rule with higher precision became a motivating goal, and CERN with its high-energy muon beam became the new center for this physics.

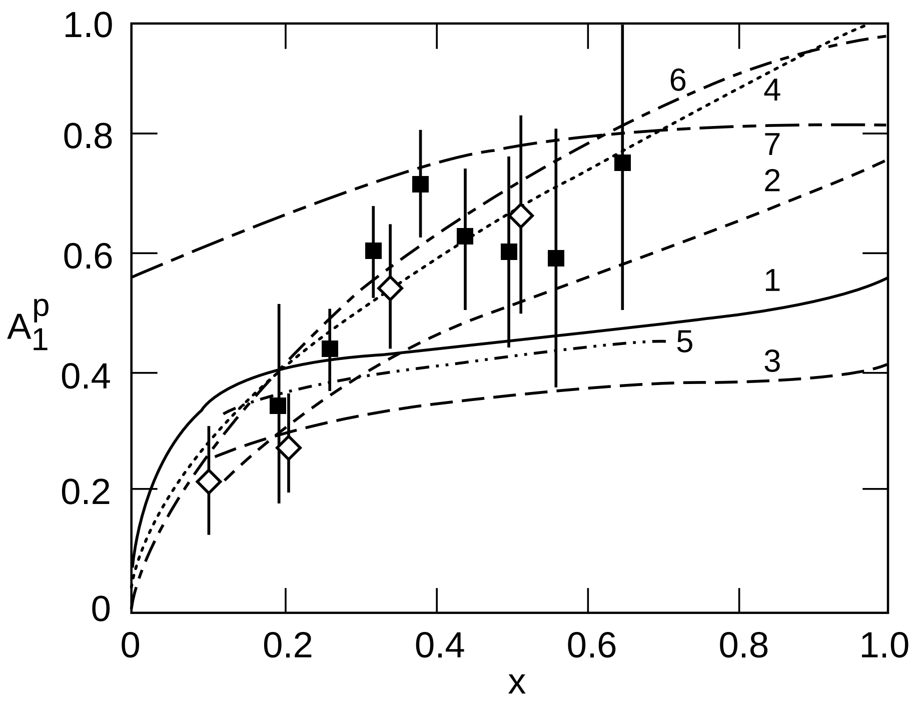

1. Symmetrical Valence Quark Model (Kuti, Weisskopf 1971).
2. Current Quarks (Close, 1974.
3. Orbitial Angular Momentom, (Look, Fischbach, Sehgal, 1977).
4. Unsymmetrical Model (Carlitz, Kaur, 1977).
5. MIT Bag Model (Jaffe, Huges, 1977).
6. Source Theory (Schwinger, 1977).
7. Quark-Geometrodynamics (Preparata, 1981).

12-93
7586A10

Fig. 24. Results of A_1^p versus x for experiments E–130 and E-80 compared to various theoretical models.

3 The CERN EMC experiment

In 1988, the European Muon Collaboration (EMC) at CERN reported on an exciting result for the low-x measurement of the proton spin structure function.[12–14] This experiment changed the field of spin physics by bringing it to the forefront of the high-energy physics community.

The EMC experiment scattered 100 to 200 GeV polarized muons off a large polarized ammonia target (NH_3) and detected the scattered muons in a well tested muon tracking spectrometer. The high beam energy allowed for high-Q^2 and low-x measurements of the proton spin structure function. However, since the muon beam is produced as a secondary beam from a primary proton beam, the luminosity of the experiment was low. The beam current for the muons was typically, 3×10^7/sec. Even with the large acceptance EMC spectrometer, the overall statistics was on the order of one million events collected for the experiment over two years of running.

The polarization of the muons comes naturally from pion and kaon decay. Since the pion is spin-0, and the decay proceeds through a parity-violating weak interaction, the muons come out naturally polarized (see Fig. 25) depending on their energy.[15] For π^+ decay, the muons are emitted left-handed as viewed in the pion rest frame; whereas in the laboratory frame, the muon polarization is a function of energy and has a full range of values. Figure 26 presents the energy dependence of the muon polarization as a function of the ratio of the muon-to-pion energy. For the EMC experiment, the beam was selected such that the average polarization of the muon beam was on the order of 80%.

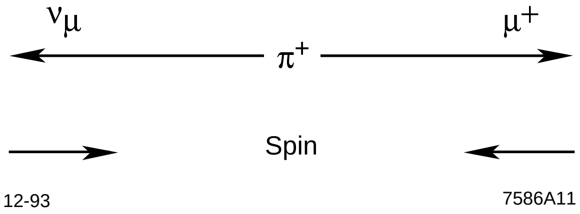

Fig. 25. Pion decay—production of polarized muons.

The EMC polarized ammonia (NH_3) target also relied on the principle of dynamic nuclear polarization. What was unique about the EMC target was its large size. It had a length of two meters in order to maximize statistics, and a large width in order to contain the fairly large transverse muon beam spot. The target ran at a

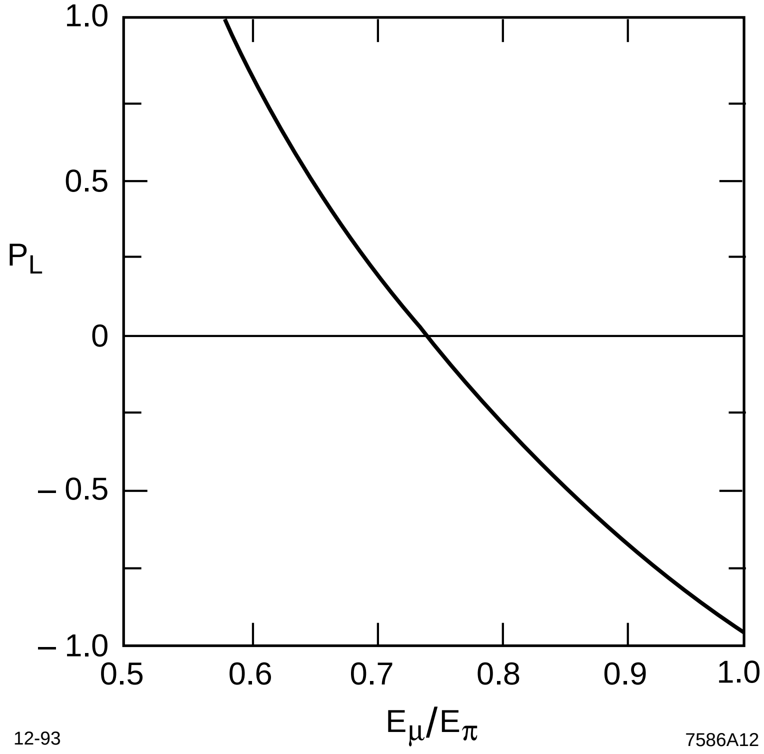

Fig. 26. Polarization versus energy fraction of outgoing muon.

temperature of 0.5° K and a magnetic field of 2.5 Tesla. Figure 27 presents a layout of the target and shows the two target halves, polarized in opposite directions so that the asymmetry measurements could be performed without normalizing to the beam flux. Nuclear Magnetic Resonance (NMR) coils were placed along the length of the EMC target in order to determine the polarization of the target as a function of its length.

The EMC spectrometer[16] was a large muon tracking device developed for the full range of structure function measurements. Figure 28 presents the spectrometer setup and its relation to the position of the polarized ammonia target. Chambers for tracking up and down stream of the target determined the vertex of the muon event. Downstream chambers tracked muons passing through an analyzing bend

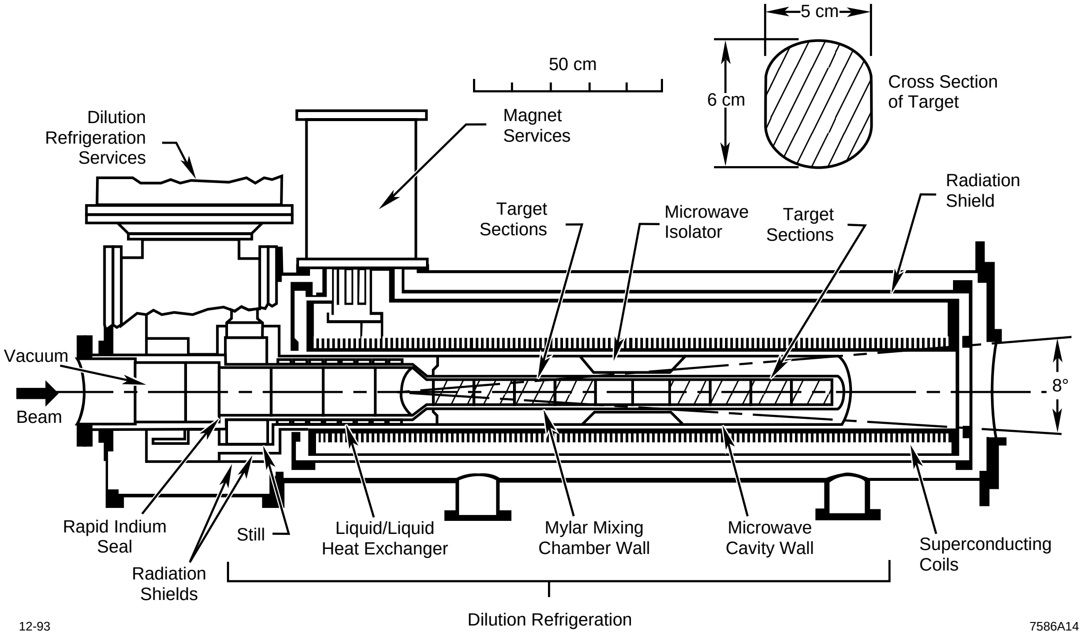

Fig. 27. European Muon Collaboration polarized ammonia target.

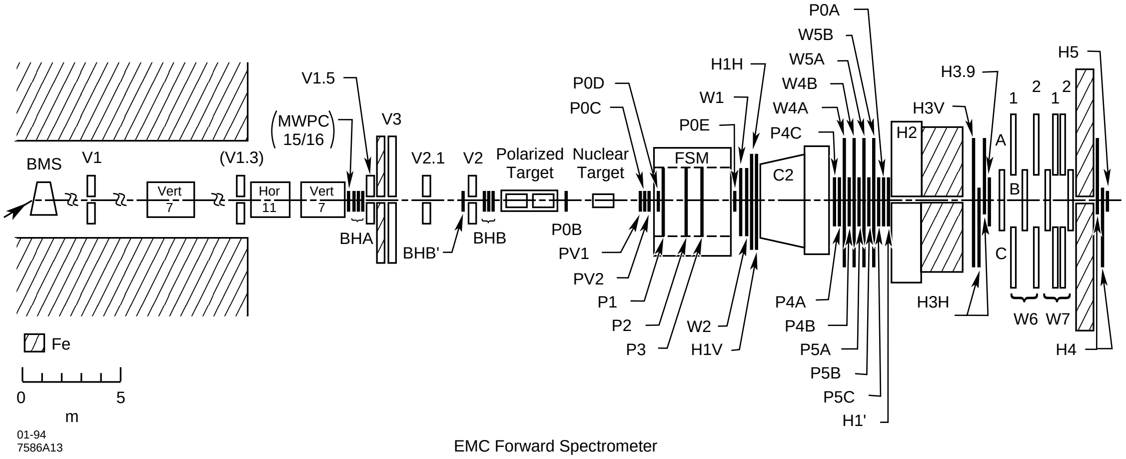

Fig. 28. European Muon Collaboration spectrometer setup.

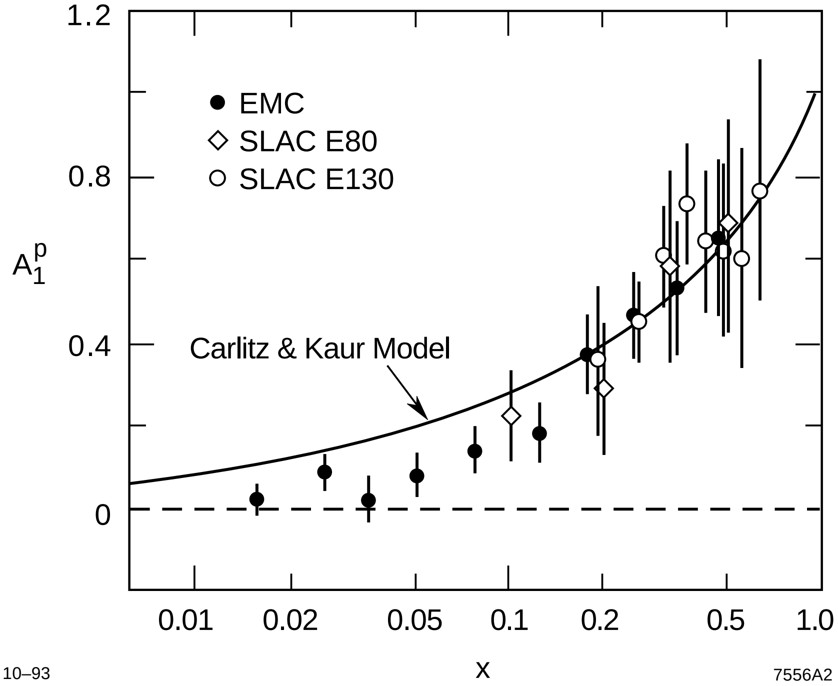

Fig. 29. Results of A_1^p versus x from the EMC experiment compared to earlier SLAC experiments and to the Carlitz-Kaur Model prediction.

magnet for momentum and production angle determination. The vertex distribution of the scattered muon events was relevant for selecting events from the appropriate polarized target half. Reversal of the target spins was performed eleven times in the experiment. Changes in the spectrometer acceptance from one spin reversal to another could produce false asymmetries. This effect was the limiting systematic uncertainty in the experiment.

Results of the proton spin structure function measurements from this experiment came as a major surprise. Figure 29 presents the EMC proton asymmetry results compared to early SLAC results from E-80 and E-130, and compared to the Carlitz-Kaur model discussed in Lecture I. The agreement with the SLAC experiments over the commen x range was fine. However, the low-x asymmetries all

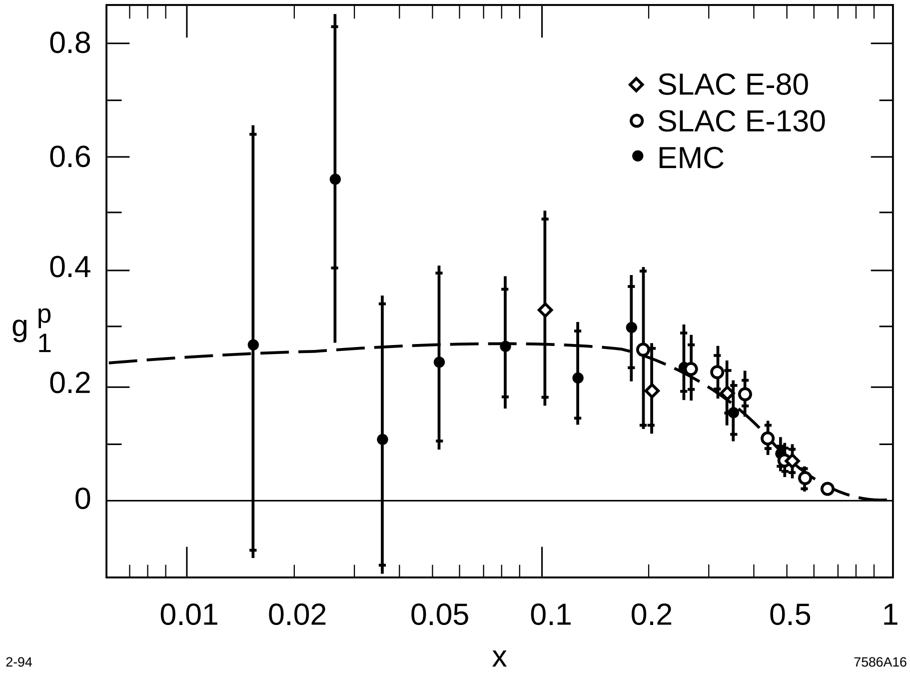

Fig. 30. Results of the proton spin structure function g_1^p versus x for the EMC experiment.

come in low compared to the Carlitz-Kaur model, which conserves the prediction of the Ellis-Jaffe sum rule. The low value for the asymmetries at low x translates into low values for the proton spin structure function g_1^p and a low value for the integral over the proton spin structure function $g_1^p(x)\,dx$. Figure 30 presents g_1^p versus x for the EMC data, and Figure 31 presents $g_1^p(x)\,dx$ integrating over the limits from x_m to one. The value of the proton integral from x of 0.01 to x of 1 is compared to the Ellis-Jaffe sum rule prediction. Assuming only a small contribution to the proton integral below x of 0.01, the disagreement between the sum rule and the measurement is at the 3.5 standard deviation level. The values of the F and D constants were quite different from today's values,[17] and the errors on the old values were underestimated.[18] Today the F and D values and their error analysis have brought the disagreement to 2.5 standard deviations.

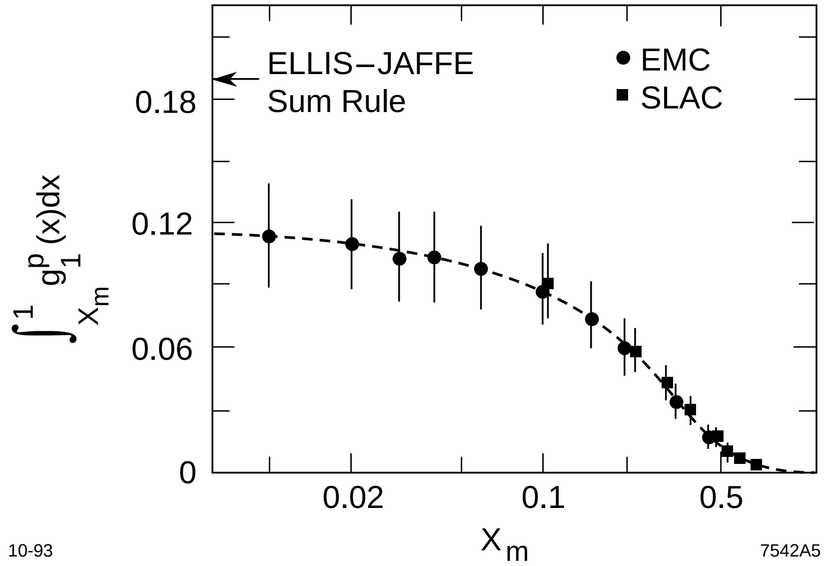

Fig. 31. Results of $\int_x^1 g_1^p(x)\,dx$ versus x for EMC compared to the Ellis-Jaffe sum rule prediction at the time.

Even more surprising, the EMC results implied the quark contribution to the proton spin is small; see Lecture III. Quarks did not carry the spin of the proton. This caused a tremendous upheaval in the field, generating hundreds of theoretical papers. A strong desire to measure the neutron spin structure function emerged, both to check the implications of the proton measurement and to test a foundational QCD equation, the Bjorken sum rule. Such a test required a measurement of the neutron spin structure function.

4 The CERN SMC experiment

Soon after the EMC result broke into the community, a new generation of muon experiments at CERN were proposed by the Spin Muon Collaboration[19] (SMC) (also covered by Bernard Frois[20]). Unlike EMC, which had done a single spin physics experiment after a long tradition of unpolarized nucleon structure function studies, the SMC experiments were focused on measurements dedicated to nucleon spin structure. The goal of these experiments was to measure the proton and neutron spin structure function with precision, using polarized proton and deuteron targets, and to test the Bjorken sum rule.

The SMC experiment (run in 1992 and published in 1993) used the same polarized target as EMC, but replaced the polarizable material of ammonia with butanol. The butanol targets provide a measurement of the spin structure functions in which the only polarized nucleons in the target are the proton and deuteron (as in E-80 and E-130), and the target spin reversal is more rapid. Rapid target-spin reversal is advantageous in order to reduce the dominant systematic uncertainty coming from false asymmetries due to changes in the spectrometer acceptance. With the alcohol targets, spin reversals took 1/2 hour and were implemented every 8 hours.

Although the SMC deuteron run of 1993 was essentially the same experiment with a different nuclear target, one significant improvement was the measurement of the beam polarization. The EMC proton experiment determined the muon beam polarization by studying the muon event distribution and inferring the polarization of the muon beam via a Monte Carlo study of muon production. In SMC, a direct measurement of the muon beam polarization was performed by studying the energy spectrum of positrons from muon decay. An asymmetry in the decay $\mu \to e^+ \nu_e \nu_\mu$, arises from parity violation.[21] Figure 32 presents the experimental setup to detect the final state positron. After traversing the spectrometer magnet, the muons from the primary beam pass through a decay region, where proportional wire chambers are able to track charged particles transverse to the primary beam. Lead-glass shower counters were used to measure the positron energies. The positron energy

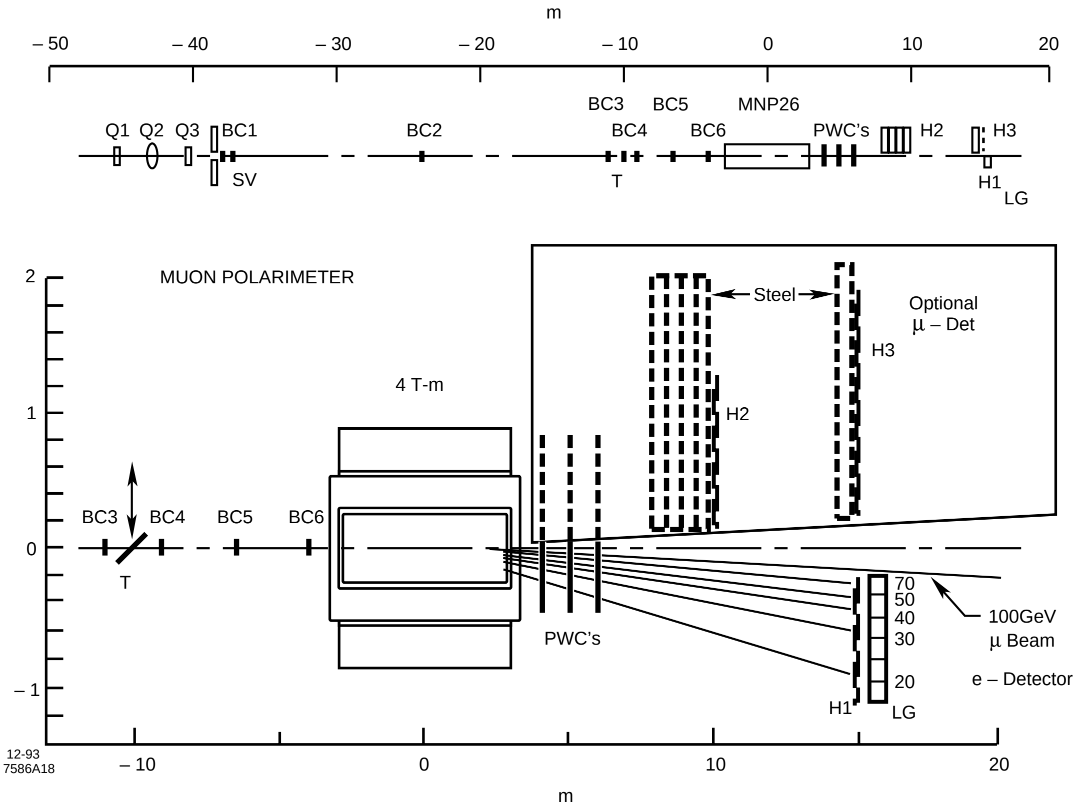

Fig. 32. Setup of Spin Muon Collaboration muon polarimeter which detects the positron decay products.

spectrum is a function of the ratio of the energy of the positron (E_e) to that of the muon (E_μ),

$$\frac{dN}{dy} = N_0 \left[\left(\frac{5}{3} - 3y^2 + \frac{4y^3}{3} \right) - \left(\frac{1}{3} - 3y^2 + \frac{8y^3}{3} \right) \; P_\mu \right] \; . \qquad (3)$$

Here P_μ is the beam polarization and $y = E_e/E_\mu$. The energy distribution for muon decay with polarization of 100%, 0, and −100% is shown in Fig. 33. Measuring the shape of this spectrum determines the average muon beam polarization.

Results from the SMC experiment were published this year. The asymmetries for the deuteron (Fig. 34) gave slightly positive values for $x > 0.1$ and were consistent with zero for $x < 0.1$. Error bars in Fig. 34 are statistical only, and are the dominant uncertainties for the point-to-point asymmetries. The band underneath

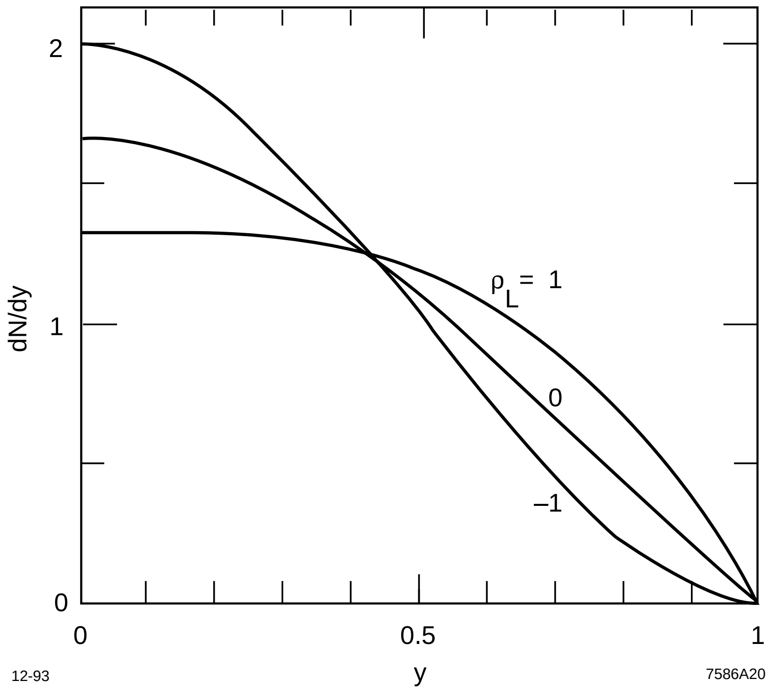

Fig. 33. Positron energy spectrum from polarized muon decay. Shown are the spectra for ±100% and 0% polarized muons.

the data points corresponds to the small contribution from systematic uncertainties. Results of the deuteron structure function xg_1^d versus x are shown in Fig. 35. It is interesting to note that plotted on a logarthmic scale, xg_1 versus log x provides a visual determination of the spin structure function integral. The area under this curve is the integral to be determined. Plotting on the log-x scale also provides a clear view of the low-x behavior of the spin structure function. In Figs. 34 and 35, the deuteron is defined by convention as being one-half (proton + neutron). Figure 36 gives the deuteron integral result (similar to Fig. 31) compared to the Ellis-Jaffe sum rule prediction. A two-standard-deviation difference is evident. Although the error bars are large, the apparent disagreement with the Ellis-Jaffe sum rule established by the EMC experiment appears confirmed by the SMC measurements.

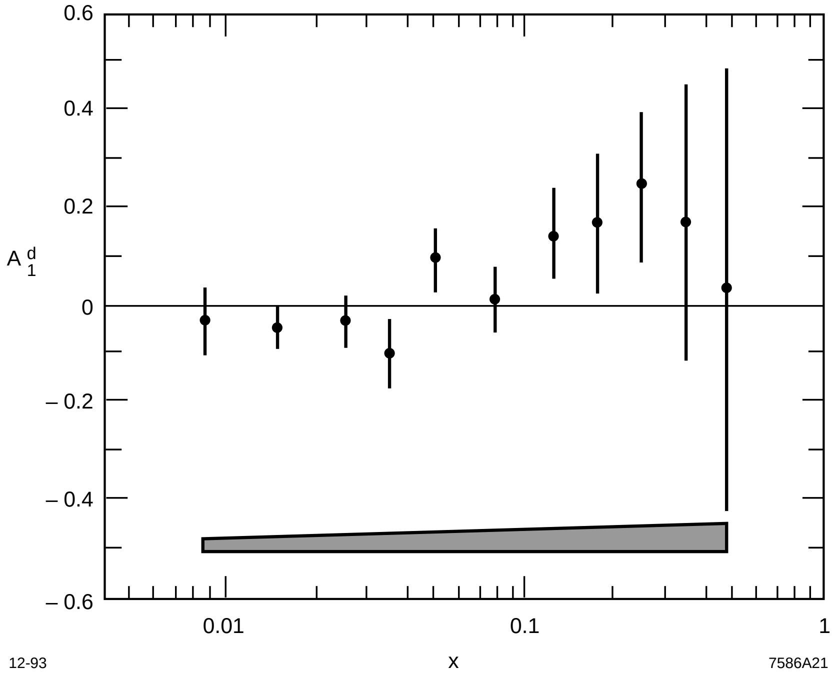

Fig. 34. Results of A_1^d versus x from the Spin Muon Collaboration experiment. The band below the data points represents the contribution of systematic uncertainties.

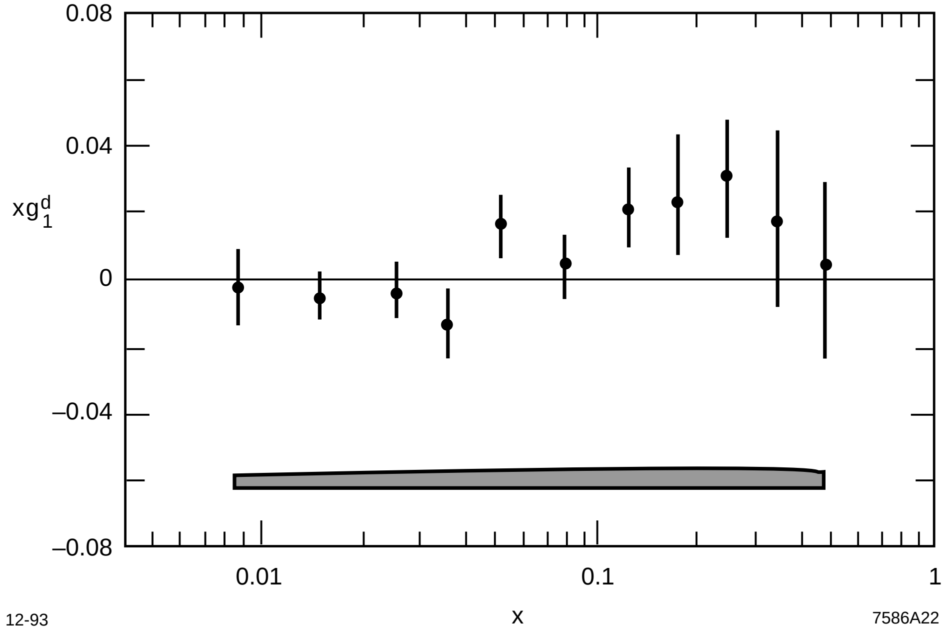

Fig. 35. Results of xg_1^d versus x from the Spin Muon Collaboration experiment. The band below the data points represents the contribution of systematic uncertainties.

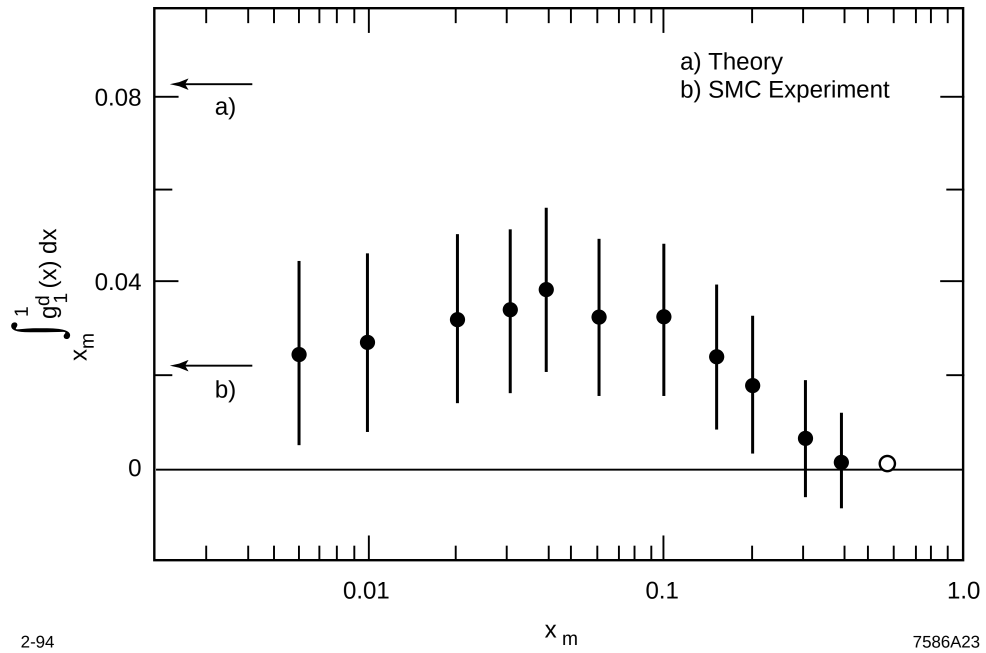

Fig. 36. Results of $\int_x^1 g_1^d(x)\,dx$ versus x for the Spin Muon Collaboration compared to the Ellis-Jaffe sum rule prediction.

5 SLAC Experiment E-142

Concurrent with the SMC experiment, SLAC experiment E-142 ran to measure the neutron spin structure function using a polarized ^{3}He target[22] (also covered by Zein-Eddine Meziani[23]). Scattering from a polarized ^{3}He target is approximately the same as scattering off a polarized neutron plus two unpolarized protons. This behavior results from the Pauli exclusion principle discussed in Lecture III. The E-142 spectrometer was conceptually an extension of the E-130 spectrometer. The spectrometer was set up, this time, with two single arms, one at a scattering angle of 4.5° and the other at 7° (see Fig. 37). The benefit of two arms located at small scattering angles gave a rather wide coverage in x and Q^2, with the smallest angles providing the lowest x data. Small scattering angles also provided high statistics,

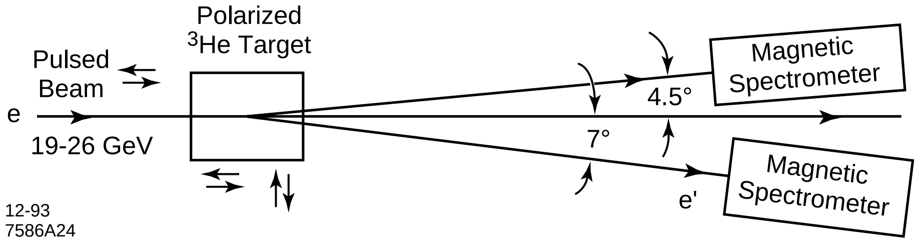

Fig. 37. Schematic of SLAC experiment E–142.

since the cross section is large. Naturally, low-x measurements of the spin structure function was a goal after the large impact of the surprising low-x EMC results.

The E-142 polarized electron source relied on developments of solid state GaAs cathodes. This technology and the recent exciting advances that have led to high polarizations are discussed in detail by Richard Prepost.[24] In experiment E-142, a 1 μsec pulse with polarizations on the order of $\sim 40\%$ was achieved. The beam ran at 120 Hz and produced a high current of typically 3×10^{11} electrons per pulse. Data was collected at beam energies of 19.4, 22.66 , and 25.5 GeV. Reversal of beam spin direction was implemented randomly on a pulse-to-pulse basis, whereas target spin reversal occurred a few times a day. As a result, effectively no uncertainty from false asymmetries was present in this experiment.

The E-142 polarized ^{3}He target is described in detail by Gordon Cates.[9] The ^{3}He nucleus is polarized using optical pumping techniques.[25,26] Circularly polarized near infrared laser light illuminates a target cell of ^{3}He and rubidium vapor. The outer shell electrons in the rubidium become polarized, and the rubidium polarization is transfered to the ^{3}He nucleus via spin exchange collisions between the rubidium and ^{3}He nucleus. The hyperfine interaction for this process is weak, and, as a result, it took hours for the ^{3}He gas to become polarized. However, once achieved, the polarization of the ^{3}He is stable due to the long time constants. Fig-

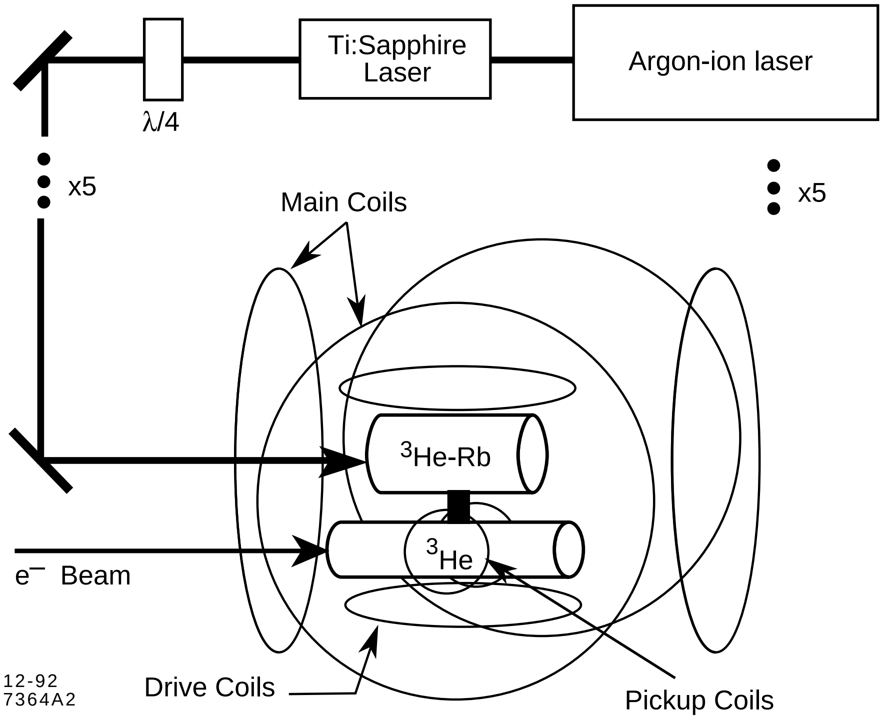

Fig. 38. The SLAC E–142 polarized ^{3}He target.

ure 38 presents a schematic view of the polarized ^{3}He target. Five sets of Argon ion lasers optically pumped five sets of Ti:sapphire lasers yielding approximately 5 W of near infrared laser power per laser set. The circularly polarized laser light was directed onto the top chamber of a double chamber ^{3}He target cell. The top cell contained ^{3}He at ~ 9 atm and rubidium vapor at a few 10^{14} atoms/cm^3. Approximately 50 torr of nitrogen is also present in the target cells to aid in the optical pumping process. The polarization collision process of ^{3}He and rubidium occurs in the top chamber, where the rubidium is trapped by controlled temperature gradients. Polarized ^{3}He then diffuses down into the bottom chamber where the electron beam passes. The entire target chamber was placed in a 30 gauss magnetic field

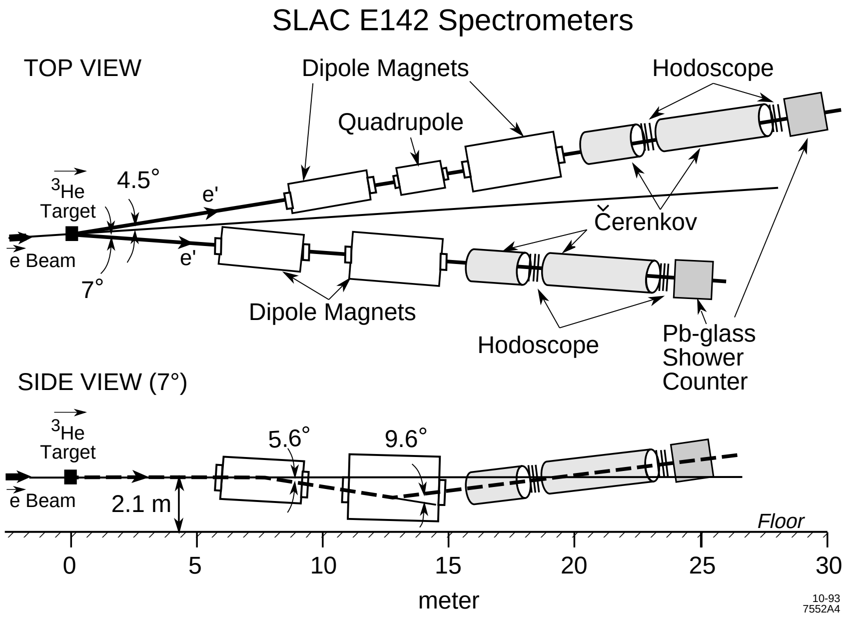

Fig. 39. The SLAC E–142 experimental setup.

which holds the spins of the ^{3}He in a particular orientation. Nuclear Magnetic Resonance techniques were used to determine the ^{3}He polarization.

An overview of the experimental setup is given in Figure 39, which shows a top and side view of the spectrometer magnets (which momentum analyze scattered electrons and sweep out neutral background spray). The Čerenkov counters were used to identify electrons, hodoscopes were used for tracking and momentum determination, and the lead-glass counters located in the rear were used for an additional determination of the electron energy from shower deposition.

Experiment E-142 collected and analyzed approximately 300 million events, more than two orders of magnitude greater than had been achieved in past spin structure function measurements. The results of the asymmetries for the neutron as extracted from the ^{3}He asymmetries is presented in Fig. 40, and for the structure function g_1^n in Fig. 41. One sees small negative asymmetries for the neutron and similarly small negative values for the neutron spin structure function. At face

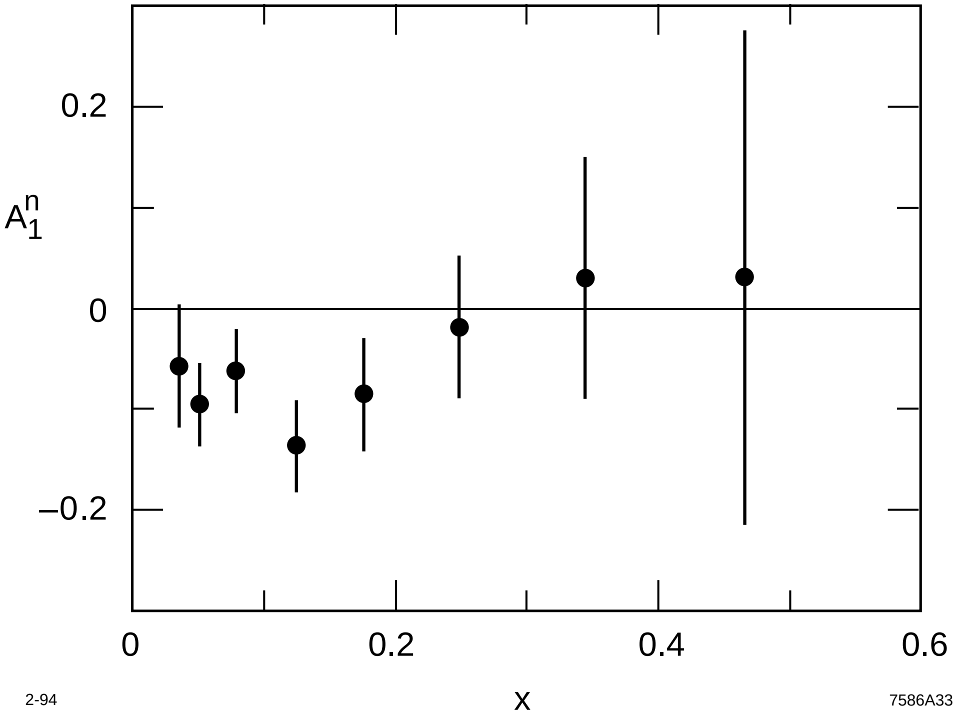

Fig. 40. Results of A_1^n versus x from experiment E–142.

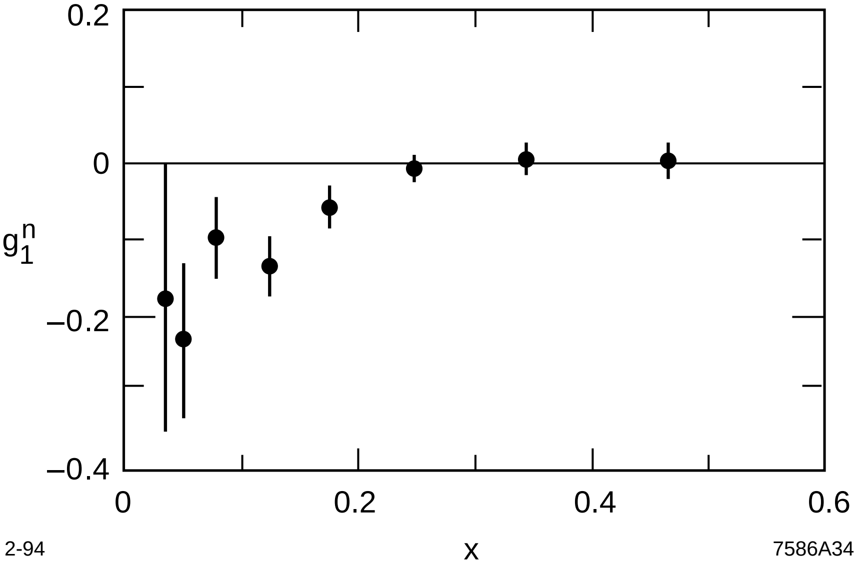

Fig. 41. Results of g_1^n versus x from experiment E–142.

value, the results support the simple QPM description of the nucleon in which the neutron spin structure function is expected to be small and negative.

6 Summary and Comparisons

Now we compare the results from the three experiments (EMC, SMC, and E-142). Figure 42 presents the proton asymmetry measurements of EMC, the deuteron asymmetry measurements of SMC, and the neutron asymmetry measurements from E-142. The smaller error bars on the neutron are a consequence of the high statistics. We can extract the neutron asymmetry measurement from CERN by taking twice the SMC deuteron results and subtracting out the EMC proton results. Comparison of the results of the asymmetry measurements of the neutron from CERN

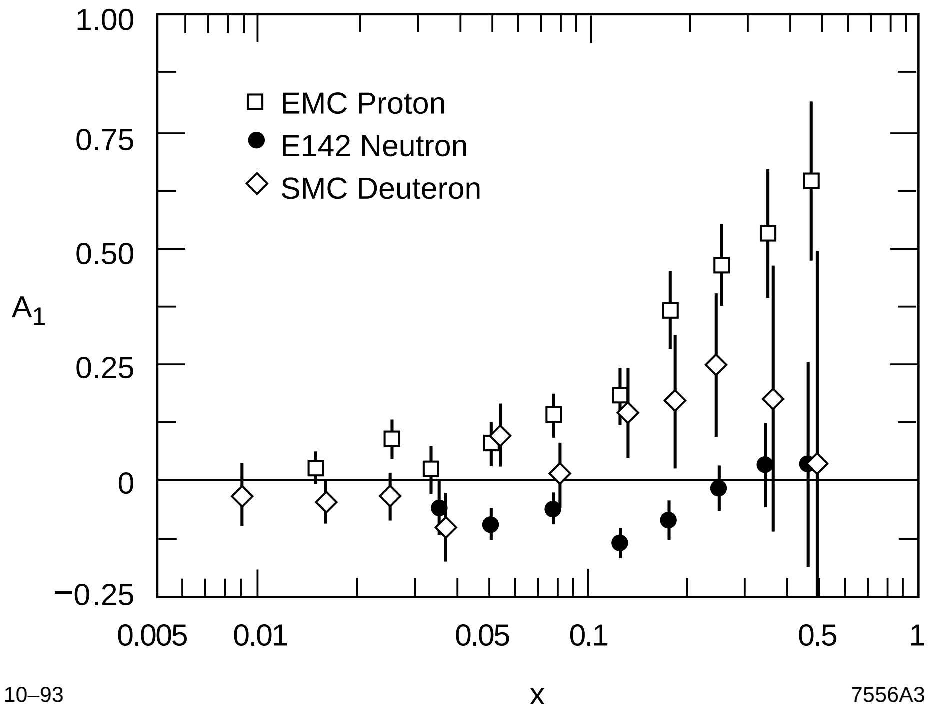

Fig. 42. Comparison of A_1 verus x of the CERN EMC proton, the SLAC E–142 neutron, and the CERN SMC deuteron.

versus those from SLAC is given in Fig. 43. Immediately, the complementary nature of the information from the two types of experiments is apparent. The CERN experiments with > 100 GeV beams penetrates to much lower x measurements. The SLAC experiment measures over a more limited x range, but with large gains in statistical precision. No disagreement in the neutron result is apparent from Fig. 43.

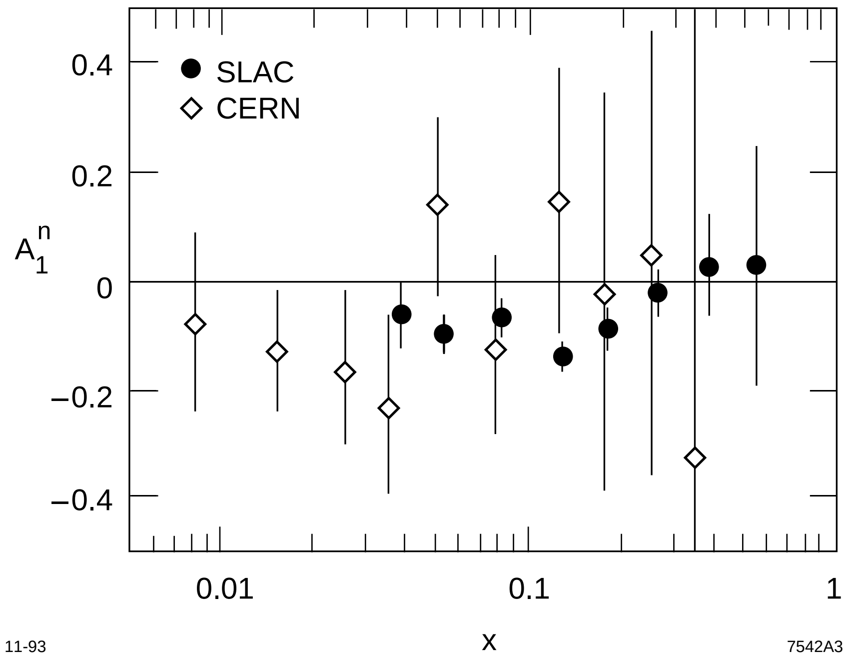

Fig. 43. Comparison of A_1^n versus x for SLAC E–142 compared to CERN (using a subtraction of the EMC proton result from the SMC deuteron result).

A comparison of the structure function measurements from CERN EMC (proton), CERN SMC (deuteron) and SLAC E–142 (neutron) is given in Fig. 44. Immediately apparent are the large positive proton results, the small negative neutron results, and the small positive deuteron results. The deuteron results are consistent with being an average of the proton and neutron results, which is just a restatement of the conclusions drawn from Fig. 43. The appearance of a rapid

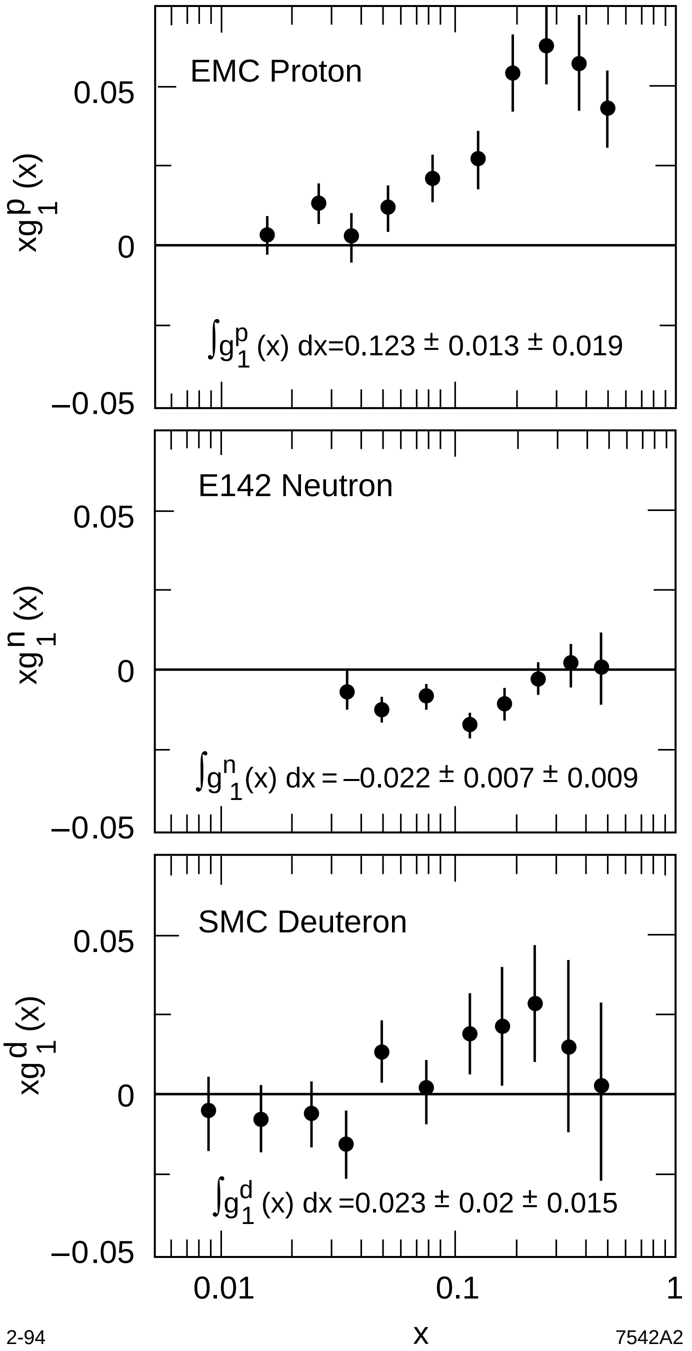

Fig. 44. Comparison of xg_1 versus x for the CERN EMC proton, the SLAC E–142 neutron, and the CERN SMC deuteron. Here the deuteron is defined by convention as being the average of a proton and a neutron.

Table 2: Systematic Uncertainties			
Uncertainty	EMC proton	SMC deuteron	E–142 neutron
Beam polarization	0.0092	0.0015	0.001
Target polarization	0.0074	0.0010	0.0016
Dilution factor	0.0054	0.0010	0.003
Acceptance variation	0.0108	0.0130	–
Extrapolation to high x	0.001	0.004	0.003
Extrapolation to low x	0.002	0.003	0.006
Uncertainty in F_2	0.0071	0.0012	0.002
Radiative corrections	0.0016	0.0009	0.001
Uncertainty on R	0.0007	0.0005	0.001
A_2	0.0030	0.0041	0.003

convergence of the small-x asymmetries as x approaches zero is evident. A comparison of systematic uncertainties from the three experiments is given in Table 2.

The largest uncertainties of the CERN muon experiments come from the false asymmetry possibility arising from possible variations in the spectrometer acceptance between target spin reversals. The largest uncertainty in the SLAC neutron integral determination comes from the small x-extrapolation, which is limited by the low electron beam energy.

The results of the nucleon integrals are given in Table 3. The first error in the table is statistical and the second is systematic.

Table 3: Nucleon Integrals	
EMC proton	$0.123 \pm 0.013 \pm 0.019$
SMC deuteron	$0.023 \pm 0.020 \pm 0.015$
E–142 neutron	$-0.022 \pm 0.007 \pm 0.009$

These are to be compared to the Ellis-Jaffe sum rule prediction that

$$\text{Proton} \qquad \int_0^1 g_1^p(x)\,dx \;\approx\; 0.17\ ,$$

$$\text{Neutron} \qquad \int_0^1 g_1^n(x)\,dx \;\approx\; -0.02\ ,$$

and the Bjorken sum rule prediction that

$$\int_0^1 g_1^p(x)dx - \int_0^1 g_1^n(x)\,dx \;\approx\; 0.18\ ,$$

where the Bjorken sum rule value depends on the Q^2 of the results being compared.

Detailed discussions on the implications of these three integral results are presented in the next lecture. With the three integral values given above, a first test of the Bjorken sum rule is possible as of 1993. Each integral also provides a statement on the quark spin contribution to the nucleon in the QPM.

Below are the references for the five polarized deep inelastic scattering spin experiments which have been published up to now:

Experiment	Reference
SLAC E-80	Phys. Rev. Lett. **37** (1976) 1261
SLAC E-130	Phys. Rev. Lett. **51** (1983) 1135
CERN EMC	Phys. Lett. **B206** (1988) 364
	Nucl. Phys. **B328** (1989) 1
CERN SMC	Phys. Lett. **B302** (1993) 553
SLAC E-142	Phys. Rev. Lett. **71** (1993) 959

Lecture III covers implications of the results, model interpretations, low-energy implications, and near future and future experimental programs to measure in detail the nucleon spin structure functions.

References

[1] M.J. Alguard et al., Phys. Rev. Lett. **37** (1976) 1258; **37** (1976) 1261.

[2] N. Sasao, Ph.D. thesis, Yale University, 1977.

[3] S. Rock et al., Phys. Rev. Lett. **24** (1970) 748.

[4] J.I. Friedman, H.W. Kendall, and R.E. Taylor, Rev. Mod. Phys. **63** (1991) 629, and references therein.

[5] For a description of Mott scattering, see Chapter 8.1.2 in J. Kessler, *Polarized Electrons* (Springer-Verlag, New York, 1985).

[6] P. Cooper, Ph.D. thesis, Yale University, 1975.

[7] W.W. Ash, Stanford Linear Accelerator Center preprints SLAC-PUB–1505 (1974) and SLAC–PUB–1797 (1976).

[8] C.D. Jeffries, *Dynamic Nuclear Orientation* (Interscience Publisher Inc., New York 1963).

[9] G.D. Cates, these proceedings.

[10] G. Baum et al., Phys. Rev. Lett. **51** (1983) 1135.

[11] R. Oppenheim, Ph.D. thesis, Yale University, 1982.

[12] J. Ashman et al., Phys. Lett. **B206** (1988) 364; Nucl. Phys. **B328** (1989) 1.

[13] V. Papavassiliou, Ph.D. thesis, Yale University, 1988.

[14] R.N. Piegaia, Ph.D. thesis, Yale University, 1988.

[15] D. Bollini et al, Nuovo Cimento **A63** (1981) 441.

[16] O.C. Allkofer et al., Nucl. Inst. Meth. **179** (1981) 445.

[17] M.Bourquin et al., Z. Phys. **C21** (1983) 27.

[18] R.L. Jaffe and A. Manohar, Nucl. Phys. **B337** (1990) 509.

[19] B. Adeva et al., Phys. Lett. **B302** (1993) 553.

[20] B. Frois, these proceedings.

[21] F. Feinstein, Proc. Conf. on High Energy Spin Physics, Nagoya, Japan, 1992, p. 927.

[22] P.L. Anthony et al, Phys. Rev. Lett. **71** (1993) 959.

[23] Z.E. Meziani, these proceedings.

[24] R. Prepost,these proceedings.

[25] M.A. Bouchiat, T.R. Carver, and C.M. Varnum, Phys. Rev. Lett. **5** (1960) 373.

[26] T.E. Chupp et al., Phys. Rev. **C36** (1987) 2244.

Lecture III: Implications and Future Programs

In this lecture, we examine the implications of the results from the three experiments that have measured the nucleon spin structure functions over a range in x, providing a reasonable test of the Ellis-Jaffe and Bjorken sum rules. SLAC experiments E-80 and E-130 do not provide much of a restriction on the proton integral value, so they are only discussed to a minimal extent. The consequence of the 1988 EMC proton result alone has had extensive theoretical implications, and has motivated the three programs that now exist at CERN, SLAC, and DESY. This lecture will begin with a discussion of theoretical implications, and will end with a review of ongoing and future experimental programs.

1 CERN versus SLAC

Experiments to date provide first tests of various sum rules and of the Quark Parton Model. An instructive way to view the results is to divide the discussion into how to interpret the results using only the CERN measurements or using only the SLAC measurements. The two experimental results from CERN are the EMC proton, which gives

$$\int_0^1 g_1^p(x)\,dx = 0.123 \pm 0.023\ ,$$

and the SMC deuteron result which gives

$$\int_0^1 g_1^d(x)\,dx = 0.046 \pm 0.050\ .$$

Here, we have added the statistical and systematic uncertainties on the integrals in quadruture, and the deuteron is written as the sum of a proton and a neutron.

From these two integrals, we extract the difference between the proton and neutron integrals,

$$\int_0^1 g_1^p(x)\,dx - \int_0^1 g_1^n(x)\,dx = 2\int_0^1 g_1^p(x)\,dx - \int_0^1 g_1^d(x)\,dx = 0.20 \pm 0.07 \ .$$

Small corrections due to the D-state wavefunction of the deuteron have been implemented,[1] but are negligible. The above result should be compared to the Bjorken sum rule, which predicts

$$\int_0^1 g_1^p(x)\,dx - \int_0^1 g_1^n(x)\,dx \ = \ \frac{1}{6}\,\frac{g_A}{g_V}\,\left[1 - \frac{\alpha_s}{\pi}\right] \ \approx \ 0.19 \ . \tag{1}$$

and the Ellis-Jaffe sum rule, which predicts,

$$\int_0^1 g_1^p(x)\,dx \ = \ \frac{1}{18}\,[9F - D] \ \approx \ 0.17 \ ,$$

$$\int_0^1 g_1^d(x)\,dx \ = \ \frac{1}{18}\,[15F - 5D] \ \approx \ 0.15 \ .$$

Conclusions from using the ‘CERN only’ results are that:

- ◇ The Bjorken sum rule is confirmed.
- ◇ The Ellis-Jaffe sum rule is violated.
- ◇ Quarks carry little of the nucleon spin.
- ◇ The strange sea has a significant polarization.

For clarification of the QPM conclusions, see the next section.

Commenting on the SLAC experiments, the ‘CERN view’ would be that the E-142 neutron and the SMC deuteron results agree over the measured range (see Fig. 43). However, the SLAC data does not extend to low enough x, where significant contributions to the neutron integral may be present.

A 'SLAC only' view of the data provides a measurement of the proton from E-80 and E-130,

$$\int_0^1 g_1^p(x)\,dx \;=\; 0.17 \pm 0.05 \;.$$

The neutron from E-142 gives

$$\int_0^1 g_1^n(x)\,dx \;=\; -0.022 \pm 0.011 \;.$$

The difference

$$\int_0^1 g_1^p(x)\,dx - \int_0^1 g_1^n(x)\,dx \;=\; 0.192 \pm 0.051$$

is still consistent with the Bjorken sum rule (Eq. 1), and agrees with the Ellis-Jaffe sum rule (for the neutron),

$$\int_0^1 g_1^n(x)\,dx \;=\; \frac{1}{18}[6F - 4D] \;\approx\; -0.02 \;.$$

Conclusions from using the 'SLAC only' results are that:

- ◇ The Bjorken sum rule is confirmed.
- ◇ The Ellis-Jaffe sum rule is confirmed.
- ◇ Quarks carry approximately half the nucleon spin, just like they carry half the nucleon momentum.
- ◇ The strange sea polarization is small.

The 'SLAC view' would be that the large statistical uncertainties of the CERN results make it difficult to draw meaningful conclusions.

2 The Quark Spin Content Δu, Δd, and Δs

The extraction of the quark spin contributions comes from SU(3) symmetry, discussed in relation to the Ellis-Jaffe sum rule (Lecture I, Sec. 7). The quantities to be determined are Δs, Δu, and Δd, and the sum over the three $\Delta q = \Delta u + \Delta d + \Delta s$. To extract these three unknowns, we need three equations. The EMC proton spin structure function integral provides one,

$$\int_0^1 g_1^p(x)\,dx \;=\; \frac{4}{18}\,\Delta u + \frac{1}{18}\,\Delta d + \frac{1}{18}\,\Delta s \;=\; 0.126 \pm 0.018\ . \tag{2}$$

Here, we take the value of the proton integral from the combined EMC, E-80, and E-130 analysis.[2] The Bjorken sum rule interpreted in the QPM provides a second equation,

$$\Delta u - \Delta d \;=\; \frac{g_A}{g_V} \;=\; 1.254 \pm 0.006\ . \tag{3}$$

Hyperon decay and the SU(3) model provides a third,

$$\Delta s - \Delta d \;=\; D - F = 0.284 \pm 0.016\ . \tag{4}$$

Here, $F = 0.485 \pm 0.012$ and $D = 0.769 \pm 0.010$.[3] With these three equations, the solutions for Δu, Δd, and Δs give,

$$\Delta u = 0.75 \pm 0.06\ , \qquad \Delta d = -0.51 \pm 0.06\ , \qquad \Delta s = -0.22 \pm 0.06\ .$$

The sum over the three parameters gives the total quark contribution to the nucleon spin,

$$\Delta q = 0.02 \pm 0.16\ .$$

We see that the EMC proton result, which differs from the Ellis-Jaffe sum rule, does indeed imply that the strange sea has a significant negative polarization, and the total quark contribution to the nucleon spin is small ("The Proton Spin Crisis").

Applying the same equations using the neutron result from SLAC E-142, results in an equation for the neutron integral that replaces the proton integral (Eq. 2),

$$\int_0^1 g_1^n(x)\,dx \;=\; \frac{4}{18}\,\Delta d + \frac{1}{18}\,\Delta u + \frac{1}{18}\,\Delta s \;=\; -0.022 \pm 0.011\;. \tag{5}$$

Solving with Eqs. (2), (3) and (4) and updated values[4] for the F and D constants ($F = 0.47 \pm 0.04$ and $D = 0.81 \pm 0.03$) gives,

$$\Delta u \;=\; 0.92 \pm 0.06\;, \qquad \Delta d \;=\; -0.33 \pm 0.04\;, \qquad \Delta s \;=\; -0.01 \pm 0.06\;.$$

The total summed quark contribution now becomes

$$\Delta q = 0.60 \pm 0.11\;.$$

For the SLAC case, the quarks are now carrying half the spin, and the strange sea polarization is small. This agrees with the Ellis-Jaffe sum rule, which assumes a zero polarization for the strange sea. No attempt is made to correct for a possible Q^2 dependence on the result from Eq. (5). This analysis reproduces approximately the published E-142 results.[5]

Figure 45 presents a comparison of published results from the three experiments on the total quark contribution to the nucleon spin. They have markedly different central values, but given the substantial error bars, there is only a mild disagreement at this point. An average of the three data points is a plausible scenario. Similarly, Fig. 46 presents a comparison of the three results on the strange sea polarization. Once again, the three results are in reasonable agreement if the

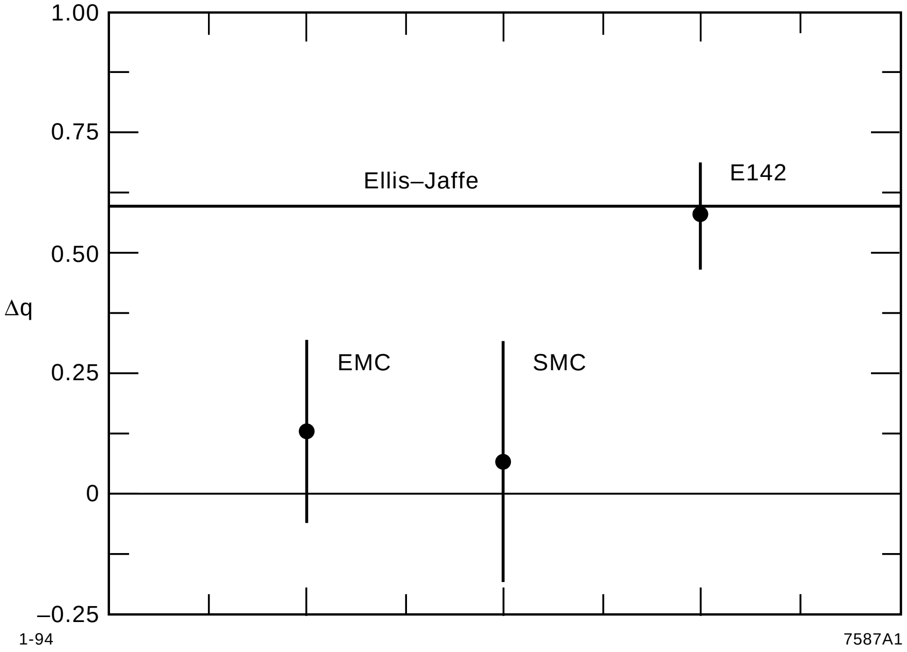

Fig. 45. Total quark contribution to the nucleon spin Δq for the EMC, SMC, and E-142 experiments.

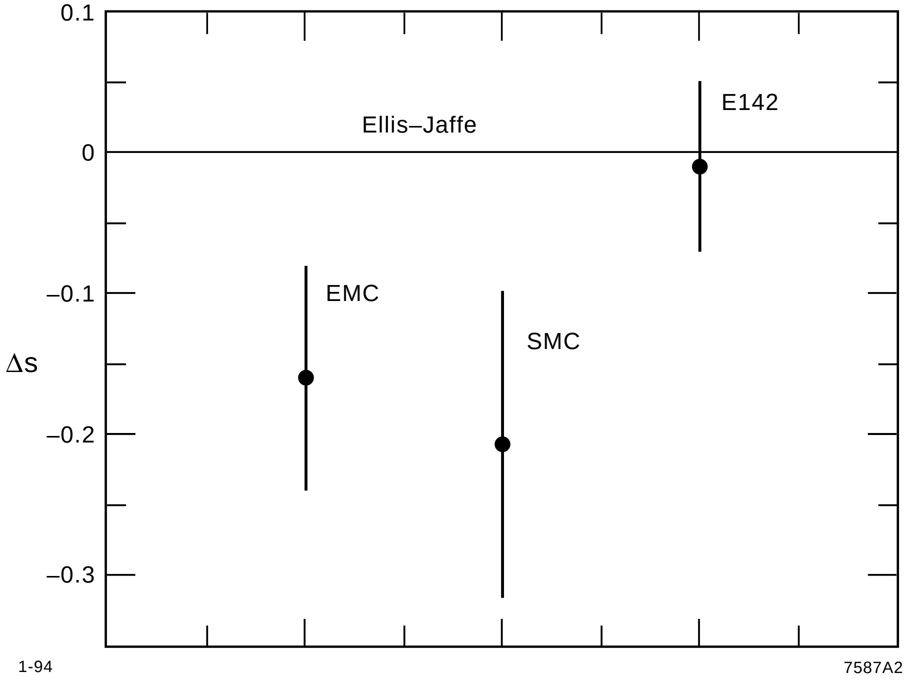

Fig. 46. Strange sea contribution to the nucleon spin Δs for the EMC, SMC and E-142 experiments.

true answer is an average of the three data points. Notice that the larger relative error bars on the strange sea polarization (as compared to the total quark contribution) is due to the larger impact of the systematic uncertainties on Δs coming from the F and D uncertainties.

The calculations in this section reproduce the published results. However, using identical F and D constants and errors, and accounting for the Q^2 dependence of the integral results from higher order QCD corrections, does bring the central values into somewhat better agreement.

3 Polarized Strange Sea

The EMC proton measurement created a great interest in studying the possible existence of a large polarized strange sea in the nucleon. Intuitively, it has been a surprise that the strange sea polarization could be so large, in light of the fact that the total strange sea in the nucleon is relatively small.

Information on the strange sea in the nucleon was established[6] in deep inelastic neutrino scattering experiments in the 1980s. The production of opposite-sign dimuon events in the final state of neutrino interactions provides some direct information on the total amount of nucleon strange sea. Figure 47 presents a diagram of a neutrino interaction and the production of two opposite-sign muons originating from scattering off a strange quark. From the measured rates of dimuons, the neutrino experiments have determined the total strange sea content of the nucleon to a reasonable precision. The ratio of the amount of strange sea to the total amount of sea was found to be,[6]

$$K = \frac{2s}{u+d} \; = \; 0.52 \pm 0.09 \; .$$

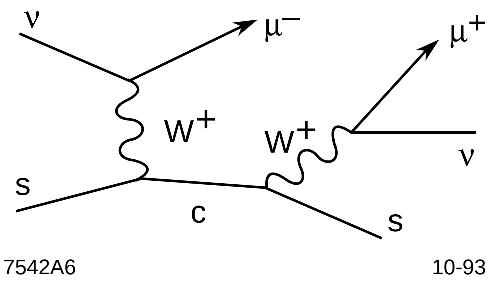

Fig. 47. Opposite-sign dimuon production.

Bounds on the strange sea momentum have been extracted[7]

$$\int_0^1 xs(x)\,dx \;\le\; 0.048 \pm 0.022\ . \tag{6}$$

This value is quite small and actually places an upper limit[8,9] on the amount of polarized strange sea Δs

$$s(x) \;=\; s^{\uparrow}(x) + s^{\downarrow}(x) \ge s^{\uparrow}(x) - s^{\downarrow}(x)\ ,$$

yielding $\Delta s \le 0.057 + 0.23(-0.057)$.

Results of the SU(3) interpretation of the EMC data support the existence of a large polarized strange sea, since

$$\Delta s = \int_0^1 [s^{\uparrow} - s^{\downarrow}]\,dx \;\approx\; -0.2\ . \tag{7}$$

The coexistence of Δs large and $s^{\uparrow} + s^{\downarrow}$ small appears to be a contradiction. Three lines of reasoning have developed to explain the possible discrepancy.

First, there is a possibility that s(x) is large at low x (though xs(x) is small), implying that the total amount of strange sea has been underestimated. There is certainly a kinematic limit to the study of the strange sea from the dimuon analysis of the neutrino data. Some fits[10,11] to the quark spin-dependent distributions appear to satisfy the constraints on both the strange sea polarization and its momentum. There has been a tremendous controversy over this point.[9]

Second, there could be a significant contribution from polarized gluons. The gluon polarization could modify the amount of strange sea measured compared to what exists in the nucleon. This model originates from the 'axial anomaly' discussed in the next section.

Third, a radical line of reasoning is that perturbative QCD (PQCD) is wrong. In this model (Sec. 5), the QPM is assumed to be fine with a small strange sea polarization and a small gluon polarization. The weak link is attributed to the Bjorken sum rule itself. If the Bjorken sum rule is wrong (due to PQCD limitation), then the extraction of Δu, Δd, and Δs using the Bjorken sum rule becomes meaningless.

The role of gluons, orbital angular momentum, and QCD violating models are discussed in the following sections.

4 Gluons and Orbital Angular Momentum

The spin crisis brought on by the EMC proton spin structure function results produced a flurry of theoretical papers. One of the most intriguing issues that arose was the possibility for a large gluon polarization in the nucleon. This effect would manifest itself as a modification to the observed amount of polarized strange sea via the 'axial anomaly'.[12–16] The diagram for the contribution of polarized gluons to the scattering process is shown in Fig. 48. This diagram couples to the polarization of each of the quark flavors and gives a modification to the amount of

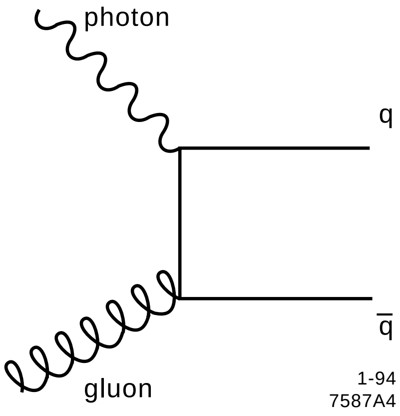

Fig. 48. Diagram of gluon contributions.

polarized quark contribution via

$$\Delta q_f^{\mathrm{true}} \ = \ \Delta q_f^{\mathrm{meas}} - \frac{\alpha_s}{\pi} \, \Delta G \ . \tag{8}$$

Here q_f is a particular quark flavor. This contribution had not initially been regarded as significant, since it is a first order correction in α_s. However, there is no theoretical limit on the size or sign of ΔG. If ΔG is as large as 5, for instance, then the true amount of polarized strange sea Δs^{true} could be close to zero, even if $\Delta s^{\mathrm{meas}} \approx -0.2$. A result such as $\Delta G = 5$ of course, is a huge polarization of the gluons and has implications for the orbital angular momentum of the constituents in the nucleon.[17]

A simple relation exists between the spin of the nucleon (1/2) and the contribution of the various constituents to the nucleon spin

$$J \ = \ \frac{1}{2} \, \Delta q + \Delta G + \Delta L \ . \tag{9}$$

Here, $J = 1/2$ is the nucleon spin, Δq is the total quark contribution to the nucleon spin, ΔG is the contribution due to the polarized gluons, and ΔL is the contribution due to the orbital angular momentum of the nucleon constituents. This relation has immediate implications:

If the total quark contribution to the nucleon spin is large, then the amount of polarized gluons and the oribital angular momentum of the quarks in the nucleon can be small. This was the old worldview of the nucleon before the EMC data was released.

If the quarks do not contribute much to the nucleon spin (Δq is small), and the proton crisis is instead explained by the axial anomaly with large gluon polarization ($\Delta G \approx 5$), then the orbital angular momentum contribution of the constituents must be large ($\Delta L \approx -4.5$). Such a large orbital angular momentum is itself surprising!

5 A Perturbative QCD Violating Model

The possible violation of the Bjorken sum rule is a carrot for the experimentalists. One idea is that perturbative QCD corrections to the Bjorken sum rule are not adequate to account for the behavior of the nucleon and its spin. As reviewed in Lecture I, the Bjorken sum rule must be tested experimentally at finite Q^2, where Perturbative (PQCD) corrections are present:

$$\int_0^1 g_1^p(x)\,dx - \int_0^1 g_1^n(x)\,dx \;=\; \frac{1}{6}\frac{g_A}{g_V}\,\left[1-\Delta^{PQCD}\right]\;.$$

For reasonably large Q^2 from deep inelastic scattering, Δ^{PQCD} is expected to be small.

The reasoning behind the QCD violating model proceeds as follows:

- ◇ The amount of strange sea is small (from neutrino scattering) and, as a consequence, the amount of polarized strange sea is small (Δs is small).

- ◇ The Quark Parton Model and SU(3) are adequate for describing the the nucleon and its structure. SU(3) symmetry breaking plays only a small role, since the strange sea contribution is anyhow small. Therefore, Eq (4) becomes $\Delta d \approx F - D$.
- ◇ The EMC measurement is taken as fine.
- ◇ A large gluon contribution to the nucleon spin is taken as unlikely (ΔG is small).
- ◇ The large strange sea implied by the EMC results imply a violation of the Bjorken sum rule [Eq. (3)] in the QPM,

  $$\Delta u - \Delta d \neq \frac{g_A}{g_V} \ .$$

  From proponents of the violation of the Bjorken sum rule, there is no surprise. PQCD is unable to explain quark confinement, and this inability shows up in the measurements of the spin asymmetries A_1 at low x. The low-x asymmetries are closer to zero for the proton and neutron than expected from the Bjorken sum rule prediction. A replacement, the Fire String Model,[18] does an excellent job at describing the EMC proton data for all x (see Fig. 49). Results from this model on the neutron prediction unfortunately were never calculated.

A closing comment on the PQCD violating model: without the Bjorken sum rule prediction, the most precise results on the nucleon spin structure function measurements to date do show an expected behavior as compared to the QPM. At x near 0.3, the results agree with SU(6). At high x there is a tendency for the asymmetries to rise to one, though this has not been confirmed by the neutron measurements yet. At low x, there is a definite rapid loss of spin information as the asymmetries quickly converge to zero (see Fig. 43). Without the constraints

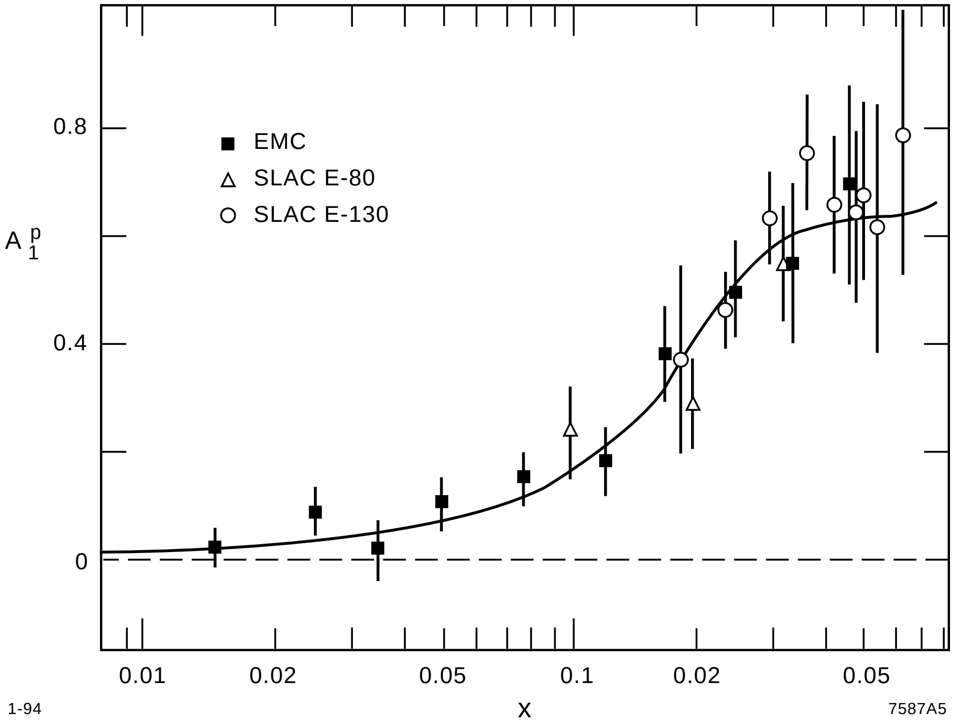

Fig. 49. A_1^p versus x from EMC compared to the Fire String Model.

of the Bjorken sum rule, the measurements are tending to agree with intuitive expectations. Future precision measurements of these structure functions should be able to nail down precise values of the QPM quantities and test the Bjorken sum rule to a level of better than 10% (see Sec. 7).

6 Nuclear Uncertainties

When the results from the various experiments are compared, one of the significant questions asked is what are the sizes of the nuclear uncertainties in extracting the proton and, even more importantly, the neutron spin structure functions, from nonpure polarized proton and neutron targets. This section briefly reviews some of the questions concerning nuclear uncertainties arising from the different target species.

For the proton, there are presently three types of targets being used to extract the proton spin structure function (solid ammonia, solid butanol, and pure hydrogen gas). The butanol target consists of carbon and oxygen that are spin-0 nuclei, and therefore do not contribute any spin dependent nuclear uncertainties. Issues such as the EMC effect[19] (i.e., that bound nucleons have different cross-sections than free nucleons) give only a small correction to the denominator of the measured asymmetries. Ammonia, on the other hand, has a subtraction that needs to be made due to the polarized nitrogen. The nitrogen in ammonia is spin-1 and polarized when the target is polarized. The shell model of nitrogen can be used to correct for this contribution. Here, a nitrogen (7 neutrons and 7 protons, and spin-1) can be approximated as a carbon (6 neutrons and 6 protons and spin-0) plus a deuteron (1 neutron and 1 proton, and spin 1).

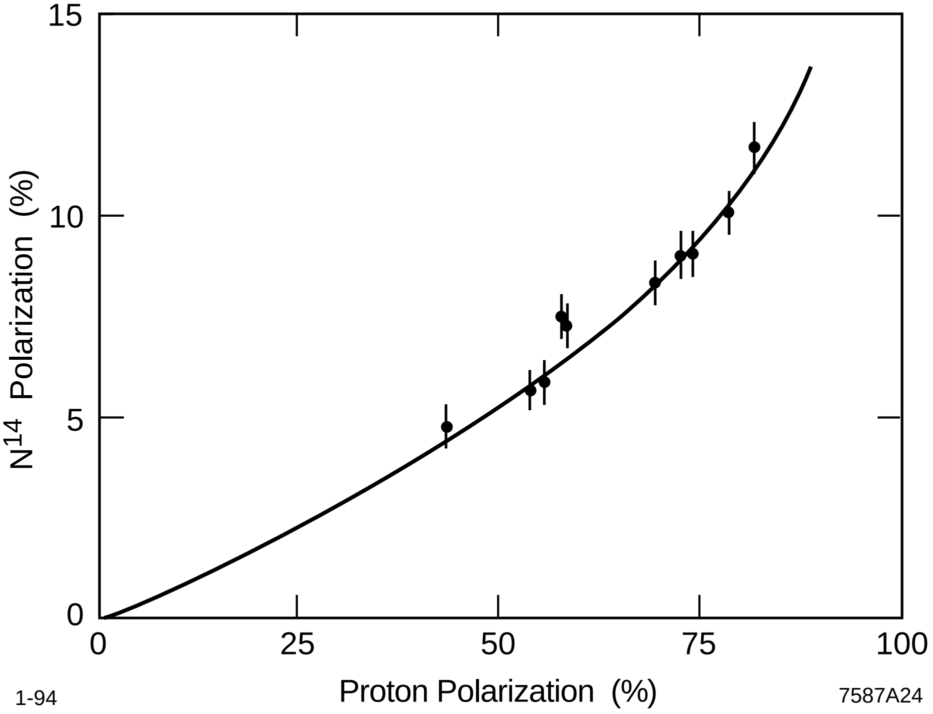

Fig. 50. Nitrogen polarization versus hydrogen polarization in polarized ammonia.

The polarization of the nitrogen in a solid, polarized ammonia target has been measured to be $\approx 13\%$ compared to the polarized hydrogens[20] (see Fig. 50). The final effect on the measured proton spin asymmetry from ammonia turns out to be quite small:

$$\Delta^{\mathrm{corr}} \;=\; \left(-\frac{1}{3}\right)\cdot\left(\frac{1}{3}\right)\cdot(13\%) \;=\; 1.5\%$$

Here Δ^{corr} is the additive correction factor that is applied to the measured asymmetry. The first factor of $(-1/3)$ comes from Clebsch-Gordon coefficients; the second factor of $(1/3)$ comes from the ratio of the number of nitrogen to hydrogen atoms, and the 13% comes from the polarization of nitrogen in a fully polarized ammonia target.

The extraction of the neutron spin structure function is generally more tricky, since a free polarized neutron target is unfeasible. There are two nuclear species which presently allow for an extraction of the neutron spin structure function: the deuteron and ^{3}He.

The difficulty of measuring the neutron spin structure function as extracted from a polarized deuterated ammonia target (ND_3) is more severe than the ammonia target (NH_3), since the nitrogen is spin-1 as are the deuterons. To alleviate this problem, modern measurements of the deuteron spin structure function extracted from ammonia use an isotope $^{15}ND_3$, and even $^{15}NH_3$, as in SLAC experiment E-143 (Sec. 9.3).

The deuteron is the simplest nucleus used for extracting neutron information, since it consists of a proton and a neutron in a relatively weak bound state (binding energy 1.1 MeV/nucleon). A polarized deuteron can be approximated as a polarized proton plus a polarized neutron. The magnetic moment of the deuteron (0.857 nuclear magnetons μ_N) is similar to the sum of the magnetic moments of the proton (2.79 μ_N) and the neutron (-1.91 μ_N); the difference is only on the order of a couple of percent.

The correction to this simple model of the deuteron comes from a small term due to the quadrupole moment of the deuteron. There is a D-state contribution in which the deuteron has the proton and neutron spins aligned antiparallel to the deuteron spin (J=1, L=2, and S=1). The D-state probability (L=2) is determined by theoretical calculations to be $P_D \sim 6\%$.[1] This D-state correction is small, but has a large uncertainty since it is not directly measureable.[21,22] The complete correction which needs to be applied in order to extract the neutron integral from the deuteron is

$$K = \frac{1}{1 + 1.5\ P_D}\ ,$$

where K is the correction factor and the multiplicative factor of 1.5 comes from evaluating Clebsch-Gordon coefficients.

A second method of extracting the neutron spin structure function comes from the use of a polarized ^{3}He target. To a large extent ($\sim$ 90%), the polarized ^{3}He nucleus can be modeled as a polarized neutron plus two protons with spins aligned in directions opposite to one another (see Fig. 51). The antiparallel alignment of the proton spins follows from the Pauli exclusion principle. The extent to which the ^{3}He nucleus is described in such a model depends on the S-state probability

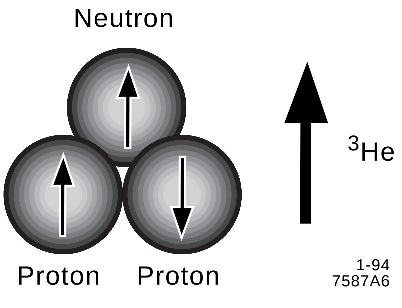

Fig. 51. Schematic of polarized ^{3}He in the S-state.

Table 1. Three nucleon wavefunction

Channel	L	S	l_α	L_α	P	K	Probability (%)
1	0	0.5	0	0	A	1	87.44
2	0	0.5	0	0	M	2	0.74
3	0	0.5	1	1	M	1	0.74
4	0	0.5	2	2	A	1	1.20
5	0	0.5	2	2	M	2	0.06
6	1	0.5	1	1	M	1	0.01
7	1	0.5	2	2	A	1	0.01
8	1	0.5	2	2	M	2	0.01
9	1	1.5	1	1	M	1	0.01
10	1	1.5	2	2	M	2	0.01
11	2	1.5	0	2	M	2	1.08
12	2	1.5	1	1	M	1	2.63
13	2	1.5	1	3	M	1	1.05
14	2	1.5	2	0	M	2	3.06
15	2	1.5	2	2	M	2	0.18
16	2	1.5	3	1	M	1	0.37

of the ^{3}He wavefunction. Table 1 presents results of a calculation of the ^{3}He wavefunction.[23] A correction for the D-state of the ^{3}He in which the proton spins are parallel (Fig. 52) must be incorporated in the extraction of the neutron spin structure function from measurements using polarized ^{3}He. Figure 53 presents a calculation[24] of the difference in the neutron spin structure function compared to ^{3}He. The overall difference is small. A more recent detailed calculation including Fermi motion refines these results.[25]

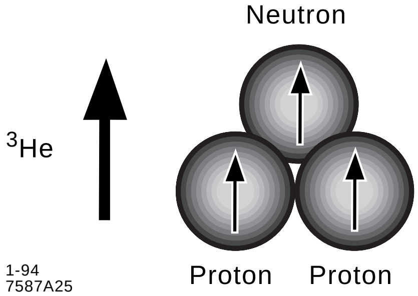

Fig. 52. Schematic of polarized ^{3}He in the D-state.

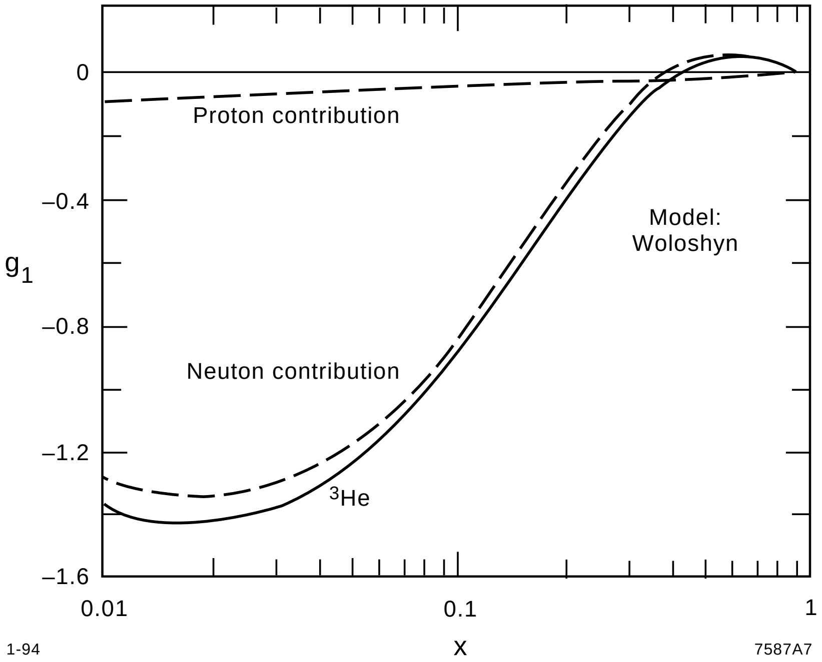

Fig. 53. Comparison of the ^{3}He and neutron spin structure function from theoretical calculations.

One of the theoretical land mines in extracting the neutron from either ^{3}He or the deuteron is the possible existence of large spin-dependent meson exchange currents. Meson exchange currents are known to exist in deep inelastic scattering, and enter as corrections to the simple Born approximation description of the scattering process. Since these currents are hard to calculate, it is difficult to know the size of the correction. Hence, it is difficult to know what theoretical uncertainty needs to be placed in extracting the neutron, for example, from the various nuclear targets.

Pion and rho production are channels that can contribute corrections to the scattering process (Fig. 54). Off hand, pion production is not believed to be a major difficulty, since this is a spin-0 particle and does not account for any spin-dependent effects. The existence of pion exchange currents will only influence the denominator of the measured asymmetry. To the extent that the asymmetry is small, pions play little role in the overall uncertainty.

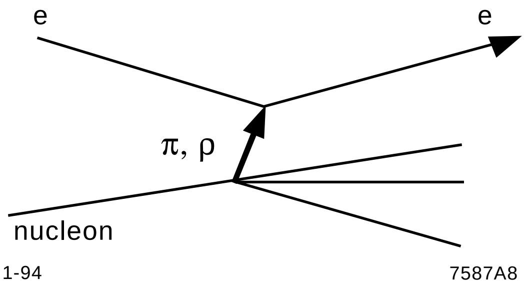

Fig. 54. Meson exchange current production.

Rho exchange currents are more problematic, since the rho is spin-1. Spin-dependent scattering with a rho may produce an asymmetry that differs from the lowest-order deep inelastic scattering process. However, the effects of scattering with rho mesons will only become a problem to the extent that rho production is large (low Q^2), the rho scattering asymmetry is large, and rho production is substantially modified by the existence of neighboring nucleons (the bound-state nucleon differs from the free nucleon). The Bjorken sum rule should not depend much on meson exchange currents, since their effect should largely cancel out in the difference between the proton and neutron integrals.

Intuitively, ^{3}He is regarded as a bit more dangerous in terms of extracting the neutron information. The binding energy (2.57 MeV/nucleon) in ^{3}He is larger than the deuteron, and the magnetic moment of the ^{3}He ($-2.12\ \mu_N$) is a worse approximation (by 11%) to the free neutron ($-1.91\ \mu_N$) than a deuteron is to the sum of a proton plus neutron. The 11% difference is usually ascribed[26] to the influence of meson exchange currents!

To summarize, the general attitude towards measurements (of the neutron spin structure function, in particular) is to measure the quantity with as many different targets as possible, so as to characterize the possible nuclear uncertainties. If the experimental results from different targets agree within experimental uncertainties, it will be (somewhat naively) assumed that the nuclear corrections are indeed small. If the results disagree, then a new storm of theoretical work is likely to erupt.

7 Testing the Bjorken Sum Rule

The greatest motivation for measuring nucleon spin structure functions is to test the Bjorken sum rule.[27] The success of this sum rule is generally considered a necessary condition for the validity of QCD, since the sum rule derivation uses tools that are essential to QCD.

In order to test the Bjorken sum rule, it is necessary to specify both experimentally and theoretically at what Q^2 the test is being performed. The sum rule is a relation valid at a particular Q^2. Ideally, an experiment is performed at a fixed Q^2, and the integral over the proton and neutron spin structure functions are compared. However, it is essentially impossible to achieve a measurement over a wide range in x at a uniform Q^2; for example, low x implies low Q^2.

Generally, the method used to test the Bjorken sum rule proceeds as follows:

- ◇ Measurements are performed on A_1 versus x at the highest possible Q^2 to ensure the results are from the deep inelastic scattering regime.
- ◇ It is *assumed* that the A_1 results are *independent* of Q^2.

This behavior is nothing more substanitive than the view that the cross sections scale similarly for $\sigma^{\uparrow\uparrow}$ and $\sigma^{\uparrow\downarrow}$. In most quark models of the nucleon, such behavior is evident. Figure 55 documents a typical quark model evolution[28] of A_1 with x and Q^2. Notice that the abscissa is a logarithmic scale in Q^2 and that the variation of

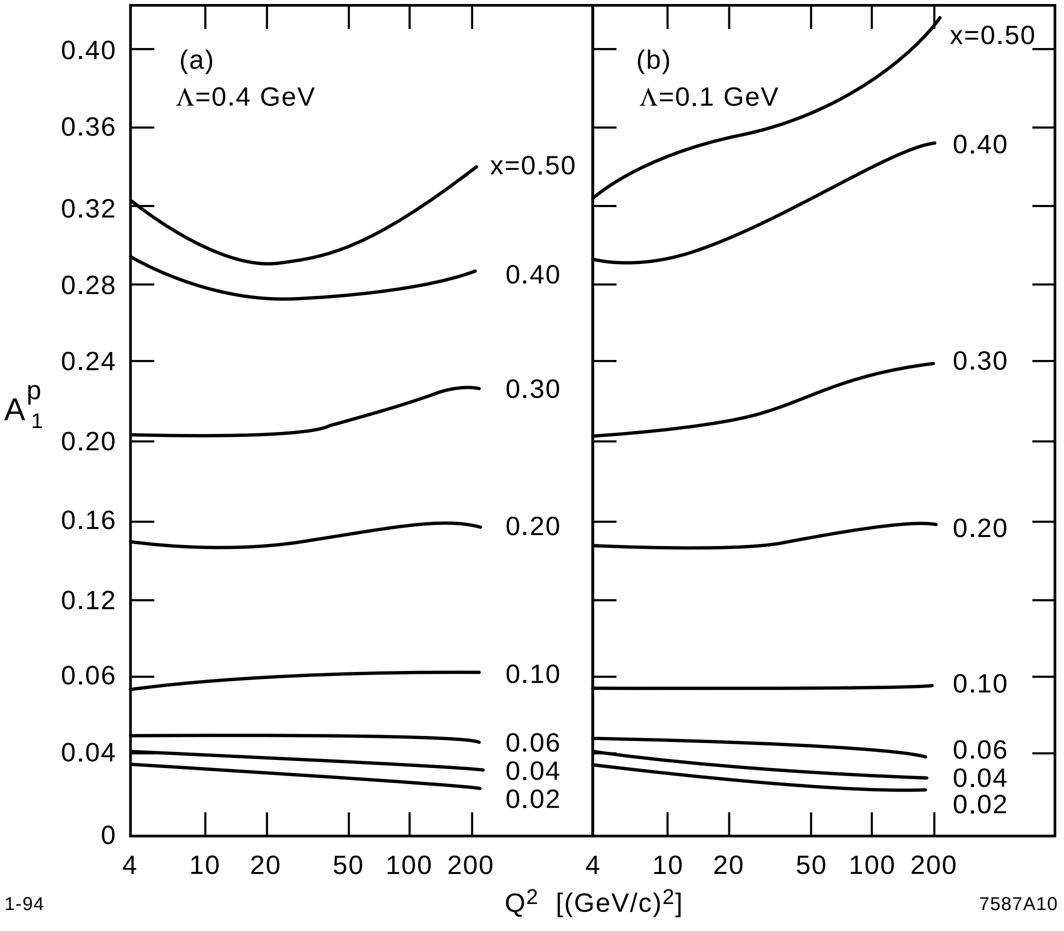

Fig. 55. Quark Parton Model prediction of A_1 versus Q^2 in different x bins.

A_1 is only evident as x gets large, typically greater than 0.4. Such small variations of A_1 with Q^2 are beyond the precision reachable by any planned spin structure function measurements. A recent preprint[29] evaluates the polarized extension of the Altarelli Parisi equations, and also finds that the asymmetry variation with Q^2 is small.

- ◇ A Q^2 independent A_1 implies that the nucleon spin structure function g_1 at a particular Q^2 varies only as a function of the unpolarized structure functions F_2 and R (ignoring the small A_2 term),

$$g_1(x,Q^2) = \frac{A_1(x)\cdot F_2(x,Q^2)}{2x[1+R(x,Q^2)]}\ , \tag{10}$$

The evolution of F_2 and R with x and Q^2 is well documented.

To summarize, from the measurement of the asymmetries $A_1(x)$ and the known Q^2 evolution of the unpolarized structures, $\int g_1(x)\,dx$ can be extracted from Eq. (10) for any value of Q^2.

For the 'right-hand side' of the Bjorken sum rule containing the weak coupling constant, QCD corrections need to be applied. The best understood corrections come from perturbative QCD that are calculated at this time up to third order in α_s. The Q^2 dependence of the Bjorken sum rule is reflected in the variation with Q^2 of α_s. Writing the Bjorken sum rule with a correction factor Δ^{PQCD} gives

$$\int_0^1 g_1^p(x)\,dx - \int_0^1 g_1^n(x)\,dx \ = \ \frac{1}{6}\,\frac{g_A}{g_V}\,\left[1-\Delta^{PQCD}\right]\ .$$

Calculations on the value of Δ^{PQCD} depend on the number of quark flavors that participate in the interaction. The first order term[31] in α_s is simple and has a coefficient of 1, independent of the number of flavors. The results for the calculations up to third order[32] give

$$\Delta^{PQCD} \ = \ \frac{\alpha_s}{\pi} + 3.58\,\left[\frac{\alpha_s}{\pi}\right]^2 + 20.22\left[\frac{\alpha_s}{\pi}\right]^3 \tag{11}$$

for three quark flavors ($N_f = 3$), and

$$\Delta^{PQCD} \;=\; \frac{\alpha_s}{\pi} + 3.25 \;\left[\frac{\alpha_s}{\pi}\right]^2 + 13.85 \left[\frac{\alpha_s}{\pi}\right]^3 \tag{12}$$

for four quark flavors ($N_f = 4$). The extraction of α_s itself depends on Q^2 and the number of quark flavors,

$$\alpha_s \;=\; \frac{12\pi}{[33 - 2N_f] \;\ln\left[Q^2/\Lambda^2_{QCD}\right]} \;. \tag{13}$$

Here Λ_{QCD} is the QCD coupling constant which has been determined in numerous fixed target and collider experiments:

$$\Lambda_{QCD} \;\approx\; 200 \text{ MeV}$$

Before comparing to the Bjorken sum rule, a few comments on the g_1 results are worth noting:

- ◇ The majority of the contribution to the proton spin structure function integral comes from the region near x of 0.3, which is naturally at a reasonably high Q^2 (see Figure 44).
- ◇ The value of the high-x measurements of the asymmetries has little impact on the spin structure function integral, since the spin structure function falls to zero as $F_2(x)$ falls to zero at high x.
- ◇ The asymmetries A_1 for the proton as measured by EMC are small at small x. Therefore, evolving the proton spin structure function to different Q^2 has little impact on the central value. Basically, the variation of $\int g_1(x)\,dx$ with Q^2 is small.
- ◇ The neutron spin structure function has the largest contribution to its own integral at much lower x near x of 0.08. Therefore, it is much more sensitive to the low Q^2 behavior of the unpolarized structure function F_2. However,

the overall value of the neutron integral is small, since A_1^n is everywhere small. Even relatively large changes in F_2 and R with Q^2 have little impact on the Bjorken sum rule, since the absolute value of the neutron integral is always small.

Evolving the experimental results from the EMC proton, SMC deuteron, and E-142 neutron measurement to various average Q^2 tests the Bjorken sum rule. Figure 56 presents the Bjorken sum rule prediction and its variation with Q^2 using 0th, 1st, and up to 3rd order PQCD corrections, compared to the integral results of EMC, SMC and E-142 evolved to different Q^2. Each pair of integral measurements provides a separate test. The difference between the measurements and the

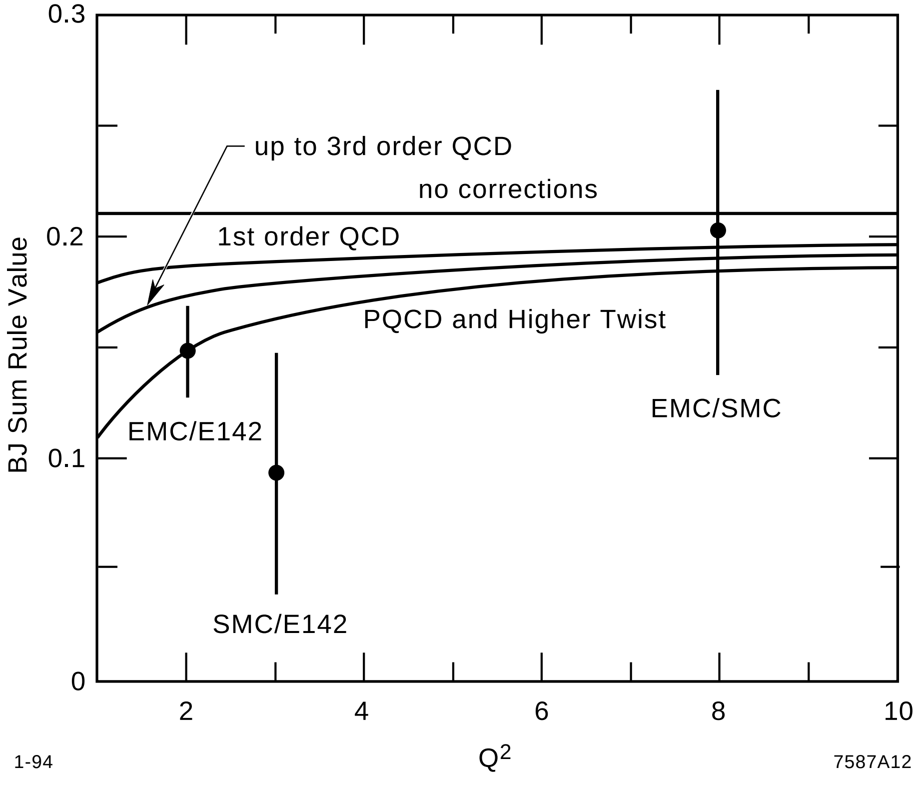

Fig. 56. Bjorken sum rule prediction versus Q^2 for 0th, 1st and up to 3rd order perturbative QCD corrections compared to results from experiments at CERN and SLAC.

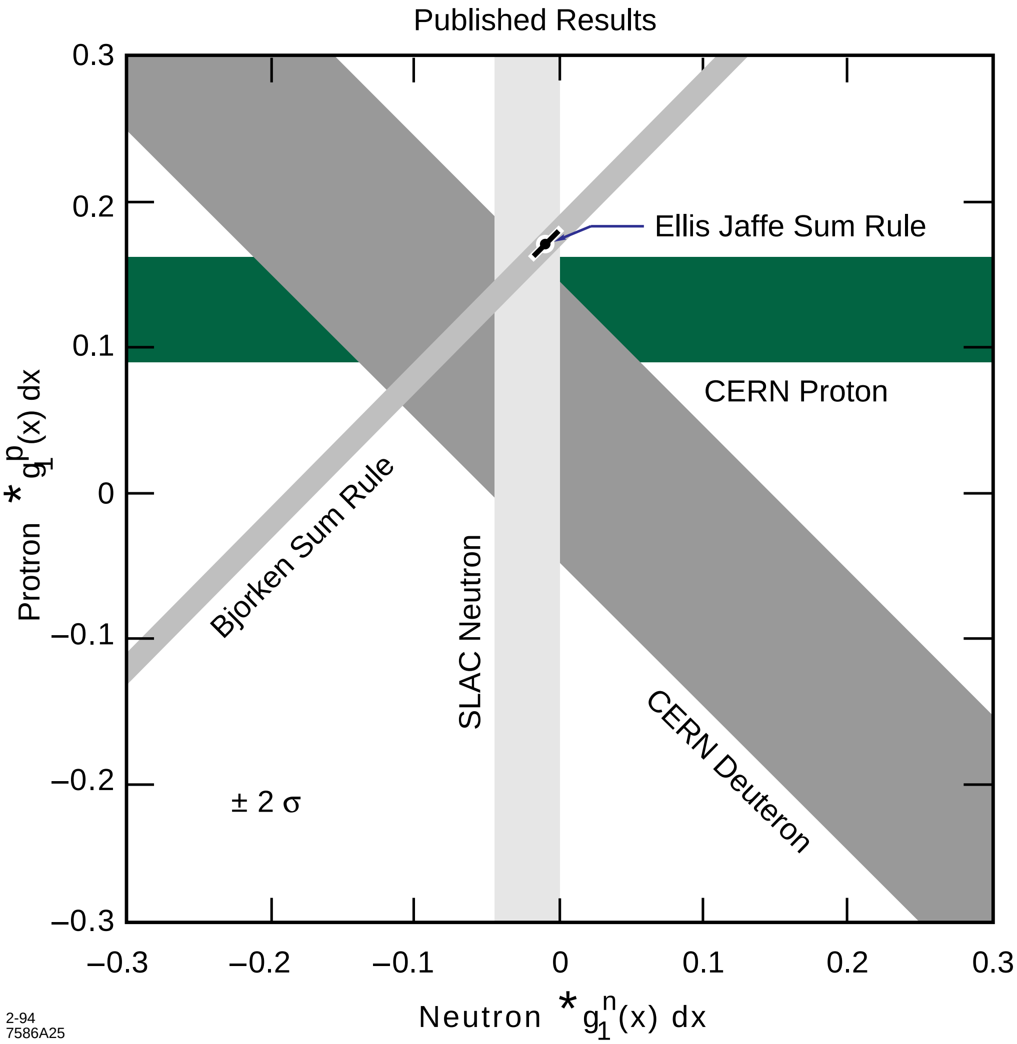

Fig. 57. Results on the integrals $\int g_1^p$ versus $\int g_1^n$ from CERN and SLAC compared to the Bjorken (a line) and the Ellis-Jaffe (a point) sum rules. Bands correspond to $\pm 2\,\sigma$.

prediction is minimal. There is no error assigned to the theoretical uncertainty coming from the lack of precision in the extraction of Λ_{QCD} in Fig. 56. No evidence for a violation of the Bjorken sum rule exists from this data, assuming that the coefficients of the PQCD corrections are indeed calculated correctly.

A nice method of presenting the world data is to plot the proton integral versus the neutron integral as bands of possible values (see Fig. 57). In such a plot, the proton and neutron integrals represent horizontal and vertical bands, respectively, and the deuteron integral represents a band at 45°. The Bjorken sum rule which gives a relation between the proton and neutron integrals represents an independent band on this plot. The Ellis-Jaffe sum rule represents a point on this plot, with a particular value for the proton and the neutron integral. All integral bands represent a range corresponding to $\pm 2\,\sigma$.

One final subject that keeps rearing its ugly head in the issue of testing the Bjorken sum rule is the role of nonperturbative QCD corrections. These corrections, which vary as a constant divided by Q^2 or Q^4, are difficult to calculate,

$$\Delta \;=\; \frac{K_1}{Q^2} + \frac{K_2}{Q^4} + \;\ldots\; .$$

Typically the coefficients such as K_1 are extracted experimentally from the data by subtracting out the normal PQCD corrections and fitting remnant variations to the higher twist coefficients. This type of analysis is dangerous in that any difficulty with the results will tend to get swept under the higher twist rug. Extractions of the higher twist terms from such a method have been employed for the unpolarized structure functions. Figure 58 shows, for example, the results of the coefficients for a higher twist analysis involving the unpolarized structure function[33] $F_2^p - F_2^n$. The precision needed to perform such an analysis for spin structure functions requires the next round of experiments.

Recent calculations using various QCD inspired models of nucleon structure have been done to try to estimate the higher twist contribution to the Bjorken sum rule.[34] These calculations were applied in a recent analysis[35] of the E-142 and SMC experimental results. The results indicated a large contribution of higher twist terms at low Q^2. The calculations were later found[36] to be based on flawed assumptions carried over from the original formalism,[37] thus implying incorrect

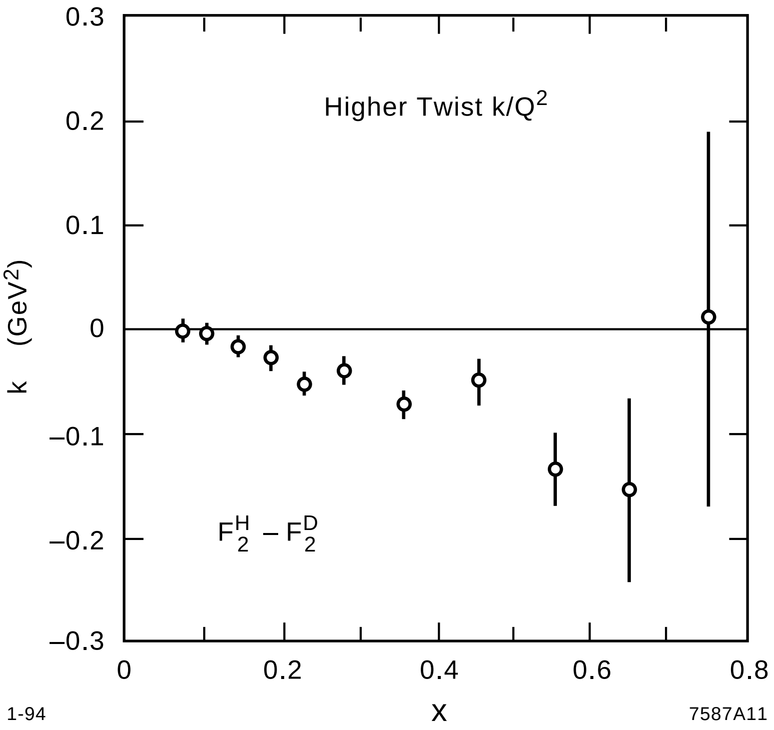

Fig. 58. Higher twist corrections to F_2^p–F_2^n versus x for unpolarized scattering.

conclusions in the updated analysis.[35] A different approach, using limits from measured unpolarized higher twist contributions, finds that the effects are small, but in a direction that would only worsen the disagreement.[38] Although higher twist effects are generally believed to be small at reasonably high Q^2, there true value is unknown. The calculations of higher twist effects are difficult and model-dependent, and at present poorly known.

To summarize, the higher twist effects present us with a number of difficulties. Since they are hard to calculate, the error on any calculation is large. They, therefore, present a significant theoretical uncertainty to interpreting measurements of the spin structure functions at finite Q^2. There is also no prescription on how to evolve the proton and neutron structure functions separately as functions of Q^2 due to the higher twist terms. Experiments performed at high Q^2 will hopefully be safe from higher twist corrections since, by definition, they decrease as Q^2 increases.

8 Low-Energy Spin Physics

A few low-energy spin-physics issues address the same questions provided by the high-energy spin physics experiments. Three relevant topics are polarized photon-nucleon scattering, neutrino-proton elastic scattering and precision hyperfine measurements in atomic physics.

A sum rule which has been arguably relevant to interpreting how the nucleon spin structure functions may evolve with Q^2 is the Drell-Hearn-Gerasimov (DHG) sum rule.[39,40] This sum rule states that at $Q^2 = 0$, there is a relationship between the spin-dependent scattering cross sections of circularly polarized photons by longitudinally polarized nucleons to the anamolous magnetic moment of the nucleon μ. The sum rule states that for the proton or neutron separately,

$$\int_0^\infty \frac{\sigma_{3/2} - \sigma_{1/2}}{\nu}\, d\nu \;=\; \frac{2\pi^2 \alpha \mu}{M} \;, \tag{14}$$

where M is the nucleon mass, α is the fine structure constant, ν is the energy of the virtual photon, and $\sigma_{1/2}$ ($\sigma_{3/2}$) is the scattering cross section for the photon and nucleon spins antiparallel (parallel). For the photon at a value of Q^2, the integral may be rewritten in terms of the structure function[41] $g_1(x, Q^2)$,

$$I(Q^2) = \frac{2m^2}{Q^2} \int g_1(x)\, dx \;. \tag{15}$$

A smooth transition is expected from Q^2 of 0 where the DHG sum rule is valid, to high Q^2 where the Bjorken sum rule is valid. Figure 59 presents a pictorial of how the sum rule and proton integral may evolve with Q^2. It is interesting to note that

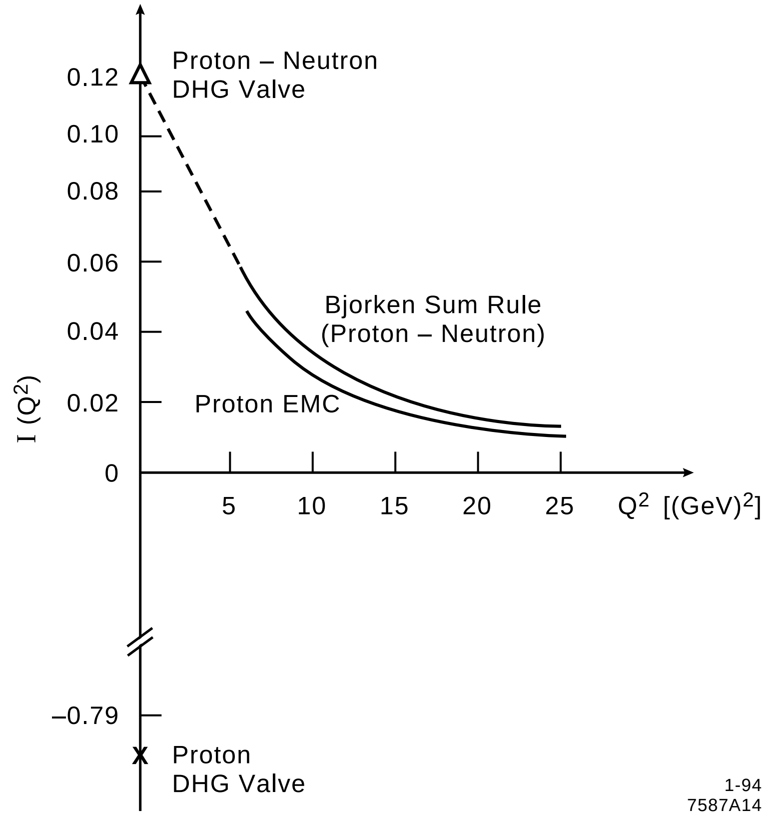

Fig. 59. A prediction for the evolution of I versus Q^2 over the range from deep inelastic scattering to $Q^2 = 0$.

the DHG value of the proton integral is negative at $Q^2 = 0$, implying that there is a crossover point where the low Q^2 corrections will make the integral change sign. This has been used as an argument that the positive proton integral will get smaller than expected in the high-energy limit, possibly explaining the low EMC proton result.

Recent criticism[42] of this type of analysis has been directed at the formalism that connects the spin structure function integral to the $Q^2 = 0$ integral. If this criticism holds, the argument presented by the DHG sum rule will not explain the proton spin crisis as originally postulated. Experiments are being planned to test this sum rule directly.[43]

The search for a large measureable polarized strange sea (implied by the EMC result) from low-energy elastic neutrino proton scattering[44] is an ongoing effort. Due to the helicity-conserving nature of neutrino scattering, neutrino interactions are sensitive to the axial vector currents Δq_i from elastic neutrino proton scattering. At $Q^2 = 0$, the Z^0 boson exchange couples to the quarks via

$$u\gamma_\mu \gamma_5 \, u - d\gamma_\mu \gamma_5 \, d - s\gamma_\mu \gamma_5 s \ ,$$

which is proportional to $\Delta u - \Delta d - \Delta s$ in the proton. This gives a completely new equation (Sec. 2) for the determination of the various quark spin contributions to the nucleon spin, and allows, for example, an independent solution for the strange sea polarization.

A significant technical challenge exists for relating the neutrino results to the theory. To obtain the $Q^2 = 0$ value from the present measured $Q^2 \neq 0$ data requires an extrapolation using a form factor, $F = 1/[1 + Q^2/M_A^2]$. The world average[45] is $M_A = 1.032 \pm 0.036$ GeV. Such a value gives the result for a polarized strange sea of $\Delta s = -0.15 \pm 0.09$. Although this appears to support the EMC result, it should be noted that a fit to $\Delta s = 0$ gives a mass of $M_A = 1.06$ which is within one standard deviation of the world average. A program of more precise elastic neutrino scattering measurements[46] at low energies avoids the extrapolation difficulty, and aims to determine Δs to a precision near ± 0.05.

An amusing connection between the high-energy world of deep inelastic scattering and the low-energy world of precision measurements in atomic physics is also addressed by the spin questions. An old problem in atomic physics is the issue of the hyperfine splitting in hydrogen, which depends on the spin-dependent polarizability of the proton. Basically, the experimental measurement of the hyperfine splitting in hydrogen has been measured to an accuracy where the spin structure function contribution from g_1 is noticeable:[47]

$$\text{Experiment} \qquad \Delta\nu = 1420405751.7667(\pm 10) \text{ Hz} .$$

From theoretical calculations,

$$\Delta\nu \;=\; \Delta\nu_F \cdot (1 + \delta_{QED} + \delta_p) \;,$$

where δ_p is a term which depends on $g_1(x)$ and is on the order of a few ppm.

9 Future Programs

Three programs now exist to study nucleon spin structure functions with precision: one at DESY, one at CERN, and one at SLAC. The three have very different experimental approaches for determining the nucleon spin structure functions ranging from high energies at moderate statistical precision to high precision at low energies.

9.1 HERMES at DESY

A new program called HERMES[48] using ultrapure polarized targets is now developing at DESY. The HERMES collaboration at DESY will build pure polarized gas targets in the HERA storage ring, and study the scattering of ~ 30 GeV polarized electrons off polarized gas targets. The scattered electrons will be detected in a large acceptance forward spectrometer. This program has a number of advantages over the SLAC and CERN experiments:

◇ The targets consist of pure gases of hydrogen, deuterium, and ^{3}He. As a result there is no background from windows, and the dilution factor will be close to one (barring beam halo scattering from side walls). The thin targets will still provide reasonable statistics, since the beam current is enormous (60 mA).

- ◇ The HERMES spectrometer should be able to tag outgoing hadronic particles, such as pions and kaons, for more detailed polarization dependent nuclear studies. Such investigations are known to extract additional spin-dependent structure functions[49] that can be used to extract new detailed information on nucleon spin structure. Among the goals is to determine the contribution of valence, sea and strange sea quarks. The statistical accuracy of the HERMES experiment should be similar to or superior to that of SLAC, assuming that HERMES can run parasitically with the collider projects at HERA.

Progress in the development of the polarized gas targets for HERMES has been impressive.[50,51] Table 2 presents the proposed specifications for densities and flow rates for the polarized targets and compares them to those achieved in storage ring tests. These tests have been accomplished in the presence of ionizing radiation (the primary source of target depolarization from electron beams) at a level comparable to that planned for the runs at DESY. Figure 60 presents a schematic layout of a

Table 2. HERMES Target Progress

Condition	Proton	^{3}He
Flow rate	8×10^6 Hz	1.2×10^{17} Hz
Density	$1.1 \times 10^{14}/\mathrm{cm}^2$	$3 \times 10^{14}/cm^2$
Polarization	45%	50%
Proposal Projection		
Density	$1 \times 10^{14}/\mathrm{cm}^2$	$3 \times 10^{14}/\mathrm{cm}^2$
Polarization	80%	50%

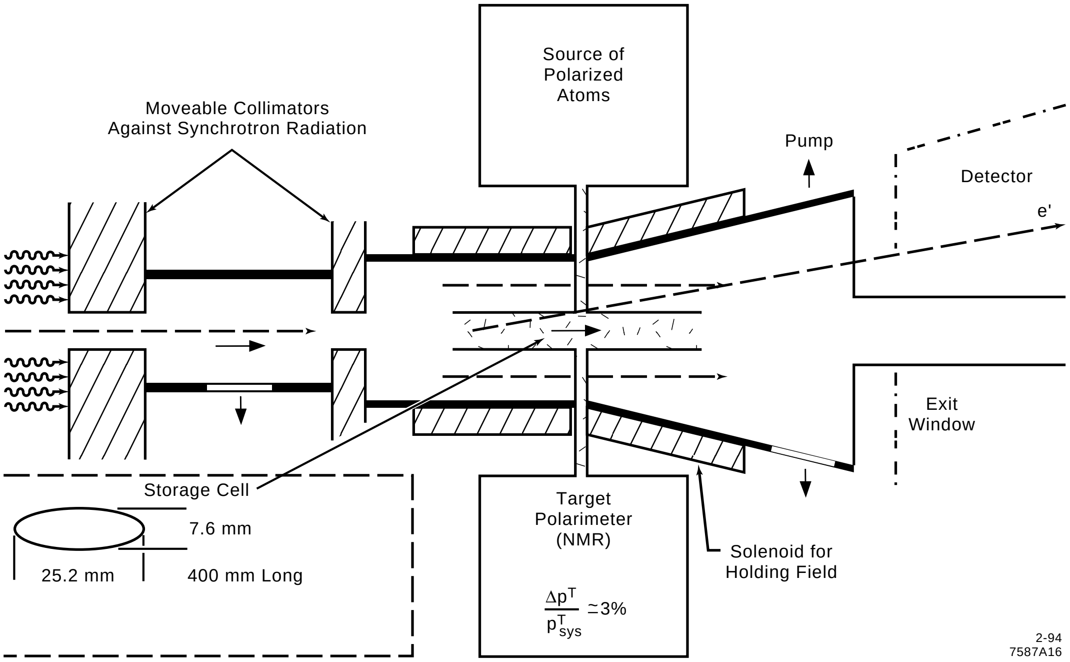

Fig. 60. Schematic of polarized gas targets at HERMES.

polarized target installed in the HERA beamline. The polarization process occurs in an upper chamber. The polarized atoms are then directed into the beamline where the interactions take place. Measurements of the target polarization are performed in a separate bottom chamber connected to the beamline. Waste gas is pumped away by diffusion pumps. No windows are present in the scattering process.

Figure 61 presents a layout of the spectrometer under construction by the HERMES collaboration. The spectrometer has a large acceptance, and multiple particle identification and energy measurement devices. To summarize, tracking chambers and hodoscopes are used for triggering, tracking, and timing; lead-glass and transition radiation detectors (TRD) are used for particle identification and energy determination. A strong magnet bends particles for momentum

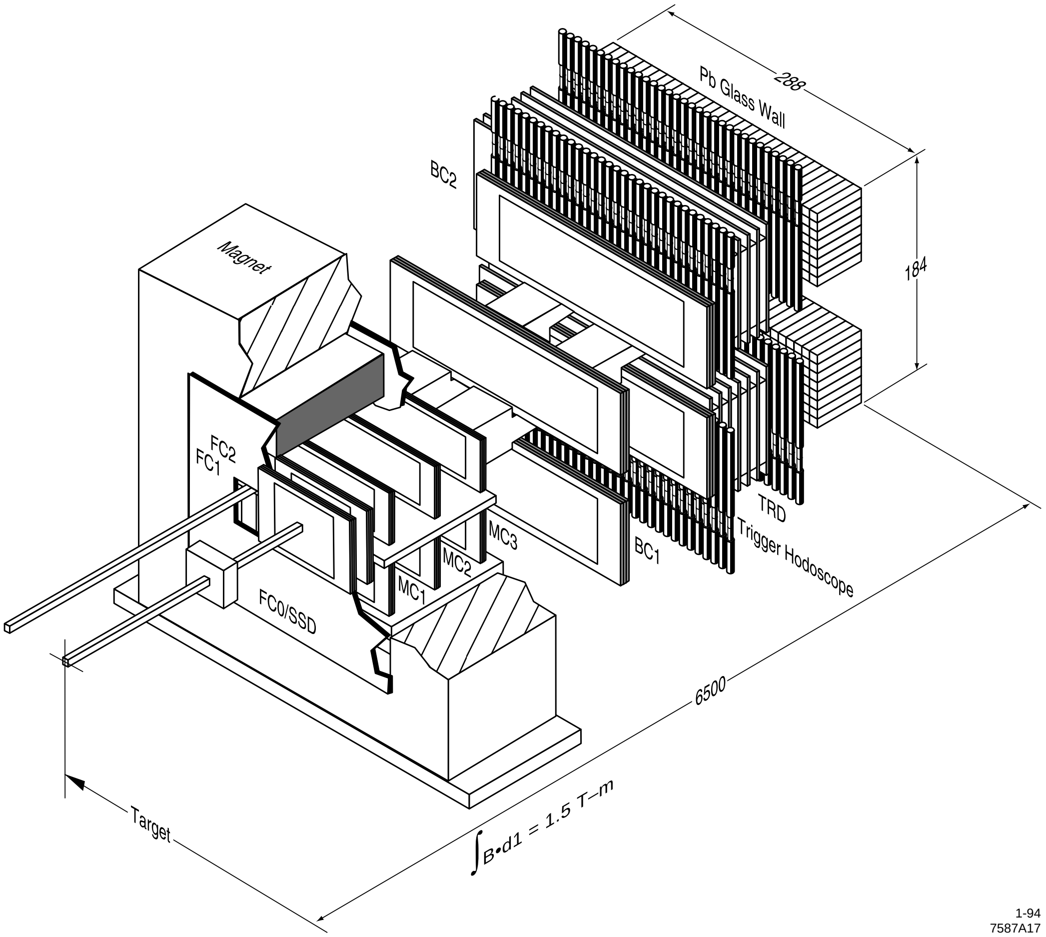

Fig. 61. HERMES spectrometer.

determination. A projection of the statistical precision of the HERMES experiment is given in Fig. 62 assuming a specified number of data collection hours.

The important issues that HERMES faces are:

(1) is the parasitic running with the collider project possible,

(2) is the beam energy limit of 30 GeV adequate for running at high Q^2 and low x, and

(3) will the results from HERMES be on a sufficiently fast time scale to be competitive.

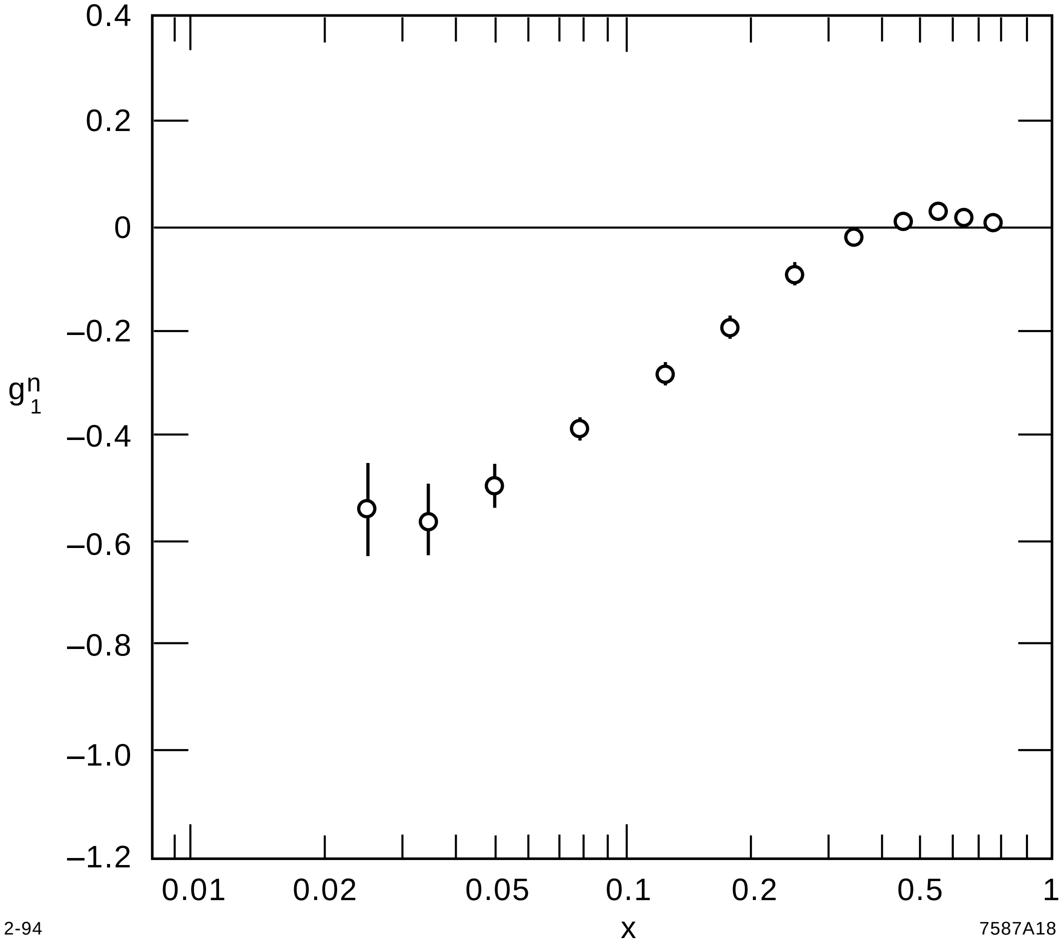

Fig. 62. Projected statistical uncertainty on g_1^n versus x for a specified number of data collection hours at HERMES.

To summarize, the HERMES program should give definitive systematically clean measurements of the proton and neutron spin structure functions at reasonably high Q^2, and provide a first look at more exotic spin structure functions.[49]

9.2 SMC at CERN

The program launched by the EMC proton experiment and now developed by the SMC collaboration[52] plans to continue running for the next couple of years. During 1993, SMC collected data using a polarized butanol target in order to extract the proton spin structure function. This experiment has recently reported[53] a preliminary result for the proton integral: $\int_0^1 g_1^p(x)\,dx = 0.152 \pm 0.015$ (stat) $\pm\, 0.018$ (syst). This value, higher than the EMC result, somewhat alleviates the nucleon spin 'crisis.' The implications of this result are a story in themselves, and an exercise remains: to calculate Δu, Δd, and Δs from the new SMC proton measurement [using Eqs. (2), (3) and (4)]. Since the result is fresh and comes after 1993, this lecture will not discuss these implications.

During 1994, SMC will run for more statistical precision on the proton. The collaboration hopes ultimately to test the Bjorken sum rule to a level of ~ 10%. Figure 63 presents the proposal statistical error on the neutron asymmetry

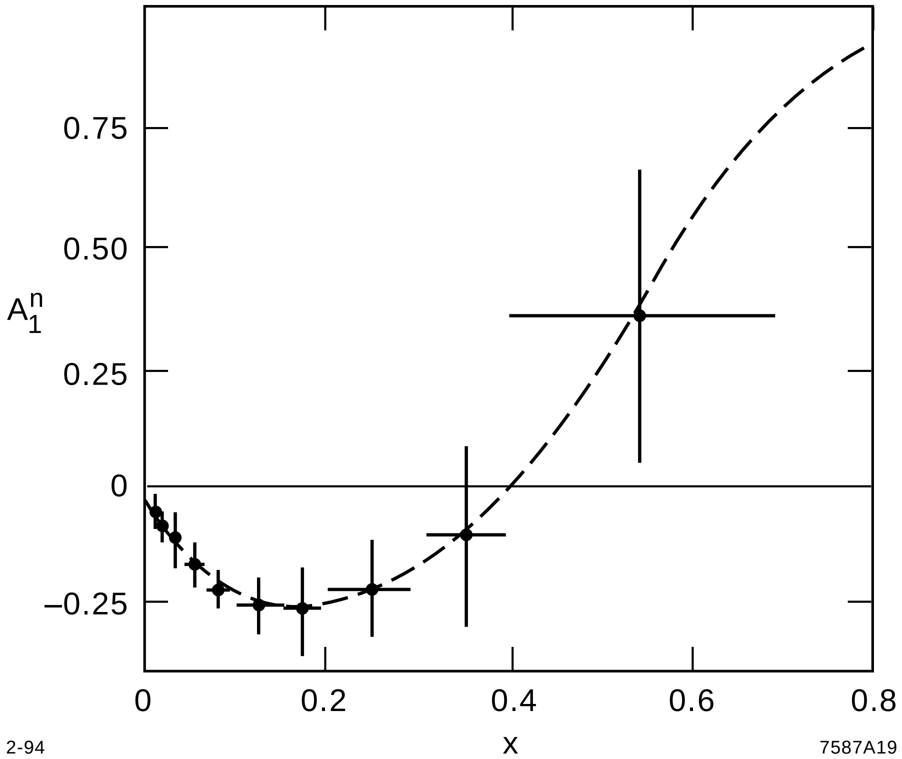

Fig. 63. Proposed statistical uncertainty on A_1^n versus x for the SMC experiment in the future.

measurement A_1^n by SMC. These are substantially larger error bars than have been achieved in the neutron measurement of experiment E-142. However, the SMC measurement will be at higher average Q^2 and will make measurements of the asymmetry to lower values of x (below x of 0.01). Even with the larger statistical error bars on the point-to-point basis, the overall statistical uncertainty on the neutron integral should be comparable to the systematic uncertainty.

9.3 Experiments E-143, E-154, and E-155 at SLAC

The third program that will measure the nucleon spin structure functions is at SLAC. Experiment E-142, which extracted the neutron spin structure function with a polarized ^{3}He target, is complete. Experiment[54] E-143 is currently running (November 1993 to January 1994). This experiment will measure the proton and deuteron spin structure functions using the polarized electron beam at 10 to 30 GeV and a polarized ammonia target. Statistical uncertainties on the proton (neutron) integral should be smaller than (similar to) those obtained in E-142 and the range in x should extend down to near 0.02 (see Fig. 64). Ammonia targets, as compared to butanol targets, are more robust in terms of their resistance to radiation damage from the electron beam.[55] In addition, the ammonia targets have a larger dilution factor than the butanol targets. The one disadvantage of the ammonia target in the electron beam, as compared to the gas targets of HERMES and E-142 and the muon experiments of CERN, is that the external radiative corrections in the E-143 experiment will be the largest. Recently, SLAC has approved two more experiments to run with a 50 GeV beam in End Station A, which are followup experiments to E-142 and E-143.

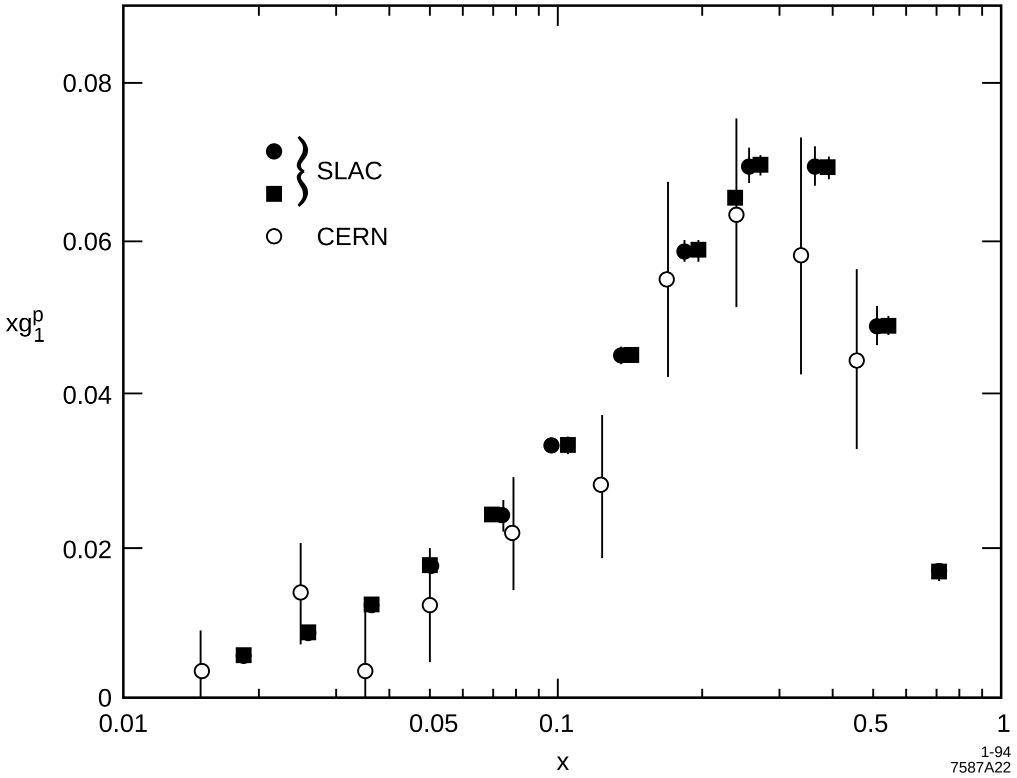

Fig. 64. Statistical error bars on the E-143 proton spin structure function g_1^p versus x, compared to the EMC proton measurement.

The experiments E-154 and E-155 (^{3}He target[56] and ammonia target,[57] respectively), will measure the nucleon spin structure functions at a high precision over a reasonably large Q^2. With a 50 GeV polarized electron beam, measurement of the nucleon structure function to lower x near 0.01 will also be possible, still maintaining $Q^2 > 1$ GeV^2. The technical challenges facing the E-154 and E-155 experiments come in the implementation of new spectrometer and detector packages in order to handle the high backgrounds from much higher instantaneous currents. At 50 GeV, the pulse length will be only 100 ns, as opposed to 1 μs used in E-142 and 2 μs being used in E-143. New, faster, and more finely segmented detector packages must be built. An example of the x-dependence of the asymmetries to be measured in E-154 ($< Q^2 > \approx 5$ GeV^2) is shown in Fig. 65 compared to that

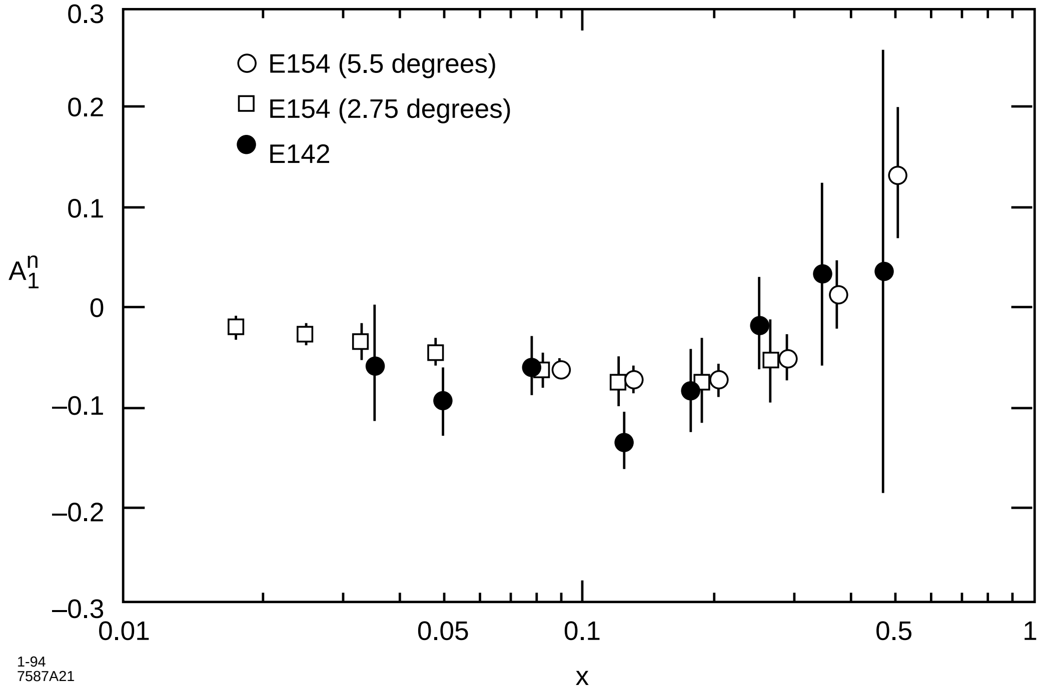

Fig. 65. Proposed statistical uncertainties on A_1^n versus x for the 50 GeV ^{3}He experiment (E–154).

achieved in E-142 ($< Q^2 > \approx 2$ GeV^2). Experiment E-155 will measure the proton and deuteron spin structure function to a precision similar to E-143. In terms of testing the sum rules, after the completion of E-154 and E-155, the precision on the sum rule tests should be impressive. Figure 66 presents a possible projection of the tests of the sum rules similar to that presented in Fig. 57. It is assumed in Fig. 66 that the E-154 and E-155 experiments measure the same central values as the EMC, SMC, and E-142 experiments for the proton, deuteron, and ^{3}He, but with the proposed precision of E-154 and E-155. Clearly, the precision is superior to the first round of experiments. Once again, the bands correspond to ±2 standard deviations.

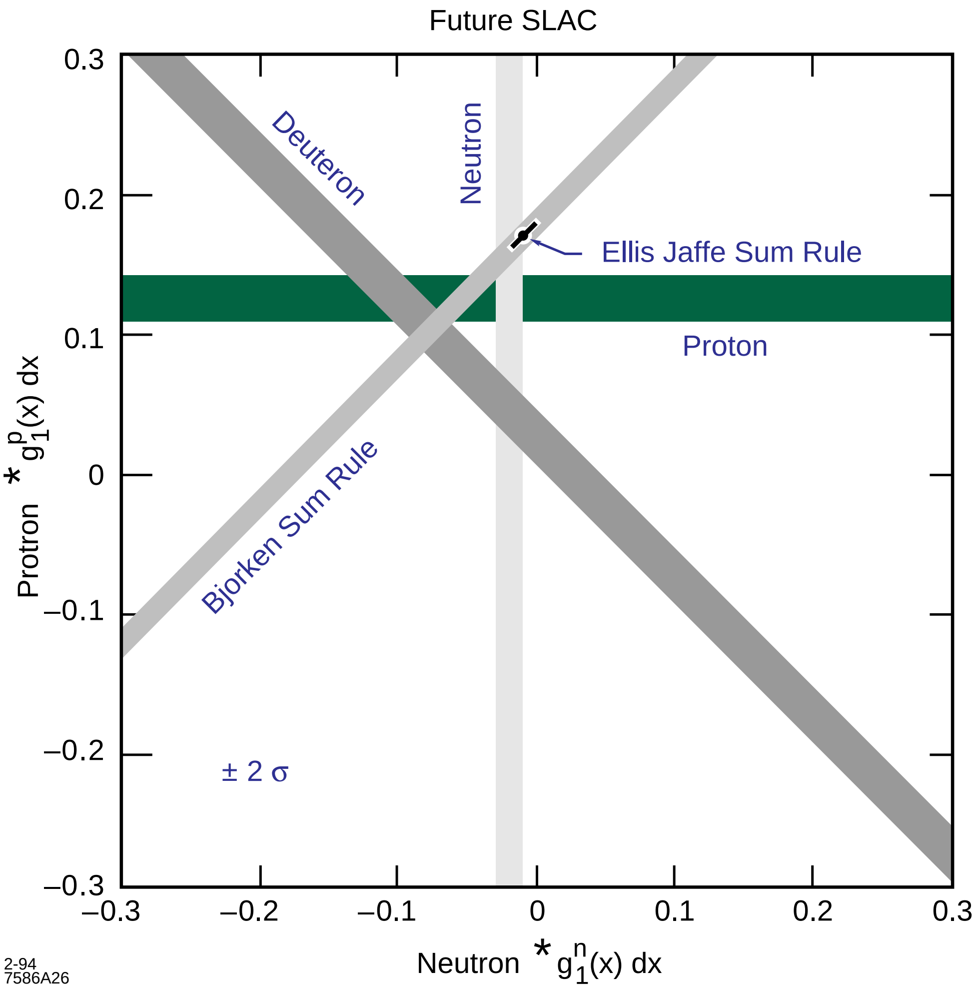

Fig. 66. Proposed error bands for the proton and neutron integrals for the future SLAC 50 GeV experiments (for both E–154 and E–155).

10 Conclusions

Table 3 summarizes the proposed and published statistical (systematic) uncertainties from the world experiments on nucleon spin structure function integrals. By the time these programs are complete, there will be a vast resource of data on nucleon spin structure functions. Each program has quite different experimental

Table 3. Proposed and published errors on nucleon spin integrals.

Experiment	Proton	Deuteron	^{3}He
EMC (1988)	0.010 (0.015)	–	–
SMC (1993)	–	0.020 (0.015)	–
SMC proposal	0.006 (0.010)	0.009 (0.007)	–
E-142 (1993)	–	–	0.007 (0.009)
E-143 proposal	0.003 (0.010)	0.005 (0.011)	–
E-154 proposal	–	–	0.003 (0.004)
E-155 proposal	0.002 (0.008)	0.003 (0.008)	–
HERMES proposal	0.003 (0.007)	0.004 (0.007)	0.005 (0.004)

approaches regarding the beams, targets, and spectrometers thus ensuring systematically independent tests of the spin structure function measurements.

Since the field of nucleon spin structure function measurements began, there has been a result appearing approximately every five years. With advances in polarized target technology and high polarization in virtually all of the lepton beams, results are now coming out each year; this is a true signature of the growth in the field. Hopefully, the experiments will provide a consistent picture of nucleon spin structure at their completion.

In summary, there are still many open questions regarding the internal spin structure of the nucleon. Tests of QCD via the investigation of the Bjorken sum rule is a prime motivator for the field, and will continue with the next round of precision experiments. The question of the origin of spin is still a fundamental problem. Our hope is that high-energy probes using spin will shed light on this intriguing mystery, in addition to characterizing the spin structure of the nucleon.

References

[1] M. Lacombe et al., Phys. Lett. **B101** (1981) 139.

[2] J. Ashman et al., Nucl. Phys. **B328** (1989) 1.

[3] M. Bourquin et al., Z. Phys. **C21** (1983) 27.

[4] R.L. Jaffe and A. Manohar, Nucl. Phys. **B337** (1990) 509.

[5] P.L. Anthony et al., Phys. Rev. Lett. **71** (1993) 959.

[6] H. Abramowicz et al., Z. Phys. **15C** (1982) 19.

[7] S.A. Rabinowitz et al., Phys. Rev. Lett. **70** (1993) 134.

[8] G. Preparata, P. Ratcliffe, and J. Soffer, Phys. Lett. B231 (1989) 483, and references therein.

[9] J. Soffer, Marseille preprint CPT–92–P–2809.

[10] B.L. Ioffe and M. Karliner, Proc. Conf. on High Energy Spin Physics, Bonn, Germany, 1990, p. 424.

[11] S. Brodsky, M. Burkhardt, and I. Schmidt, SLAC preprint SLAC–PUB–6087 (1993).

[12] A.V. Efremov and O.V. Teryaev, Czech. Hadron Symp., 1988, p. 302.

[13] R.L. Jaffe, Phys. Lett. **B193** (1987) 101.

[14] G.Altarelli and G.G. Ross, Phys. Lett. **B212** (1988) 391.

[15] R.D. Carlitz, J.C. Collins, A.H. Mueller, Phys. Lett. **B214** (1988) 229.

[16] M. Anselmino and E. Leader, preprint NSF–ITP–88–142 (1988).

[17] L.M. Seghal, Phys. Rev. **D10** (1974) 1663.

[18] G. Preparata, P. Ratcliffe and J. Soffer, Phys. Lett. **B231** (1989) 483.

[19] J.J. Aubert et al., Phys. Lett. **B123** (1983) 275.

[20] S.C. Brown et al., Proc. of 4th Int. Workshop on Polarized Target Materials and Techniques, Bonn, Germany, 1984, p. 102.

[21] R.D. Amado, Phys. Rev. **C19** (1979) 1473.

[22] J.L. Friar, Phys. Rev. **C20** (1979) 325.

[23] B. Blankleider and R.M. Woloshyn, Phys. Rev. **C29** (1984) 538.

[24] R.M. Woloshyn, Nucl. Phys. **496A** (1989) 749.

[25] C. Ciofi degli Atti, University of Perugia preprint DFUPG–75/93 (1993).

[26] J.L. Friar et al., Phys. Rev. **C42** (1990) 2310.

[27] J.D. Bjorken, Phys. Rev. **148** (1966) 1467; **D1** (1970) 1376.

[28] O. Darrigol and F. Hayot, Nucl. Phys. **B141** (1978) 391.

[29] G. Altarelli, P. Nason, and G. Ridolfi, CERN preprint CERN–TH–7023–93 (October 1993).

[30] J. Kodaira et al., Phys. Rev. **D20** (1979) 627.

[31] J. Kodaira et al., Nucl. Phys. **B159** (1979) 99; **B165** (1980) 129.

[32] S.A. Larin and J.A.M. Vermaseren, Phys. Lett. **B259** (1991) 345.

[33] M. Virchaux and A. Milsztajn, Phys. Lett. **B274** (1992) 221.

[34] I.I. Balitsky et al., Phys. Lett. **B242** (1990) 245.

[35] J. Ellis and M. Karliner, Phys. Lett. **B313** (1993) 131.

[36] X. Ji and P. Unrau, MIT preprint MIT–CTP–2232 (1993).

[37] E.V. Shuryak and A.I. Vainshtein, Phys. Lett. **B105** (1981) 65; Nucl. Phys. **B199** (1982) 951.

[38] P.G. Ratcliffe, Milano preprint MITH–28–93 (1993).

[39] S.D. Drell and A.C. Hearn, Phys. Rev. Lett. **16** (1966) 908.

[40] S.B. Gerasimov, Sov. Jour. of Nucl. Phys. **2** (1966) 430.

[41] M. Anselmino, B.L. Ioffe and E. Leader, Sov. J. Nucl. Phys. **49** (1989) 136.

[42] X. Ji, Phys. Lett. **B309** (1993) 187.

[43] N. de Botton, Proce. Conf. on High Energy Spin Physics, Bonn, Germany, 1990, p. 419.

[44] D. Kaplan and A. Manohar, Nucl. Phys. **B310** (1988) 527.

[45] L. A. Ahrens et al., Phys. Rev. **D35** (1987) 785.

[46] G. Garvey et al., Preprint LA–UR–93–0037 (1992).

[47] J. Kuti and V.W. Hughes, Ann. Rev. Nucl. Part. Sci. **33** (1983) 611.

[48] HERMES proposal, R. Milner and K. Rith et al., DESY (1990).

[49] R.L. Jaffe, Proc, Conf. on High Energy Spin Physics, Nagoya, Japan, 1992, p. 19.

[50] K. Zapfe, Proc. AIP Conf. on Polarized Ion Sources and Polarized Gas Targets, Madison, WI, 1993, p. 3.

[51] R. G. Milner, Proc. AIP Conf. on Polarized Ion Sources and Polarized Gas Targets, Madison, WI, 1993, p. 235.

[52] SMC proposal, V.W. Hughes et al. , CERN/SPSC 88–47 (1988).

[53] G.K. Mallot, Talk given at Nucleon Spin Structure Meeting, Yale University, January 1994.

[54] J. McCarthy and C.Y. Prescott et al., SLAC Proposal E-143, February 1992.

[55] M.L. Seely et al., Nucl. Instrum. Methods **201** (1982) 303.

[56] E.W. Hughes et al., SLAC Proposal E-154, October 1993.

[57] R.G. Arnold and J. McCarthy et al., SLAC Proposal E-155, October 1993.